AD-A148 527 TRANSITION FROM DEFLAGRATION TO DETONATION AND EFFECT OF HEAT AND MASS AD..(U) OHIO STATE UNIV RESEARCH FOUNDATION COLUMBUS R EDSE ET AL. JUN 83 1/2

UNCLASSIFIED AFOSR-TR-84-1103 AFOSR-78-3604 F/G 21/2 NL

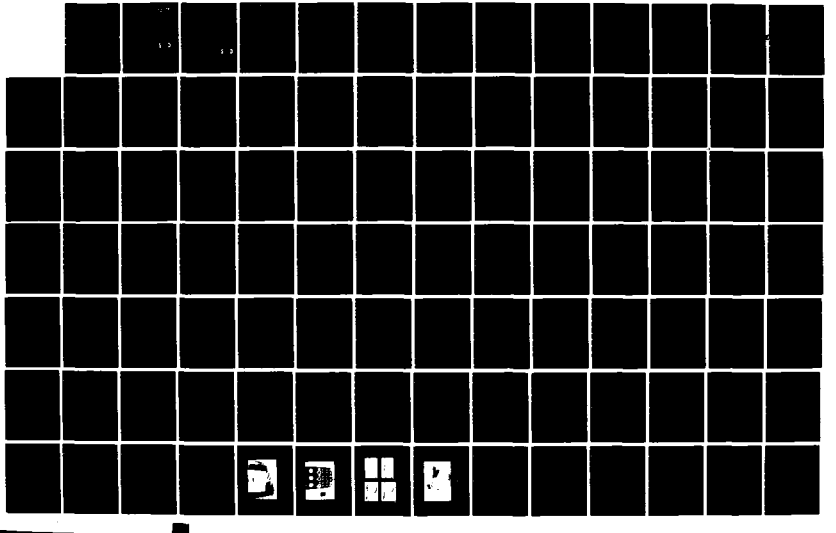

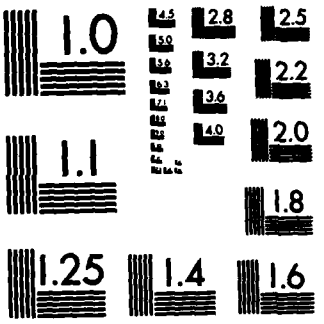

AFOSR-TR- 84-1103

12

RF Project 761050/711050
Final Report

TRANSITION FROM DEFLAGRATION TO DETONATION AND EFFECTS OF HEAT AND MASS ADDITION ON THE PARAMETERS OF A SUBSONIC FLOW THROUGH A DUCT

R. Edse, T. D. Costello, and T. Sheaf
Department of Aeronautical and Astronautical Engineering

For the Period
September 1, 1981 - May 31, 1983

U.S. DEPARTMENT OF THE AIR FORCE
Air Force Office of Scientific Research
Bolling Air Force Base, D.C. 20332

Grant No. AFOSR-78-3604

June, 1983

OSU
The Ohio State University Research Foundation
1314 Kinnear Road
Columbus, Ohio 43212

THE OHIO STATE UNIVERSITY RESEARCH FOUNDATION
1314 KINNEAR ROAD
COLUMBUS, OHIO 43212

TRANSITION FROM DEFLAGRATION TO DETONATION AND EFFECTS OF HEAT AND MASS ADDITION ON THE PARAMETERS OF A SUBSONIC FLOW THROUGH A DUCT

R. EDSE, T. D. COSTELLO, AND T. SHEAF

FOR THE PERIOD

SEPTEMBER 1, 1981 - MAY 31, 1983

U.S. DEPARTMENT OF THE AIR FORCE
AIR FORCE OFFICE OF SCIENTIFIC RESEARCH
BOLLING AIR FORCE BASE, D.C. 20332

JUNE 1983

SECURITY CLASSIFICATION OF THIS PAGE (When Data Entered) UNCLASSIFIED

REPORT DOCUMENTATION PAGE

READ INSTRUCTIONS BEFORE COMPLETING FORM

1. REPORT NUMBER: AFOSR-TR- 84-1103	2. GOVT ACCESSION NO.: AD-A148 587
3. RECIPIENT'S CATALOG NUMBER	
4. TITLE (and Subtitle): Transition from Deflagration to Detonation and Effect of Heat and Mass Addition on the Parameters of a Subsonic Flow Through a Duct	5. TYPE OF REPORT & PERIOD COVERED: 5/1/81 - 5/31/83 Final
	6. PERFORMING ORG. REPORT NUMBER: 761050/711050
7. AUTHOR(s): R. Edse, T. D. Costello, T. Sheaf	8. CONTRACT OR GRANT NUMBER(s): AFOSR-78-3604
9. PERFORMING ORGANIZATION NAME AND ADDRESS: The Ohio State University Research Foundation, 1314 Kinnear Road, Columbus, Ohio 43212	10. PROGRAM ELEMENT, PROJECT, TASK AREA & WORK UNIT NUMBERS: 61102F 2308/A2
11. CONTROLLING OFFICE NAME AND ADDRESS: U.S. Department of the Air Force, Air Force Office of Scientific Research, Bolling Air Force Base, D.C. 20332 /NA	12. REPORT DATE: June 1983
	13. NUMBER OF PAGES
14. MONITORING AGENCY NAME & ADDRESS (if different from Controlling Office)	15. SECURITY CLASS. (of this report): Unclassified
	15a. DECLASSIFICATION/DOWNGRADING SCHEDULE

16. DISTRIBUTION STATEMENT (of this Report)

Approved for public release; distribution unlimited.

17. DISTRIBUTION STATEMENT (of the abstract entered in Block 20, if different from Report)

18. SUPPLEMENTARY NOTES

19. KEY WORDS (Continue on reverse side if necessary and identify by block number)

Deflagration, Detonation, Transition, Induction Distance, Energy Transfer, Hydrogen, Oxygen, Diluent, Flame Speed, Gas Speed, Wave Speed, C-J Wave, Calculations, Transducers, Measurements, Frozen Speed of Sound, Shifting Speed of Sound, Compressor Stall.

20. ABSTRACT (Continue on reverse side if necessary and identify by block number)

The mechanism of the transition from deflagration to detonation was investigated by searching for a correlation between the detonation induction distance and various properties of the unburned mixture such as density, temperature, speed of sound, and the energy transfer to the gas behind the wave front. The magnitudes of theoretically calculated energy transfer in steady waves were compared with experimentally determined induction distances for various hydrogen-oxygen-inert gas mixtures at 1 atm and initial temperatures ranging from 140 to 300 K. The energy transfer was also calculated for pressures

DD FORM 1 JAN 73 1473

UNCLASSIFIED

SECURITY CLASSIFICATION OF THIS PAGE (When Data Entered)

ranging from 0.1 to 5 atm. It was found that the induction distances decrease somewhat when the initial pressure is increased but decrease greatly when the initial temperature is decreased. However, more experimental data are needed for ~~the~~ formulation of a quantitative relationship between induction distance and the initial properties of the combustible gas mixture.

Computational techniques (were ~~have been~~ developed to calculate the changes of the initial static pressure of subsonic flows of air through constant area ducts which are caused by heat and mass addition. These data provide information which will ~~are to~~ be used to predict the effect of fuel flow changes in turbojet combustion chambers and/or afterburners on the performance of high efficiency compressors.

PART I

TRANSITION FROM DEFLAGRATION TO DETONATION

TABLE OF CONTENTS

ABSTRACT		iii
LIST OF TABLES		v
LIST OF FIGURES		vi
LIST OF SYMBOLS		vii
CHAPTER 1 :	INTRODUCTION	1
1.1	General Introduction	1
1.2	Statement Of The Problem	4
CHAPTER 2 :	LITERATURE SURVEY	6
CHAPTER 3 :	THEORETICAL ANALYSIS	17
3.1	General Method	17
3.2	Composition Equations	30
3.3	Initial Pressure Vs. Initial Temperature	37
CHAPTER 4 :	EXPERIMENTAL ANALYSIS	41
4.1	Apparatus	42
4.2	Data Reduction	43
4.3	Experimental Results	44
CHAPTER 5 :	CONCLUSIONS	46
REFERENCES		88
APPENDICES		92

LIST OF TABLES

TABLE 3-1	Equations For Equilibrium Constants	51
TABLE 3-2	Coefficients Of Equilibrium Constants	52
TABLE 3-3	Coefficients Of Equilibrium Constants	53
TABLE 3-4	Reduced Sensible Enthalpies	54
TABLE 3-5	Reduced Sensible Enthalpies	55
TABLE 3-6	Absolute Formation Enthalpies At 0 Degrees Kelvin	56
TABLE 3-7	Dimensionless Specific Heats	57
TABLE 3-8	Dimensionless Specific Heats	58
TABLE 3-9	Relative Formation Enthalpies	59
TABLE 3-10	Detonation Parameters For hydrogen/oxygen/carbon dioxide	60
TABLE 3-11	Detonation Parameters For hydrogen/oxygen/nitrogen	61
TABLE 3-12	Detonation Parameters For hydrogen/oxygen/helium	62
TABLE 3-13	Detonation Parameters For hydrogen/oxygen/argon	63
TABLE 3-14	Relative Energy Transfer Per Unit Volume	64
TABLE 4-1	Wave Velocities Vs. Distance From Ignitor	65
TABLE 4-2	Wave Velocities Vs. Distance From Ignitor	66
TABLE 4-3	Wave Velocities Vs. Distance From Ignitor	67
TABLE 4-4	Wave Velocities Vs. Distance From Ignitor	68
TABLE 4-5	Wave Velocities Vs. Distance From Ignitor	69
TABLE 4-6	Wave Velocities Vs. Distance From Ignitor	70
TABLE 4-7	Flame Speed, Speed Of Sound, Initial Flame Front Mach Number, Initial Density and Induction Distance (approx. 300 K initial temp.)	71
TABLE 4-8	Flame Speed, Speed Of Sound, Initial Flame Front Mach Number, Initial Density and Induction Distance (approx. 140 K initial temp.)	72

LIST OF FIGURES

FIGURE 3-1	Dimensionless Relative Energy Transfer Vs. Initial Temperature	73
FIGURE 3-2	Dimensionless Relative Energy Transfer Vs. Initial Temperature	74
FIGURE 3-3	Dimensionless Relative Energy Transfer Vs. Initial Temperature	75
FIGURE 3-4	Dimensionless Relative Energy Transfer Vs. Initial Temperature	76
FIGURE 4-1	Combustion Tube	77
FIGURE 4-2	Ignitor And Inlet Assembly	78
FIGURE 4-3	Gas Control Panel	79
FIGURE 4-4	Typical Oscilloscope Photographs	80
FIGURE 4-5	Experimental Setup	81
FIGURE 4-6	Wave Velocity Vs. Distance From Ignitor	82
FIGURE 4-7	Wave Velocity Vs. Distance From Ignitor	83
FIGURE 4-8	Wave Velocity Vs. Distance From Ignitor	84
FIGURE 4-9	Wave Velocity Vs. Distance From Ignitor	85
FIGURE 4-10	Wave Velocity Vs. Distance From Ignitor	86
FIGURE 4-11	Wave Velocity Vs. Distance From Ignitor	87

LIST OF SYMBOLS

a_i^T	coefficient of equilibrium constant of species i at temperature T
f_C	ratio of global mole number of carbon to global mole number of diatomic hydrogen
f_{O_2}	ratio of global mole number of diatomic oxygen to global mole number of diatomic hydrogen
$f_{O_2}^{calc}$	calculated value of f_{O_2}
f_{N_2/O_2}	ratio of global mole number of diatomic nitrogen to global mole number of diatomic oxygen
f_{N_2/O_2}^{calc}	calculated value of f_{N_2/O_2}
$\left(\frac{c_p}{\mathcal{R}}\right)_i^T$	dimensionless specific heat of species i at temperature T
$\left(\frac{H-E_o}{\mathcal{R}T}\right)_i^T$	reduced sensible enthalpy of species i at temperature T
$\left(\frac{H_f^o}{\mathcal{R}}\right)_i$	absolute formation enthalpy of species i at zero degrees Kelvin
$\left(\frac{h_f}{\mathcal{R}}\right)_i^T$	reduced enthalpy of species i at temperature T
K^i	equilibrium constant of species i
M_f	initial flame front Mach number
$\mathcal{M}_{CG}$	molecular mass of combustion gas
$\mathcal{M}_i$	molecular mass of species i

LIST OF SYMBOLS (Continued)

$\mathcal{M}_1$	molecular mass of unburned gas mixture
p_1	pressure of unburned gas mixture
p_3	pressure of combustion gas
$\mathcal{R}$	universal gas constant
R_{CG}	specific gas constant of combustion gas
T_1	unburned gas mixture temperature
T_3	combustion gas temperature
u_f	flame speed of unburned gas mixture
u_3	combustion gas speed
$\left(\frac{v_3}{v_1}\right)$	ratio of specific volume of burned to unburned gas
$w_{a,3}$	speed of sound in combustion gas
w_1	detonation wave velocity relative to unburned gas mixture
w_3	velocity of tail of detonation wave relative to combustion gas
η_i	mole fraction of species i
$\gamma_{T_3}^{EST}$ $_F$	frozen ratio of specific heats in combustion gas
$\gamma_{T_3}^{EST}$ $_{eff}$	effective ratio of specific heats in combustion gas

CHAPTER 1

INTRODUCTION

1.1 General Introduction.

The mechanism of the formation of a detonation wave in a combustible gas mixture has been studied extensively in the past, both theoretically and experimentally. Whereas many aspects of the transition process are still not fully understood, the process of the stable detonation wave has been fully clarified.

The transition of deflagration to detonation is a fairly rapid and rather complex process. Its duration is affected in part by the temperature, pressure and composition of the initial reactants and by both the amount of turbulence present before ignition and the amount generated by the flame. Another important factor is the shape of the vessel in which the combustion takes place. Burning gas mixtures in long cylindrical tubes is a common method for investigating detonation phenomena.

From profiles of the average wave velocity along

the length of a combustion tube, the detonation induction distance can be determined. The induction distance is ordinarily defined as the distance from the ignitor to the point where a detonation wave forms. This distance varies from one gas mixture to another, and is affected by the initial conditions.

When a combustible gas mixture contained in a cylindrical tube of constant diameter is ignited at one end, a flame front is produced which propagates into the unburnt mixture. Because of the temperature rise behind the flame front, the pressure of the burnt gas increases. This increase in pressure leads to the formation of a shock wave at some distance ahead of the flame. The zone between the front of the shock wave and the tail of the combustion wave constitutes the detonation wave during the transition period.

Behind the shock wave, the unburned gas is compressed. The formation of the shock wave by the propagation of the flame front is similar to that produced by a moving piston.

Because of the heating of the unburned gas behind the shock wave, the flame speed increases. In analogy to the piston, the expanding combustion gas does work on the unburned gas behind the shock wave and, thereby,

produces detonation temperatures which are higher than the corresponding adiabatic flame temperatures at constant volume. Because of this temperature rise the flame front continually accelerates and thus produces additional pressure waves which increase the strength of the shock wave. At some point, the flame front is travelling fast enough to catch up with the tail of the shock wave. The resulting structure of a shock wave and adjacent combustion wave is called an overdriven detonation wave.

In this state the detonation wave is unstable because it has not attained its final speed. The Mach number of the tail of this detonation wave (with respect to the burned gas) is less than one. The detonation wave is considered stable after the tail Mach number reaches unity. The wave is then called a Chapman-Jouguet detonation wave.

An overshoot in combustion gas pressure and shock wave velocity occurs as the flame front rushes up to the tail of the shock wave. The magnitude of this pressure overshoot depends on the volume of the heated but unburned gas in the region between the shock wave and the flame front at the time of merging. The merging process is fast enough that the unburned gas in

this region explodes almost instantaneously.

A region of low pressure exists at the ignitor end of the tube as a result of the forward momentum imparted to the combustion gas by the passage of the shock wave. This low pressure region propagates rarefaction waves upstream which catch up to and reduce the strength of the overdriven detonation wave. These waves reduce the speed of the detonation wave by reducing the gas pressures within it. The net result is a continual increase in the Mach number of the tail of the detonation wave.

Eventually, the tail Mach number becomes equal to one, and the expansion waves no longer weaken the detonation wave. At this point, the detonation wave is considered stable and proceeds down the rest of the length of the tube at a constant rate.

1.2 Statement Of The Problem.

The question of whether induction distance is affected more by changes in initial pressure or temperature has never been completely resolved. Furthermore, the role of the speed of sound in the unburned gas mixture and how it affects the length of

the induction distance has yet to be fully understood.

A study is undertaken here to provide better insight into the relative importance of the initial pressure and temperature on the induction distance. This is done by calculating the relative energy transfer to the stable detonation wave in several hydrogen/oxygen/diluent gas mixtures. The induction distances for these gas mixtures are experimentally determined by burning them in a cylindrical combustion tube at initial conditions of room temperature and atmospheric pressure.

By studying the initial flame front Mach number, more insight into the concept of detonation induction due to flame front acceleration is obtained. The initial flame front Mach number is calculated for the various mixtures in this study based on experimentally determined flame speeds. The investigation of this parameter results in a conclusion as to whether relatively high initial Mach numbers correspond to low induction distances.

CHAPTER 2

LITERATURE SURVEY

There is much literature concerning the transition from deflagration to detonation, but the majority of it deals with the process occurring in solid explosives rather than in gaseous mixtures (references 1, 2 and 3 for example). The main literature available concerning transition in combustible gas mixtures still have not yet resolved the question of what mechanism causes the detonation induction distance to change (either lengthen or shorten) as the initial conditions of the mixture are changed.

Experiments have verified many times that the detonation induction distance is affected by changes in initial gas mixture pressure, temperature, composition, vessel configuration (i.e. length and diameter) and the amount of turbulence present before and after ignition. Early work by Sokolik and Schelkin (ref. 4) showed that initial pressure changes the length of the induction distance. These investigators performed experiments using hydrogen and oxygen mixtures as well as various

hydrocarbon fuels and oxygen. The inital pressure ranged from 30 to 300 mm of mercury (.04 to 4 atmospheres). The results clearly showed that induction distance decreases as initial gas mixture pressure increases. This effect of initial pressure has been confirmed many times since then (references 8, 26, 27, 28, 29 and 30).

Lafitte (ref. 5) did various early experiments with hydrogen/oxygen mixtures at different initial temperatures. The results of his work (which are discussed in ref. 9) showed that induction distance increased as initial temperature increased. The experiments by Lafitte involved inital temperatures ranging from 15 to 350 degress centigrade (288 to 623 degrees Kelvin).

Edse and Lawrence (ref. 6) did similar experiments only to obtain the same trend in induction distance with initial temperature. These authors used initial temperatures ranging from 123 to 300 degrees Kelvin. They concluded that the reason for the change in length of the induction distance in a combustible gas mixture depends primarily on the acceleration of the flame front as well as on the rate at which the pressure of the combusted gases increases. This conclusion was

supported by use of an empirical equation that inversely related the detonation induction distance to an empirical factor whose dimensions were that of an acceleration. It was therefore postulated that this factor was some unknown function of the acceleration of the flame front.

Bollinger, Fong, Laughrey and Edse (ref. 7) concluded that turbulence is an important mechanism by measuring the detonation induction distance in hydrogen/oxygen mixtures where longitudinal rod inserts of various diameters were placed in the combustion tube before ignition. The mixtures were ignited at a temperature of approximately 313 degrees Kelvin and both rod diameter and initial pressure was varied. They further concluded that as both initial pressure and rod diameter increased, detonation induction decreased. A final conclusion was that turbulence increases both due to the pressure waves generated and the resulting interactions as the combustion wave encounters area discontinuities.

Bollinger and Edse (ref. 8) also gave another insight into the effect of turbulence on the detonation induction distance. This conclusion represents a contradiction to some previous views which is

illustrative of the problems inherent in describing the complicated combustion process of transition.

Briefly, it is known (from the work by Shchelkin discussed in ref. 9) that as tube diameter decreases, the detonation induction distance increases. If the amount of turbulence per unit volume of gas mixture is considered, this ratio decreases as tube diameter increases. Therefore, it should be expected that detonation induction distance should increase. This behaviour would be expected because the flame propagation rate decreases as the amount of turbulence decreases and the detonation process should therefore occur in a longer period of time. However, as stated above, induction distance has been experimentally observed to decrease as tube diameter decreases.

The same type of contradiction is obtained when the Reynolds number of the unburnt gas mixture set in motion by the passage of the shock wave is considered. If this ratio is based on tube diameter, it is proportional to the diameter and decreases as tube diameter decreases. Since the Reynolds number is in turn proportional to the amount of turbulence, from this reasoning we would also expect the induction distance to increase as tube diameter decreases. Once

again, the expected result is in disagreement with experimentally observed behaviour. These conclusions exemplify the need for a better understanding of the role of turbulence in the induction process.

Lafitte and Shchelkin have shown that detonation wave velocities in rough tubes are only 40 to 50 percent that of those observed in tubes with smooth walls. Rybanin (ref. 10) summarizes the reason for these results as being due to the gas mixture being ignited at the points of wave reflection from the wall roughness. The temperature at these reflection points has been shown to be higher than the temperature behind the shock wave. Combustion propagates toward the center of the tube and fills the cross section. Thus, the combustion occurs before the mixture has time to ignite as a result of the compression process behind the shock wave.

The question of whether the unburnt but shocked gases between the shock wave and the flame front ignite spontaneously or by a less rapid process whereby the flame front merges with the tail of the shock wave, has been investigated quite thoroughly. Oppenheim, Stern and Urtiew (ref. 11) have analyzed in detail the results of experiments by Schmidt, Steinicke and Neubert

(ref. 12) using propane and air mixtures and Schleiren photographs of the combustion process. The idea of pre-ignition due to the formation of high temperature areas close to the shock wave causing ignition of the gas mixture between the shock wave and the flame front was investigated. Oppenheim, Stern and Urtiew concluded that the phenomenon of pre-ignition does cause, but is not neccessary for the formation of a detonation wave. In either case, it was further concluded, an overshoot in both detonation wave pressure and velocity would be observed.

Meyer, Urtiew and Oppenheim (ref. 13) have concluded that the gasdynamic process of compression between the shock wave and the flame front contribute, at most, only 4 percent to the enhancement of the transition process in hydrogen/air mixtures. Thus, the phenomenon of transition to detonation must be associated with heat or mass transfer from the flame front although the effects of the unsteady boundary layer should also be considered. These authors' conclusions are based on the results of the calculated value of the fractional progress of the induction process which takes the value one when detonation occurs. Values that they calculated for this fraction

were at most equal to .04 . This means that a particle in the shocked but unburnt gas mixture would have only achieved a pressure and temperature of 4 percent the value that it has at detonation if the transition process were the result of gasdynamic compression only.

Strehlow, Crooker and Cusey (ref. 14) have concluded by both theory and experiment that the accelerating shock wave preceding the combustion process can lead to the formation of 'hot spots' (pre-ignition points) near the shock wave which initiates an explosion and produces a detonation wave. Both Strehlow et al. and Meyer et al. conclude that the transition process can be modelled once the complicated kinetics between the shock wave and flame front are fully understood.

Atkinson, Bull and Shuff (ref. 15) have investigated the formation of spherical detonation waves in hydrogen/oxygen mixtures. They introduced a relation for calculating the detonation induction distance, [ ], as a function of the induction time, t, and the velocity, u, of particles transmitting the combustion wave just prior to detonation, [ ] = ut. A plot of t versus ϕ, the stoichiometric ratio of hydrogen to air in the mixture, was made after t had

been calculted for various values of the induction distance obtained from measurements and u was assumed to equal the speed of the stable C-J wave for each mixture. Another conclusion was that the most detonable mixture of hydrogen/air occurred when # was approximately equal to 1.2 .

Work in the area concerning the development of relations for the the speed of the flame front as it accelerates into a combustible gas mixture has not progressed much further than analysis of the flame front immediately after ignition. Studies by Urtiew, Laderman and Oppenheim (ref. 16) have produced relations that are based on the principal that the particle velocity of the shocked but unburnt gases, prior to when the flame front reaches the walls of the detonation tube, is a linear function of the flamefront area. In their investigation, these authors have considered cases in which the flame front initially propagates away from the ignitor in a hemispherical shape and where it propagates in the shape of a prolate spheroid. The justification for using such shapes is that they are based on photographic records of the combustion process. Use of their method is dependent on the experimentally determined values of

the initial area of the flame front and its initial average velocity. What is important about this research is the emphasis on the importance of the initial Mach number of the flame front.

Other work by Edse and Strauss (references 17, 18, 19 and 20) has produced data concerning the flame speeds of various carbon monoxide/air mixtures at high ambient pressures. The data obtained by these authors has shown that flame speeds for carbon monoxide/air mixtures decrease with pressure, whereas the flame speeds of hydrogen/oxygen mixtures increase with pressure. A major problem in experimentally determining the flame speeds of mixtures that behave like the carbon monoxide/air system is controlling flashback. In other words, higher ambient pressures require higher gas speeds which, coupled with the lower flame speeds, can make it impossible to maintain a flame. Empirically derived relations for the flame speed can therefore not be applied to pressures and temperatures that are much higher than those at which the experiments were conducted.

Since it is possible to apply the energy, continuity and Hugoniot equations to the combustion process within a stable detonation wave, several

methods exist in the literature for calculation of C-J detonation wave parameters. An early method used by Lewis and Friauf (ref. 21) calculates values based on the frozen speed of sound in the combusted gases at the tail of the detonation wave. This method, which is generally considered to be the first developed, does not include the presence of atomic oxygen in the combusted gases. The authors believed that the amount of atomic oxygen formed was not enough to affect the results of their calculations. However, if one wishes to obtain a complete description of the state of the combusted gases, atomic oxygen should be taken in to account since in mixtures involving only hydrogen and oxygen, the mole fraction of atomic oxygen is usually on the order of .02 which is not negligible.

Berets, Greene and Kistiakowsky (ref. 22) and Dunn and Wolfson (ref. 23) base their methods on the frozen speed of sound in the combusted gases and therefore obtain values of the temperature at the tail of the detonation wave which is less than actual. Comparison of temperatures calculated by the above authors has shown differences as much as 130 degrees Kelvin. The reason for these differences is generally attributed to their use of thermodynamic functions which are not of

the same accuracy.

Eisen, Gross and Rivlin (ref. 24) introduced a method that bases results on both the frozen and equilibrium speed of sound in the combusted gases. Bollinger and Edse (ref. 25) introduced a simplified method for calculating stable detonation wave parameters in hydrogen/oxygen mixtures in which the Hugoniot equation for a chemically reacting gas mixture is solved for the ratio of the pressure of the unburnt to burnt gases at the tail of the detonation wave. This iterative procedure calculates the partial pressures of each specie present in the combustion gas and produces correct results which are obtained without having to calculate either the frozen or equilibrium speed of sound.

The procedure presented in chapter three of this paper iterates until the C-J condition at the tail of the detonation wave is obtained. Equations for calculation of parameters in gases containing up to eleven species is presented.

CHAPTER THREE

THEORETICAL ANALYSIS

This chapter deals with the calculation of stable detonation wave parameters in combustible gas mixtures. An iterative method is presented for determining the pressure and temperature of a combustion gas at the tail of a stable detonation wave, and the associated wave velocities and gas speeds. Equations for calculating the combustion gas composition in several hydrogen/oxygen/diluent mixtures are presented where the diluent gas is either nitrogen, carbon dioxide or some inert species.

3.1 General Method.

The Hugoniot equations, the energy and continuity equations, and the equation of state are useful in describing the kinetic and gasdynamic processes that occur as a stable detonation wave passes through a combustible gas mixture. The fact that we calculate

parameters for stable detonation waves enables us to check the accuracy of the results since we know that the velocity of the tail of a stable wave is equal to the equilibrium speed of sound in the gases behind it.

Since the thermodynamic functions of the combustion gas are complex functions of temperature, and the composition is dependent on both temperature and pressure, an iterative procedure is required. The procedure begins by specifying initial estimates of the temperature and pressure of the combustion gas. These estimates are continually improved until the calculated value of the tail Mach number is unity. Also, it is assumed that the combustion process occurs in both thermal and chemical equilibrium.

Since this study deals with hydrogen/oxygen based mixtures that have a third gas additive of either carbon dioxide, nitrogen or an inert gas, the following equilibria are considered:

$$\tfrac{1}{2}\,O_2 \rightleftharpoons O \qquad \Delta v^{(O)} = \tfrac{1}{2}$$

$$\tfrac{1}{2}\,H_2 \rightleftharpoons H \qquad \Delta v^{(H)} = \tfrac{1}{2}$$

$$\tfrac{1}{2}\,N_2 \rightleftharpoons N \qquad \Delta v^{(N)} = \tfrac{1}{2}$$

$$\tfrac{1}{2}\,O_2 + \tfrac{1}{2}\,H_2 \rightleftharpoons OH \qquad \Delta v^{(OH)} = 0$$

$$\tfrac{1}{2}\,O_2 + \tfrac{1}{2}\,N_2 \rightleftharpoons NO \qquad \Delta v^{(NO)} = 0$$

$$\tfrac{1}{2}\,O_2 + CO \rightleftharpoons CO_2 \qquad \Delta v^{(CO_2)} = -\tfrac{1}{2}$$

$$\tfrac{1}{2}\,O_2 + H_2 \rightleftharpoons H_2O \qquad \Delta v^{(H_2O)} = -\tfrac{1}{2}$$

In the calculation of the overall mole number change,

$$\Delta\nu^{(1)} = \sum_i \nu_i^{(1)} \qquad (3.1\text{-}1)$$

where mole numbers on the left side of the reactions are considered negative, and the mole numbers on the right side are considered positive. Also, i sums over all of the species in the particular reaction.

For instance, if the gas mixture in consideration was $O_2 + H_2 + CO_2$, we might order the equilibria in the following manner,

(1)	$\frac{1}{2}\,O_2 + \frac{1}{2}\,H_2 \rightleftharpoons OH$	1=OH
(2)	$\frac{1}{2}\,O_2 \rightleftharpoons O$	1=O
(3)	$\frac{1}{2}\,H_2 \rightleftharpoons H$	1=H
(4)	$\frac{1}{2}\,O_2 + CO \rightleftharpoons CO_2$	1=CO_2
(5)	$\frac{1}{2}\,O_2 + H_2 \rightleftharpoons H_2O$	1=H_2O

Numbering the equilibria will make them easier to

reference while calculating the elements of several subsequent matrices.

An initial estimate of the pressure at the tail of the detonation wave can be obtained by considering the effect of heat addition to a supersonic flow of a calorically perfect gas. In particular, when q Joules of heat are added to one kilogram of the moving gas, the pressure ratio across the resulting thermal wave is,

$$\left(\frac{p_3}{p_1}\right)^{M_{w_3}=1} = 1 + \frac{\gamma q}{C_p T_1}\left[1 + \sqrt{1 + \frac{2/(\gamma+1)}{q/C_p T_1}}\right] \qquad (3.1\text{-}2)$$

The dimensionless heat release factor, $\frac{q}{C_p T_1}$, can be expressed in terms of the combustion enthalpy of the fuel and the dimensionless specific heat of the combustion gas as follows,

$$\frac{q}{C_p T_1} = \delta \frac{\left|\Delta H^{T_1}_{comb,f}\right|}{\mathcal{R}\, T_1} \cdot \frac{1}{\sum_i \nu_{i,o}\left(\frac{C_p}{\mathcal{R}}\right)_i^{T_{avg}}} \qquad (3.1\text{-}3)$$

where $\left|\Delta H^{T_1}_{comb,f}\right|$ is the absolute value of the combustion enthalpy of one mole of the fuel at the unburnt gas temperature T_1. The $v_{i,o}$ are the mole numbers of the constituents of the undissociated combustion gas obtained from the stoichiometric equation for the reaction. $\left(\frac{c_p}{\mathcal{R}}\right)^T_i$ is the dimensionless specific heat of species i between the temperatures T_3 and T_1. The empirical correction factor δ takes dissociation into consideration and is equal to approximately .5. A reasonable estimate for γ is approximately 1.3.

Next, the specific volume of the combustion gas can be estimated from the following relation,

$$\left(\frac{v_3}{v_1}\right)^{M_{w_3}=1} = 1 + \frac{q}{c_p T_1}\left[1 - \sqrt{1 + \frac{2/(\gamma+1)}{q/c_p T_1}}\right] \quad (3.1\text{-}4)$$

Finally, the initial estimate of the combusted gas temperature is obtained,

$$\left(\frac{T_3}{T_1}\right)^{M_{w_3}=1} = \left(\frac{p_3}{p_1}\right)^{M_{w_3}=1} \cdot \left(\frac{v_3}{v_1}\right)^{M_{w_3}=1} \quad (3.1\text{-}5)$$

In equations (3.1-2) to (3.1-5), the subscript 1 refers to the conditions of the unburnt, unshocked gas mixture. The subscript 3 refers to the conditions at the tail of the detonation wave. In subsequent equations, the superscript EST refers to an estimated value of a quantity which will equal the actual value at the end of the iteration.

With these initial estimates of temperature, T_3^{EST}, and pressure, P_3^{EST}, the equilibrium constants for the dissociation equilibria are calculated. Table (3-1) lists the K-relations for the equilibria of page 18. The a_i^T is the coefficient of the equilibrium constant of species i at temperature T and is interpolated from Tables (3-2) and (3-3).

Following calculation of the equilibrium constants, the mole fractions of the species in the combustion gas are calculated. Since the equations for calculating the composition are unique to the amount and types of species present in the combustion gas for particular initial gas mixtures, it will suffice at the present time to refer to the composition equations of section 3.2 for the mixtures considered in this study. These composition calculation procedures require at

least an initial estimate of the mole fraction of diatomic oxygen in the combustion gas. Gas mixtures containing nitrogen and carbon (as well as hydrogen and oxygen) require initial estimates of both diatomic oxygen and diatomic nitrogen.

Once the composition for the estimated temperature and pressure has been determined, the molecular mass of the combustion gas is calculated,

$$\mathcal{M}_{CG}^{T_3^{EST}} = \sum_i \eta_i \mathcal{M}_i \qquad (3.1\text{-}6)$$

Followed by the reduced enthalpy,

$$\left(\frac{h_f}{\mathcal{R}}\right)_{CG}^{T_3^{EST}} = \frac{T_3^{EST}}{\mathcal{M}_{CG}}\left[\sum_i \eta_i \left|\left(\frac{H-E_o}{\mathcal{R}T}\right)_i^{T_3^{EST}} + \left(\frac{H_f^o}{\mathcal{R}}\right)_i \frac{1}{T_3^{EST}}\right|\right] \qquad (3.1\text{-}7)$$

where the individual $\left(\frac{H-E_o}{\mathcal{R}T}\right)_i^T$ are interpolated from Tables (3-4) to (3-5). The universal gas constant, $\mathcal{R}$, is equal to 8314.33 J/Kmol K, and the specific gas constant is equal to,

$$R_{CG}^{T_3^{EST}} = \mathcal{R}/\mathcal{M}_{CG}^{T_3^{EST}} \qquad (3.1\text{-}8)$$

The absolute formation enthalpies, $\left(\frac{H_f^o}{\mathcal{R}}\right)_i$, are

obtained from Table (3-6).

From the equation of state, we determine the ratio of the specific volume of the combustion gas to that of the unburnt, unshocked gas mixture to be,

$$\left(\frac{v_3}{v_1}\right) = \frac{\left(T_3^{EST}\, p_1\, \mathcal{M}_1\right)}{\left(T_1\, p_3^{EST}\, \mathcal{M}_{CG}\right)} \qquad (3.1\text{-}9)$$

From the Hugoniot equation for a chemically reacting gas, we calculate a value for the pressure at the tail of the detonation wave,

$$p_3^{calc} = p_1\left[1 + \frac{2\mathcal{M}_1}{T_1}\left\{\left(\frac{h_f}{\mathcal{R}}\right)_{CG}^{T_3^{EST}} - \left(\frac{h_f}{\mathcal{R}}\right)^{T_1}\right\} + \left(1 + \frac{v_3}{v_1}\right)\right] \qquad (3.1\text{-}10)$$

If the absolute value of the difference between the estimated and calculated pressures is large (greater than .0000001 for instance), we reestimate the pressure in the following manner,

$$p_3^{EST(n+1)} = p_3^{EST(n)} + x_{p_3} \cdot \left(p_3^{calc(n)} - p_3^{EST(n)}\right) \qquad (3.1\text{-}11)$$

where x_{p_3} is approximately equal to .5.

The composition is recalculated using the new estimate of pressure and the old estimate of temperature. If the difference is small, we proceed by calculating the dimensionless specific heat of the combustion gas,

$$\left(\frac{C_p}{\mathcal{R}}\right)_{CG}^{T_3^{EST}} = \sum_i \eta_i \left(\frac{C_p}{\mathcal{R}}\right)_i^{T_3^{EST}} \qquad (3.1\text{-}12)$$

where the individual $\left(\frac{C_p}{\mathcal{R}}\right)_i^T$ are interpolated from Tables (3-7) to (3-8).

The frozen ratio of specific heats is calculated next,

$$\gamma_F^{T_3^{EST}} = \frac{\left(\frac{C_p}{\mathcal{R}}\right)_{CG}^{T_3^{EST}}}{\left(\frac{C_p}{\mathcal{R}}\right)_{CG}^{T_3^{EST}} - 1} \qquad (3.1\text{-}13)$$

Since the C-J condition is based on the equilibrium speed of sound in the combustion gas at the tail of the detonation wave, the effective ratio of specific heats must be calculated. This ratio is a function of the specific heat from equation (3.1-12), a chemically reacting specific heat ratio and the effect of the local mole number changes as sound waves

traverse the equilibrium combustion gas. The relation for the effective specific heat ratio is,

$$\gamma_{eff}^{T_3^{EST}} = \frac{\left[\left(\frac{C_p}{\mathcal{R}}\right)_{CG}^{T_3^{EST}} + \left|\frac{\Delta H_f^{(1)}}{\mathcal{R}T}\right| \cdot \left[a_{1,j}\right]^{-1} \cdot \left|\frac{\Delta H_f^{(j)}}{\mathcal{R}T}\right|\right]}{\left[\left(\frac{C_p}{\mathcal{R}}\right)_{CG}^{T_3^{EST}} - 1 + \left|\frac{\Delta H_f^{(1)}}{\mathcal{R}_T} - \Delta v^{(1)}\right| \cdot \left[b_{1,j}\right]^{-1} \cdot \left|\frac{\Delta H_f^{(j)}}{\mathcal{R}_T} - \Delta v^{(j)}\right|\right]}$$

$$\cdot \left[\frac{1 + \left|\frac{\Delta H_f^{(1)}}{\mathcal{R}_T} - \Delta v^{(1)}\right| \cdot \left[b_{1,j}\right]^{-1} \cdot \left|\Delta v^{(j)}\right|}{1 + \left|\frac{\Delta H_f^{(1)}}{\mathcal{R}_T}\right| \cdot \left[a_{1,j}\right]^{-1} \cdot \left|\Delta v^{(j)}\right|}\right] \quad (3.1\text{-}14)$$

The quantity in the first set of square brackets is ref ered to as the chemically reacting ratio of specific heats. It has a value of,

$$\gamma_{eff}^{T_3^{EST}} < \gamma_{c.r.}^{T_3^{EST}} < \gamma_{F}^{T_3^{EST}}$$

The quantity in the second set of brackets takes into account the mole number changes.

The inverted [illegible] square matrices $\left[a_{1,j}\right]^{-1}$ and $\left[b_{1,j}\right]^{-1}$, are defined as the inversions of the matrices whose elements are,

$$\left[b_{1,j}\right] = \sum_i \frac{v_i^{(1)} \cdot v_i^{(j)}}{n_i} \qquad (3.1\text{-}15)$$

$$\left[a_{1,j}\right] = \left[b_{1,j}\right] - \Delta v_i^{(1)} \cdot \Delta v_i^{(j)} \qquad (3.1\text{-}16)$$

The letters 1 and j refer to the chemical change. For example, if the equilibria on page 21 are being considered,

$$1 = OH, O, H, CO_2, H_2O \qquad j = OH, O, H, CO_2, H_2O$$

Since the reactions are numbered, the subscripts 1 and j can be written as numbers, for example,

$$b_{1,1}=b_{OH,OH} \; ; \; b_{1,2}=b_{OH,O} \; ; \; b_{1,3}=b_{OH,H} \quad \text{etc...}$$

The elements of the row matrix $\left|\frac{\Delta H_f^{(1)}}{RT}\right|$ and column matrix $\left|\frac{\Delta H_f^{(j)}}{RT}\right|$, are obtained from Table (3-9).

The values of the row and column matrices,

$$\left|\frac{\Delta H_f^{(1)}}{RT} - \Delta v^{(1)}\right|$$

and

$$\left| \frac{\Delta H_f^{(j)}}{\mathcal{R}_T} - \Delta v^{(j)} \right|$$

are easily obtained since the $\frac{\Delta H_f^{(1)}}{\mathcal{R}_T}$ and $\Delta v^{(1)}$ are known. Likewise, the column matrix $\left| \Delta v^{(j)} \right|$ is easily determined.

Once the effective ratio of specific heats is calculated, the equilibrium speed of sound is obtained,

$$w_{a,3} = \sqrt{\gamma_{eff}^{T_3^{EST}} \; R_{CG} \; T_3^{EST}} \qquad (3.1\text{-}17)$$

and the Hugoniot equation for a normal shock wave produces the velocity of the head of the detonation wave as follows,

$$w_1 = \sqrt{R_1 T_1 \left(\frac{P_3}{P_1} - 1 \right) \div \left(1 - \frac{v_3}{v_1} \right)} \qquad (3.1\text{-}18)$$

The continuity equation produces the velocity of the tail of the detonation wave,

$$w_3 = w_1 \cdot \left(\frac{v_3}{v_1} \right) \qquad (3.1\text{-}19)$$

If the absolute value of the difference between w_3 and $w_{a,3}$ is large (greater than .0000001 for instance), we make a new estimate of the temperature from the following relation,

$$T_3^{EST(n+1)} = T_3^{EST(n)} + x_{T_3} \cdot (w_3 - w_{a,3}) \qquad (3.1\text{-}20)$$

where x_{T_3} is approximately equal to .5 . The entire iteration routine is begun again until the magnitude of the difference between w_3 and $w_{a,3}$ is very small.

Lastly, the velocity imparted to the combustion gas by the passage of the shock wave is obtained as follows,

$$u_3 = w_1 - w_3 \qquad (3.1\text{-}21)$$

The following section 3.2 contains the composition equations that are used to compute the mole fractions of the combustion gas. They are presented in an algorithm form to demonstrate the iterative nature of the calculation.

3.2 Composition Equations.

To introduce the equations for calculating the combustion gas composition, the case of the hydrogen/oxygen/carbon dioxide mixture will be considered. First, the ratio of the global mole number of diatomic oxygen to that of diatomic hydrogen is calculated,

$$f_{O_2} = v^g_{O_2} / v^g_{H_2} \qquad (3.2\text{-}1)$$

This ratio remains constant during the combustion process. It is calculated during each iteration and is denoted by $f^{calc}_{O_2}$. One of the conditions for ending the composition iteration is the requirement that,

$$\left| f^{calc}_{O_2} - f_{O_2} \right| < .0000001$$

Next, the ratio of the global mole numbers of carbon to diatomic hydrogen is calculated,

$$f_C = v^g_C / v^g_{H_2} \qquad (3.2\text{-}2)$$

This ratio is also constant during the combustion process.

An initial estimate of the mole fraction of diatomic oxygen is required and is generally initialized as,

$$\eta_{O_2}^{EST(o)} \leftarrow .1$$

At this point, the mole fraction of atomic oxygen is calculated,

$$\eta_O = K^O \sqrt{\eta_{O_2}^{EST}} \qquad (3.2\text{-}3)$$

followed by,

$$A = \left(K^{OH}\sqrt{\eta_{O_2}^{EST}} + K^H\right)\cdot\left(1 + f_C/2\right) \qquad (3.2\text{-}4)$$

$$B = \left(K^{H_2O}\sqrt{\eta_{O_2}^{EST}} + 1\right)\cdot\left(1 + f_C\right) \qquad (3.2\text{-}5)$$

The mole fraction of diatomic hydrogen is now determined,

$$\eta_{H_2} = \left\{\sqrt{\left(\frac{A}{2B}\right)^2 + \left(1 - \eta_{O_2}^{EST} - \eta_O\right)/B} - \left(\frac{A}{2B}\right)\right\}^2 \qquad (3.2\text{-}6)$$

which allows the mole fraction of water to follow,

$$\eta_{H_2O} = K^{H_2O}\ \eta_{H_2}\sqrt{\eta_{O_2}^{EST}} \qquad (3.2\text{-}7)$$

and the mole fraction of OH,

$$\eta_{OH} = K^{OH}\sqrt{\eta_{O_2}^{EST}}\ \sqrt{\eta_{H_2}} \qquad (3.2\text{-}8)$$

as well as atomic hydrogen,

$$\eta_H = K^H \sqrt{\eta_{H_2}} \qquad (3.2\text{-}9)$$

Now the global mole fraction of diatomic hydrogen is calculated,

$$\eta_{H_2}^g = \eta_{H_2} + \eta_{H_2O} + \left(\eta_{OH} + \eta_H\right)/2 \qquad (3.2\text{-}10)$$

followed by the global mole fraction of carbon,

$$\eta_C^g = \eta_{H_2}^g \cdot f_C \qquad (3.2\text{-}11)$$

Next, the mole fractions of CO and CO_2 are obtained,

$$\eta_{CO} = \eta_C^g \Big/ \left(1 + K^{CO_2} \sqrt{\eta_{O_2}^{EST}}\right) \qquad (3.2\text{-}12)$$

$$\eta_{CO_2} = \eta_C^g - \eta_{CO} \qquad (3.2\text{-}13)$$

and finally the global mole fraction of diatomic oxygen,

$$\eta_{O_2}^g = \eta_{O_2}^{EST} + \eta_{CO_2} + \left(\eta_{CO} + \eta_O + \eta_{OH} + \eta_{H_2O}\right)/2 \qquad (3.2\text{-}14)$$

Using the above mole fractions that are based on the estimated mole fraction of diatomic oxygen, a calculated value of f_{O_2} is determined,

$$f_{O_2}^{calc} = \eta_{O_2}^g \Big/ \eta_{H_2}^g \qquad (3.2\text{-}15)$$

If the absolute value of $f_{O_2} - f_{O_2}^{calc}$ is large (greater than .0000001 for example) a new estimate of the mole fraction of diatomic oxygen is made using the following empirical relation,

$$\eta_{O_2}^{EST(n+1)} = \eta_{O_2}^{EST(n)} \cdot \left(f_{O_2} / f_{O_2}^{calc} \right)^{.8} \qquad (3.2\text{-}16)$$

and the iteration is started again by returning to equation (3.2-3).

For gas mixtures involving only hydrogen and oxygen, the above iteration can be used by specif ying that f_C is equal to zero.

For gas mixtures containing both carbon and nitrogen (as well as hydrogen and oxygen), the ratio of the global mole number of diatomic nitrogen to oxygen is also calculate

$$f_{N_2/O_2} = \nu_{N_2}^{g} / \nu_{O_2}^{g} \qquad (3.2\text{-}17)$$

and an initial estimate of the mole fraction of diatomic nitrogen is required,

$$\eta_{N_2}^{EST(0)} = .6$$

These relations are inserted after equation (3.2-2).

The mole fractions of NO and atomic nitrogen are

calculated from the following relations,

$$\eta_{NO} = K^{NO}\sqrt{\eta_{N_2}^{EST}}\sqrt{\eta_{O_2}^{EST}} \qquad (3.2\text{-}18)$$

$$\eta_{N} = K^{N}\sqrt{\eta_{N_2}^{EST}} \qquad (3.2\text{-}19)$$

and are inserted after equation (3.2-3).

The equation for the mole fraction of diatomic hydrogen, eq. (3.2-6), is replaced by,

$$\eta_{H_2} = \left\{ \sqrt{\left(\frac{A}{2B}\right)^2 + \left(1 - \eta_{N_2}^{EST} - \eta_{O_2}^{EST} - \eta_{NO} - \eta_{O} - \eta_{N}\right)/B} - \left(\frac{A}{2B}\right) \right\}^2 \qquad (3.2\text{-}20)$$

and the equation for the global mole fraction of diatomic oxygen, eq. (3.2-14), is replaced by,

$$\eta_{O_2}^{g} = \eta_{CO_2} + \eta_{O_2}^{EST} + \left(\eta_{CO} + \eta_{H_2O} + \eta_{OH} + \eta_{NO} + \eta_{O}\right)/2 \qquad (3.2\text{-}21)$$

The global mole fraction of diatomic nitrogen is obtained from,

$$\eta_{N_2}^{g} = \eta_{N_2}^{EST} + \left(\eta_{NO} + \eta_{N}\right)/2 \qquad (3.2\text{-}22)$$

and is inserted after equation (3.2-21). A calculated value of f_{N_2/O_2} is determined as,

$$f_{N_2/O_2}^{calc} = \eta_{N_2}^{g} / \eta_{O_2}^{g} \qquad (3.2\text{-}23)$$

which is inserted after equation (3.2-15).

If the absolute value of $f_{N_2/O_2} - f_{N_2/O_2}^{calc}$ is large

(greater than .0000001 for example) then the estimate of the mole fraction of diatomic nitrogen is improved by the following empirical relation,

$$\eta_{N_2}^{EST(n+1)} = \eta_{N_2}^{EST(n)} \cdot \left(f_{N_2/O_2} / f_{N_2/O_2}^{calc} \right)^{.6} \qquad (3.2\text{-}24)$$

This relation is placed after equation (3.2-16) which improves the previous estimate of the mole fraction of diatomic oxygen. If the gas mixture contains only hydrogen, oxygen and nitrogen, the value of f_C is set equal to zero.

When the diluent component of the gas mixture is an inert species, the composition iteration is started with determination of the ratio of the global mole number of the inert gas to that of the diatomic hydrogen,

$$f_x = v_x^g / v_{H_2}^g \qquad (3.2\text{-}25)$$

This is in turn followed by calculation of f_{O_2} from equation (3.2-1) and an initial estimate of the mole fraction of diatomic oxygen,

$$\eta_{O_2}^{EST(o)} = .1$$

The mole fraction of atomic oxygen is determined from egaution (3.2-3). This is in turn followed by

calculation of the following two quantities,

$$A = \left(K^{OH}\sqrt{\eta_{O_2}^{EST}} + K^{H}\right)\cdot\left(1 + f_x/2\right) \qquad (3.2\text{-}26)$$

$$B = \left(K^{H_2O}\sqrt{\eta_{O_2}^{EST}} + 1\right)\cdot\left(1 + f_x\right) \qquad (3.2\text{-}27)$$

The mole fractions of atomic hydrogen, water and OH are obtained from equations (3.2-7) to (3.2-9) . The global mole fraction of diatomic hydrogen is obtained from eq. (3.2-10). The global mole fraction of diatomic oxygen is obtained from,

$$\eta_{O_2}^{\varepsilon} = \eta_{O_2}^{EST} + \left(\eta_{H_2O} + \eta_{OH} + \eta_{O}\right)/2 \qquad (3.2\text{-}28)$$

The value of $f_{O_2}^{calc}$ is determined from equation (3.2-15). A new estimate of the mole fraction of diatomic oxygen is made from equation (3.2-16). The iteration is continued until $f_{O_2} - f_{O_2}^{calc}$ is small.

The procedure described in section 3.1 for calculation of the detonation parameters of a stable detonation wave was used to determine the parameters of the following gas mixtures,

$$\tfrac{1}{2}O_2 + H_2 + \tfrac{1}{2}CO_2$$

$$\tfrac{1}{2}O_2 + H_2 + N_2$$

$$\tfrac{1}{2}O_2 + H_2 + He$$

$$\tfrac{1}{2}O_2 + H_2 + Ar$$

The detonation parameters of T_3 , p_3 , w_3 , w_1 and the gas speed u_3 were calculated for different initial temperatures of 100, 200, 300, 400 and 500 degrees Kelvin. The initial pressures considered were .1, .5, 1.0, 2.0, and 5.0 atmospheres. The results of these calculations are compiled in Tables (3-10) to (3-13).

3.3 Initial Pressure Vs. Initial Temperature.

The results obtained by calculating the parameters of a stable detonation wave describe only the steady state motion of the wave. It is therefore difficult to apply them in explicitly calculating the induction distance. However, it is interesting to notice that the pressure ratio, $\frac{p_3}{p_1}$, may be related to the magnitude of this distance. By observing plots (Figures (3-1) to (3-4) for example) of this ratio as a function of the initial gas mixture temperature, T_1 , we see a relatively sharp increase as the initial temperature decreases.

From the energy equation considered before and after the detonation wave, it can be shown that the dimensionless relative energy transfer from the burned gas behind the detonation wave to the shocked, but

unburnt gas in the region between the shock wave and the combustion wave is,

$$\frac{\Delta h^{\circ}}{R_1 T_1} = \left(\frac{P_3}{P_1}\right) - 1 \qquad (3.3\text{-}1)$$

A complete derivation of equation (3.3-1) is given in the appendix.

Equation (3.3-1) shows that the dimensionless relative energy transfer is directly proportional to the pressure ratio $\frac{P_3}{P_1}$, and inversely proportional to the initial temperature of the gas mixture. This result is reasonable since a combustible gas mixture will generally have a higher enthalpy at a higher temperature. This in turn lowers the amount of relative energy transfered prior to the formation of the stable detonation wave. Furthermore, the definition of the detonation induction distance is relative to whether we are considering the point where the unstable wave forms, or the point where it has become stable. Therefore, we can justifiably relate the relative energy transfer to this distance.

It is particularly interesting to note that the ratio $\frac{P_3}{P_1}$, does not change substantially as the initial pressure, P_1, is changed. This result allows

us to conclude that initial temperature, rather than initial pressure has a more important effect on the length of the induction distance. However, the induction distance does change markedly with changes in initial pressure.

It is interesting to observe that by multiplying both sides of equation (3.3-1) by R_1T_1 we obtain,

$$\Delta h^\circ = R_1T_1 \left(\frac{P_3}{P_1} - 1\right) \qquad (3.3\text{-}2)$$

Equation (3.3-2) is the relative energy transfer per unit mass of gas mixture. Of course, a plot of this parameter (for different initial pressures) as a function of the initial temperature would show the same trend as that in Figures (3-1) to (3-4) and would allow us to draw the same conclusions.

However, by multiplying both sides of eq. (3.3-2) by the initial density the relative energy transfer per unit volume is obtained,

$$\Delta h^\circ = P_3 - P_1 \qquad (3.3\text{-}3)$$

By observing values of this parameter (Table (3-14)) for the hydrogen/oxygen/nitrogen gas mixture for example, this parameter is observed to increase dramatically both as initial pressure is increased and initial temperature decreased. Because the relative energy transfer per unit volume is inversely proportional to initial temperature and proportional to initial pressure, it is therefore proportional to the initial density of the gas mixture.

CHAPTER FOUR

EXPERIMENTAL ANALYSIS

In order to determine the effect of the speed of sound and the initial density on the induction distance, several hydrogen/oxygen/diluent gas mixtures initially at room temperature (approximately 300 degrees K) and atmospheric pressure were ignited in a 0.4 meter long combustion tube.

The proportion and types of diluent species used were nitrogen (N_2), argon (Ar), helium (He) and carbon dioxide (CO_2). The mole numbers of the hydrogen and oxygen were one and one half respectively. Originally, the mole number for the carbon dioxide was one, but it was lowered to one half after it was discovered that its detonation induction distance was longer than the length of the combustion tube for the given initial conditions.

Also, the hydrogen/oxygen/helium and hydrogen/oxygen/argon gas mixtures were burned at atmospheric pressure and an initial temperature of 140 degrees Kelvin.

4.1 Apparatus.

The cylindrical combustion tube in the experiment had an inside diameter of five centimeters. Along it (see Figure (4-1)) was an array of thirteen randomly spaced holes into which mounts containing piezoelectric quartz pressure transducers could be placed. The entire tube was encased in a steel cooling jacket through which liquid nitrogen could be passed in order to cool the gas mixtures before ignition in the low temperature part of this experiment.

The gases for the experiment were obtained from commercially available cylinders and were of industrial purity. The individual gases were premixed in a remote mixing chamber before injection into the combustion tube. Injection of the gases was accomplished through an orifice in the ignitor assembly (see Figure (4-2)). The mixture ratios were controlled through a series of regulators, valves and gauges contained within a control panel (see Figure (4-3)).

After injection of the gas mixture into the tube, both ends were closed by use of valves. The mixture was then ignited at one end by passing an electrical current through a thin piece of nichrome wire wrapped

across two electrodes in the ignitor.

4.2 Data Reduction.

Wave speed was measured at each of the thirteen locations along the tube using the pressure transducers in conjunction with a dual beam oscilloscope. Two successive transducer locations were monitored per run. The transducer closest to the ignitor was used to trigger the pair of beams on the oscilloscope. The wave speed was determined by first measuring the distance that the second (lower) beam travelled before the wave passed the second transducer. Passage of the wave was accompanied by an abrupt jump in the trace due to the momentary pressure increase. This distance corresponded to the wave time between tranducers. This time was then divided into the distance between the transducers which yielded the average wave speed.

Because the wave passage was on the order of microseconds, a photograph of the oscilloscope beams (see Figure (4-4) for example) traversing the screen was required for each run. The two transducers were successively repositioned until a complete profile of the average wave velocity along the tube had been

obtained.

4.3 Experimental Results.

The detonation induction distances for each of the gas mixtures were determined by observing the approximate (plus or minus 15 cm.) position on the velocity profiles where the overshoot described in section 1.1 occurred. Wave velocities obtained are compiled in Tables (4-1) to (4-6) and these values are plotted in Figures (4-6) to (4-11).

It is interesting to note that the induction distance for the hydrogen/oxygen/nitrogen and the hydrogen/oxygen/helium gas mixtures are identical for the initial conditions used in this experiment. This observation is consistent with the data of Bollinger, Fong and Edse (ref. 28) who found that for the same initial conditions but only half the amount of diluent, the induction distances were the same. The distances obtained by Bollinger, Fong and Edse are less than those found in this experiment which is to be expected since, in general, the greater the amount of diluent, the longer the induction distance.

To calculate the initial Mach number of the flame

front, flame speeds obtained by Jones (ref. 31) for each of the mixtures were used. The Mach number relationship is,

$$M_f = u_f/(\gamma_1 R_1 T_1)^{\frac{1}{2}} \qquad (4.3\text{-}1)$$

The induction distances, initial flame front Mach numbers and flame speeds are compiled in Table (4-7) where the data of Bollinger, Fong and Edse have also been included. Table (4-8) contains the data from the experiments at low initial temperature.

CHAPTER FIVE

CONCLUSIONS

Even though there is much evidence available that confirms the effect of both initial temperature and initial pressure on the induction distance of a combustible gas mixture, it is inherently difficult to draw conclusions as to the relative importance between these two parameters. This is particularly true if they are to be based solely on experimental data. Therefore, it would be convenient to determine a theoretical relationship that would clearly show which is the more important factor.

In this study, the dimensionless relative energy transfer to the gases behind the head of a stable detonation wave has been analyzed theoretically in detail for several hydrogen/oxygen/diluent gas mixtures. Plots of this quantity (Figures (3-1) to (3-4)) as a function of the initial temperature for various initial pressures show that the initial temperature appears to be the more significant factor in changing this parameter.

In fact, the maximum change in the relative energy transfer is only on the order of ten percent when the initial pressure is increased by a factor of fifty. The maximum difference occurs when the initial temperature is very low (100 degrees Kelvin in this study) and decreases rapidly as the initial temperature is increased. These results are based on the gas mixtures considered in this study but there is no reason to believe that other combustible gas mixtures would not behave in this manner. Considering the relative energy transfer per unit mass (equation (3.3-2)) results in the same conclusion.

When the relative energy transfer per unit volume is plotted as a function of the initial temperature for various initial pressures (Figure (3-5) for example), this parameter is observed to change markedly with initial pressure as well as with initial temperature. Therefore, no insight into the relative importance between temperature and pressure is obtained, particularly in describing detonations in fixed volumes. This is because in a fixed volume, changes in density neccessitate changes in mass. This result leads back to consideration of the dimensionless relative energy transfer or the relative energy

transfer per unit mass.

As far as applying the relative energy transfer to the detonation induction distance, because it is proportional to initial temperature, it is easy to say that it is therefore proportional to the induction distance. However, there are two major disagreements with this conclusion. The first arises because the induction distance for two different gas mixtures can be the same but the relative energy transfer may not. The hydrogen/oxygen/helium and hydrogen/oxygen/nitrogen systems are an example. The second conflict arises when two different gas mixtures with the same relative energy transfer do not have the same induction distance. The hydrogen/oxygen/helium and hydrogen/oxygen/argon systems are examples of this case.

It is therefore difficult to say whether a relationship for the length of the induction distance in a combustible gas mixture can be obtained based on the concept of relative energy transfer to the stable detonation wave.

When the initial flame front Mach number and its relationship with the induction distance is studied, one major problem arises. The relationship is

complicated by the fact that different gas mixtures can have the same induction distance but different initial flame front Mach numbers. From the data obtained in this study and the data compiled by other investigators, it is seen that gas mixtures with relatively high flame front Mach numbers can have either long or short induction distances. The hydrogen/oxygen/argon and hydrogen/oxygen/carbon dioxide mixtures display this effect.

Therefore, consideration of the relative energy transfer and the speed of sound in the unburnt gas mixture show these parameters to be inadequate in themselves to describe the behaviour of the detonation induction distance in combustible gas mixtures.

The combustion tube used in this study did not have transducer mounts in the region very close to the ignitor. This presents a problem in judging the accuracy of the value obtained for the induction distance in each of the low temperature hydrogen/oxygen/inert gas mixtures. This is particularly true in the case where the inert species was argon.

It must be mentioned that the wave speeds after detonation for the low temperature mixtures do not agree well with the calculated values for the stable

detonation waves. This is observed by looking at the profiles of Figures (4-10) and (4-11) and comparing the wave speeds after detonation with those compiled in Tables (3-12) and (3-13). The calculated values are consistently higher than what was actually measured.

To improve the experimental results of this study, it is suggested that a combustion tube of approximately ten feet in length be built containing transducer locations at three inch intervals from the ignitor. In addition to construction of a new tube, the use of at least four transducers per run is advised such that more data can be obtained in a shorter amount of time. In general, the use of many transducer mounts along the length of the combustion tube will produce much more complete profiles and allow more accurate estimation of the detonation induction distance.

TABLE 3-1

Equations For Equilibrium Constants

K^i

$$K^{CO_2} = a^T_{CO_2} \cdot T^{.125} \cdot \exp\left\{\left(\frac{H_f^o}{\mathcal{R}}\right)_{CO} - \left(\frac{H_f^o}{\mathcal{R}}\right)_{CO_2} / T\right\} \cdot p^{\frac{1}{2}}$$

$$K^{H_2O} = a^T_{H_2O} \cdot T^{-\frac{1}{2}} \cdot \exp\left\{-\left(\frac{H_f^o}{\mathcal{R}}\right)_{H_2O} / T\right\} \cdot p^{\frac{1}{2}}$$

$$K^{OH} = a^T_{OH} \cdot \exp\left\{-\left(\frac{H_f^o}{\mathcal{R}}\right)_{OH} / T\right\}$$

$$K^{NO} = a^T_{NO} \cdot \exp\left\{-\left(\frac{H_f^o}{\mathcal{R}}\right)_{NO} / T\right\}$$

$$K^{H} = a^T_{H} \cdot T^{\frac{1}{2}} \cdot \exp\left\{-\left(\frac{H_f^o}{\mathcal{R}}\right)_{H} / T\right\} \cdot p^{-\frac{1}{2}}$$

$$K^{O} = a^T_{O} \cdot T^{\frac{1}{2}} \cdot \exp\left\{-\left(\frac{H_f^o}{\mathcal{R}}\right)_{O} / T\right\} \cdot p^{-\frac{1}{2}}$$

$$K^{N} = a^T_{N} \cdot T^{\frac{1}{2}} \cdot \exp\left\{-\left(\frac{H_f^o}{\mathcal{R}}\right)_{N} / T\right\} \cdot p^{-\frac{1}{2}}$$

TABLE 3-2

Coefficients Of Equilibrium Constants

a_i^T

T(^{O}K)	$\frac{1}{2}H_2 \rightleftharpoons H$	$\frac{1}{2}O_2 \rightleftharpoons O$	$\frac{1}{2}O_2+\frac{1}{2}H_2 \rightleftharpoons OH$	$\frac{1}{2}O_2+H_2 \rightleftharpoons H_2O$
2500	16.351	41.289	5.8457	.08531
2600	16.405	41.207	5.8133	.08483
2700	16.451	41.112	5.7810	.08440
2800	16.495	40.993	5.7490	.08403
2900	16.543	40.862	5.7171	.08370
3000	16.585	40.719	5.6854	.08352
3100	16.602	40.553	5.6594	.08328
3200	16.620	40.391	5.6334	.08307
3300	16.635	40.225	5.6076	.08295
3400	16.624	40.061	5.5820	.08288
3500	16.645	39.901	5.5564	.08284
3600	16.645	39.738	5.5310	.08282
3700	16.638	39.575	5.5056	.08283
3800	16.625	39.413	5.4804	.08286
3900	16.612	39.256	5.4553	.08929
4000	16.602	39.087	5.4303	.08300

TABLE 3-3

Coefficients Of Equilibrium Constants

a_i^T

T(^{o}K)	$\frac{1}{2}N_2 \rightleftharpoons N$	$\frac{1}{2}O_2+\frac{1}{2}N_2 \rightleftharpoons NO$	$\frac{1}{2}O_2+CO \rightleftharpoons CO_2$
2500	39.865	4.4620	1.5090 -5
2600	39.865	4.4651	1.5137 -5
2700	39.861	4.4669	1.5199 -5
2800	39.845	4.4687	1.5236 -5
2900	39.809	4.4696	1.5300 -5
3000	39.734	4.4705	1.5366 -5
3100	39.701	4.4709	1.5441 -5
3200	39.666	4.4705	1.5526 -5
3300	39.630	4.4696	1.5615 -5
3400	39.586	4.4687	1.5703 -5
3500	39.539	4.4669	1.5786 -5
3600	39.488	4.4647	1.5870 -5
3700	39.428	4.4620	1.5956 -5
3800	39.369	4.4564	1.6040 -5
3900	39.302	4.4549	1.6128 -5
4000	39.220	4.4513	1.6214 -5

TABLE 3-4

Reduced Sensible Enthalpies

$$\left(\frac{H-E_0}{\mathcal{R}T}\right)_i^T$$

T(^oK)	H_2	H	O_2	O	OH
2500	3.799	2.5	4.188	2.543	3.877
2600	3.819	2.5	4.208	2.542	3.894
2700	3.839	2.5	4.227	2.541	3.911
2800	3.859	2.5	4.245	2.540	3.928
2900	3.878	2.5	4.263	2.539	3.944
3000	3.897	2.5	4.281	2.538	3.959
3100	3.916	2.5	4.298	2.537	3.974
3200	3.934	2.5	4.315	2.537	3.989
3300	3.952	2.5	4.332	2.537	4.003
3400	3.969	2.5	4.348	2.536	4.017
3500	3.987	2.5	4.364	2.536	4.031
3600	4.003	2.5	4.379	2.536	4.044
3700	4.020	2.5	4.395	2.537	4.056
3800	4.037	2.5	4.409	2.537	4.069
3900	4.053	2.5	4.424	2.537	4.081
4000	4.069	2.5	4.438	2.538	4.093

TABLE 3-5

Reduced Sensible Enthalpies

$$\left(\frac{H-E_o}{RT}\right)_i^T$$

T(°K)	H_2O	N_2	NO	N	CO	CO_2
2500	5.238	3.992	4.114	2.500	4.026	6.316
2600	5.286	4.008	4.128	2.501	4.042	6.358
2700	5.333	4.024	4.141	2.501	4.057	6.398
2800	5.378	4.038	4.153	2.501	4.071	6.435
2900	5.421	4.052	4.165	2.502	4.085	6.470
3000	5.463	4.066	4.176	2.502	4.098	6.504
3100	5.503	4.078	4.187	2.503	4.110	6.536
3200	5.542	4.090	4.197	2.504	4.122	6.566
3300	5.580	4.102	4.207	2.505	4.133	6.595
3400	5.616	4.113	4.216	2.506	4.144	6.623
3500	5.651	4.124	4.226	2.508	4.154	6.649
3600	5.685	4.134	4.234	2.509	4.164	6.674
3700	5.717	4.144	4.243	2.511	4.174	6.698
3800	5.749	4.154	4.251	2.513	4.183	6.722
3900	5.779	4.163	4.258	2.515	4.192	6.744
4000	5.809	4.172	4.266	2.518	4.200	6.765

TABLE 3-6

Absolute Formation Enthalpies At 0 Degrees Kelvin

$$\left(\frac{H_f^\circ}{\mathcal{R}}\right)_i$$

Specie	Abs. Formation Enthalpy (K)
CO	-13,688
CO_2	-47,286
H	25,982
H_2	0
H_2O	-28,736
N	56,613
N_2	0
NO	10,799
O	29,685
O_2	0
OH	4,675

TABLE 3-7

Dimensionless Specific Heats

$\left(\frac{C_p}{\mathcal{R}}\right)_i^T$

T(°K)	H_2	H	O_2	O	OH
2500	4.315	2.5	4.681	2.508	4.339
2600	4.347	2.5	4.707	2.509	4.339
2700	4.378	2.5	4.733	2.511	4.360
2800	4.407	2.5	4.758	2.513	4.381
2900	4.433	2.5	4.782	2.516	4.400
3000	4.458	2.5	4.806	2.518	4.418
3100	4.484	2.5	4.829	2.521	4.435
3200	4.510	2.5	4.851	2.525	4.452
3300	4.535	2.5	4.872	2.529	4.467
3400	4.560	2.5	4.893	2.533	4.481
3500	4.584	2.5	4.913	2.537	4.495
3600	4.609	2.5	4.931	2.541	4.508
3700	4.632	2.5	4.949	2.546	4.521
3800	4.656	2.5	4.966	2.551	4.533
3900	4.679	2.5	4.982	2.557	4.545
4000	4.701	2.5	4.998	2.562	4.556

TABLE 3-8

Dimensionless Specific Heats

$\left(\frac{C_p}{\mathcal{R}}\right)_i^T$

T(°K)	N_2	N	NO	CO_2	CO	H_2O
2500	4.406	2.505	4.467	7.393	4.430	6.473
2600	4.418	2.507	4.476	7.415	4.441	6.524
2700	4.428	2.510	4.485	7.433	4.451	6.572
2800	4.438	2.513	4.492	7.451	4.460	6.615
2900	4.448	2.517	4.499	7.468	4.468	6.657
3000	4.456	2.522	4.506	7.485	4.476	6.695
3100	4.464	2.527	4.513	7.499	4.484	6.730
3200	4.472	2.534	4.519	7.513	4.491	6.764
3300	4.479	2.541	4.525	7.526	4.497	6.795
3400	4.486	2.550	4.530	7.539	4.503	6.825
3500	4.492	2.559	4.535	7.551	4.509	6.852
3600	4.498	2.570	4.540	7.564	4.515	6.879
3700	4.504	2.582	4.545	7.575	4.521	6.903
3800	4.510	2.595	4.550	7.586	4.526	6.926
3900	4.515	2.608	4.554	7.597	4.531	6.949
4000	4.521	2.623	4.558	7.608	4.536	6.970

TABLE 3-9

$$\frac{\Delta H_f^{(CO_2)}}{RT} = \left(\frac{H_f}{RT}\right)^T_{CO_2} - \left(\frac{H_f}{RT}\right)^T_{CO} - \tfrac{1}{2}\left(\frac{H_f}{RT}\right)^T_{O_2}$$

$$\frac{\Delta H_f^{(H)}}{RT} = \left(\frac{H_f}{RT}\right)^T_{H} - \tfrac{1}{2}\left(\frac{H_f}{RT}\right)^T_{H_2}$$

$$\frac{\Delta H_f^{(H_2O)}}{RT} = \left(\frac{H_f}{RT}\right)^T_{H_2O} - \left(\frac{H_f}{RT}\right)^T_{H_2} - \tfrac{1}{2}\left(\frac{H_f}{RT}\right)^T_{O_2}$$

$$\frac{\Delta H_f^{(N)}}{RT} = \left(\frac{H_f}{RT}\right)^T_{N} - \tfrac{1}{2}\left(\frac{H_f}{RT}\right)^T_{N_2}$$

$$\frac{\Delta H_f^{(NO)}}{RT} = \left(\frac{H_f}{RT}\right)^T_{NO} - \tfrac{1}{2}\left(\frac{H_f}{RT}\right)^T_{N_2} - \tfrac{1}{2}\left(\frac{H_f}{RT}\right)^T_{O_2}$$

$$\frac{\Delta H_f^{(OH)}}{RT} = \left(\frac{H_f}{RT}\right)^T_{OH} - \tfrac{1}{2}\left(\frac{H_f}{RT}\right)^T_{O_2} - \tfrac{1}{2}\left(\frac{H_f}{RT}\right)^T_{H_2}$$

$$\frac{\Delta H_f^{(O)}}{RT} = \left(\frac{H_f}{RT}\right)^T_{O} - \tfrac{1}{2}\left(\frac{H_f}{RT}\right)^T_{O_2}$$

where: $$\left(\frac{H_f}{RT}\right)^T_i = \left(\frac{H-E_o}{RT}\right)^T_i + \left(\frac{H_f^o}{R}\right)_i \cdot \left(\frac{1}{T}\right)$$

TABLE 3-10

Detonation Parameters For

$\frac{1}{2}O_2 + H_2 + \frac{1}{2}CO_2$

At .1 And 5 Atmospheres Initial Pressure

p_1 = .1 atm.

$T_1(^oK)$	$T_3(^oK)$	p_3(atm)	w_1(m/s)	w_3(m/s)	u_3(m/s)
100	3250.52	4.28	1926.87	1026.53	900.34
200	3168.72	2.10	1897.46	1021.87	875.59
300	3127.24	1.39	1875.65	1021.25	854.40
400	3101.54	1.03	1856.93	1023.44	833.49
500	3082.58	.82	1838.09	1025.80	812.29

p_1 = 5 atm.

100	3813.00	231.8	2014.50	1079.07	935.43
200	3733.38	114.6	1992.25	1077.69	914.5o
300	3695.45	76.0	1975.94	1080.03	895.91
400	3674.75	56.9	1962.31	1083.60	878.71
500	3659.86	45.3	1948.11	1087.67	860.44

TABLE 3-11

Detonation Parameters For

$\frac{1}{2}O_2 + H_2 + N_2$

At .1 And 5 Atmospheres Initial Pressure

p_1 = .1 atm.

$T_1(^oK)$	$T_3(^oK)$	p_3(atm)	w_1(m/s)	w_3(m/s)	u_3(m/s)
100	3076.23	4.92	2167.68	1162.83	1004.9
200	3015.84	2.41	2134.08	1154.05	980.0
300	2986.41	1.59	2109.01	1150.98	958.0
400	2968.67	1.18	2085.90	1150.08	935.8
500	2957.45	.94	2066.37	1150.41	915.9

p_1 = 5 atm.

100	3499.02	269.0	2281.36	1236.06	1045.3
200	3457.83	133.0	2255.86	1230.62	1025.2
300	3442.43	88.1	2236.92	1229.86	1007.1
400	3436.98	65.8	2220.38	1230.96	989.4
500	3435.83	52.4	2204.57	1232.85	971.7

TABLE 3-12

Detonation Parameters For

$\frac{1}{2}O_2 + H_2 + He$

At .1 And 5 Atmospheres Initial Pressure

p_1 = .1 atm.

$T_1(^oK)$	$T_3(^oK)$	p_3(atm)	w_1(m/s)	w_3(m/s)	u_3(m/s)
100	3253.20	5.35	3277.05	1764.49	1512.6
200	3165.57	2.61	3215.48	1743.50	1471.9
300	3120.12	1.71	3171.56	1734.03	1437.5
400	3091.03	1.27	3134.12	1729.06	1405.1
500	3070.13	1.00	3099.15	1726.28	1372.9

p_1 = 5 atm.

100	3866.85	303.6	3522.64	1922.12	1600.5
200	3776.10	148.8	3467.82	1902.13	1565.7
300	3730.89	98.0	3429.70	1893.64	1536.1
400	3703.49	72.9	3397.92	1889.73	1508.2
500	3684.85	57.8	3368.86	1888.03	1480.8

TABLE 3-13

Detonation Parameters For

$\frac{1}{2}O_2 + H_2 + Ar$

At .1 And 5 Atmospheres Initial Pressure

$p_1 = .1$ atm.

$T_1(^oK)$	$T_3(^oK)$	p_3(atm)	w_1(m/s)	w_3(m/s)	u_3(m/s)
100	3253.20	5.35	2019.80	1087.54	932.26
200	3165.59	2.61	1981.90	1074.61	907.30
300	3120.09	1.71	1954.70	1068.76	885.95
400	3090.99	1.27	1931.61	1065.70	865.91
500	3070.14	1.00	1910.19	1063.99	846.20

$p_1 = 5$ atm.

100	3866.85	303.6	2171.17	1184.70	986.47
200	3776.10	148.8	2137.38	1172.37	965.01
300	3730.89	98.0	2113.89	1167.14	946.74
400	3703.49	72.9	2094.30	1164.73	929.57
500	3684.85	57.8	2076.39	1163.68	912.71

TABLE 4-1

Wave Velocities, w_1 , Vs. Distance From Igniter

$\frac{1}{2}O_2 + H_2 + \frac{1}{2}CO_2$

(1 Atm. Initial Pressure and °300 K Initial Temp.)

Distance (m)	Run #1 (m/s)	Run #2 (m/s)	Run #3 (m/s)
1.49	162	162	162
2.41	941	941	941
3.01	1360	1360	1580
3.31	1613	1741	1613
3.94	2511	2651	2511
4.53	2162	2179	2214
4.84	2191	2125	2093
5.77	2169	2126	2105
6.23	2044	2007	2032

TABLE 3-14

Relative Energy Transfer Per Unit Volume

$\frac{1}{2}O_2 + H_2 + N_2$

$T_1(^oK)$		p_3-p_1 (atm.)
100		4.82
200		2.32
300	p_1 = .1 atm.	1.49
400		1.08
500		.84
100		264.04
200		128.04
300	p_1 = 5 atm.	83.14
400		60.81
500		47.44

TABLE 4-2

Wave Velocities, W_1, Vs. Distance From Ignitor

$\frac{1}{2}O_2 + H_2 + N_2$

(1 Atm. Initial Pressure and °300 K Initial Temp.)

Distance (m)	Run #1 (m/s)	Run #2 (m/s)	Run #3 (m/s)
1.80	633	639	645
3.01	1799	1705	2020
3.31	3193	3193	3048
3.94	2852	2913	2883
4.53	2794	2736	2736
4.84	2580	2683	2580
5.77	2474	2445	2460

TABLE 4-3

Wave Velocities, w_1 , Vs. Distance From Ignitor

$\frac{1}{2}O_2 + H_2 + He$

(1 Atm. Initial Pressure and °300 K Initial Temp.)

Distance (m)	Run #1 (m/s)	Run #2 (m/s)	Run #3 (m/s)
.90	752	767	784
1.49	560	582	577
3.01	2692	2500	1313
3.31	4868	4801	4963
3.40	4311	4501	4402
4.53	4014	4038	4224
4.84	3895	3939	3895
5.77	3702	3734	3734
6.23	3533	3533	3533

TABLE 4-4

Wave Velocities, w_1, Vs. Distance From Ignitor

$\frac{1}{2}O_2 + H_2 + Ar$

(1 Atm. Initial Pressure and ~300 K Initial Temp.)

Distance (m)	Run #1 (m/s)	Run #2 (m/s)	Run #3 (m/s)
1.49	312	298	319
1.80	960	1131	1002
2.41	2674	2508	2362
3.01	2347	2406	2367
3.31	2336	2336	2336
3.94	2272	2272	2236
4.53	2179	2197	2179
4.84	2262	2262	2262
5.77	2236	2147	2147
6.23	2146	2191	2168

TABLE 4-5

Wave Velocities, W_1, Vs. Distance From Ignitor

$\frac{1}{2}O_2 + H_2 + He$

(1 Atm. Initial Pressure and °140 K Initial Temp.)

Distance (m)	Run #1 (m/s)	Run #2 (m/s)	Run #3 (m/s)
.43	280	286	320
.90	570	545	600
1.49	868	995	1194
1.80	762	469	554
2.41	1051	----	----
3.01	2172	2389	2275
3.31	1353	1449	966
3.94	1296	----	----
4.53	1003	841	1152

* ---- Data not usable

TABLE 4-6

Wave Velocities, W_1, Vs. Distance From Ignitor

$\frac{1}{2}O_2 + H_2 + Ar$

(1 Atm. Initial Pressure and ~140 K Initial Temp.)

Distance (m)	Run #1 (m/s)	Run #2 (m/s)	Run #3 (m/s)
.43	609	563	----
.90	2213	2326	----
1.49	1843	1393	1528
1.80	442	1637	1707
2.41	2121	1840	2015
3.01	2120	2222	----
3.31	2018	1945	----

* ---- Data not usable

TABLE 4-7

Flame Speed, Speed of Sound, Initial Flame Front Mach Number, Initial Density And Induction Distance

T_1 approx. 300 ^{o}K and p_1 = 1 atm.

Diluent	u_f (m/s)	$w_{a,f}$ (m/s)	M_f	ρ_1 (Kg/m**3)	d_i (cm.)
N_2	4.60	435.62	.0106	.7479	325
Ar	4.43	398.68	.0111	.9418	225
He	6.44	646.87	.0099	.3578	325
$\frac{1}{2}CO_2$	6.07	367.94	.0147	.8129	375
$\frac{1}{2}N_2$	7.89	467.18	.0168	.6504	228*
$\frac{1}{2}$Ar	8.00	435.73	.0184	.7716	179*
Ar	4.43	398.68	.0111	.9418	240*
$\frac{1}{2}$He	9.34	600.28	.0156	.4065	228*
$\frac{1}{2}CO_2$	6.07	412.54	.0147	.8129	---

* Data from reference 28 (15 mm diameter tube)

TABLE 4-8

Flame Speed, Speed of Sound, Initial Flame Front Mach Number, Initial Density And Induction Distance

T_1 approx. 140 ^{o}K and p_1 = 1 atm.

Diluent	u_f(m/s)	$w_{a,1}$(m/s)	M_f	ρ_1(Kg/m**3)	d_i(cm.)
He	3.076	454.07	.0068	.7666	275
Ar	2.117	279.85	.0076	2.018	75

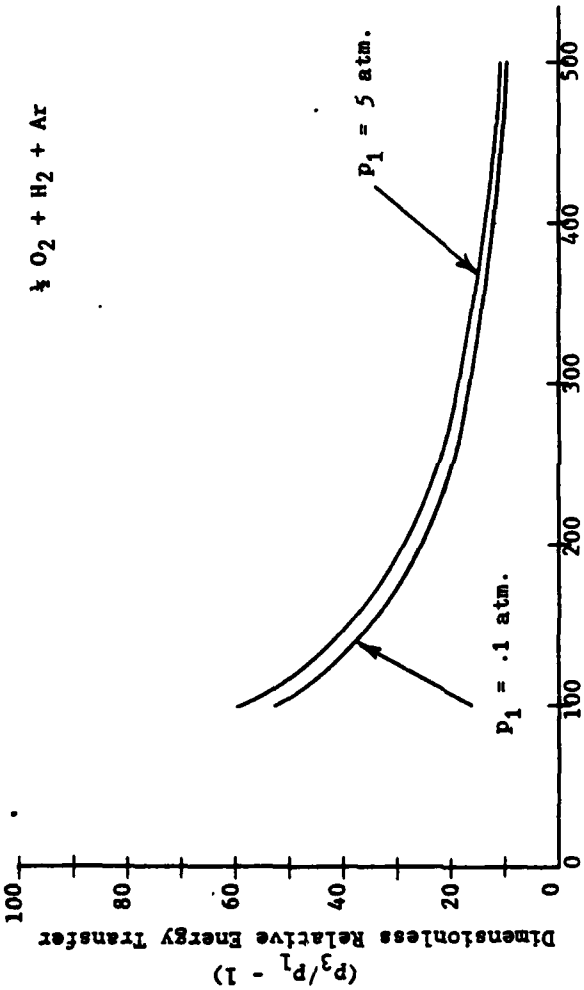

Figure 3-1

Dimensionless Relative Energy Transfer Vs. Initial Temperature

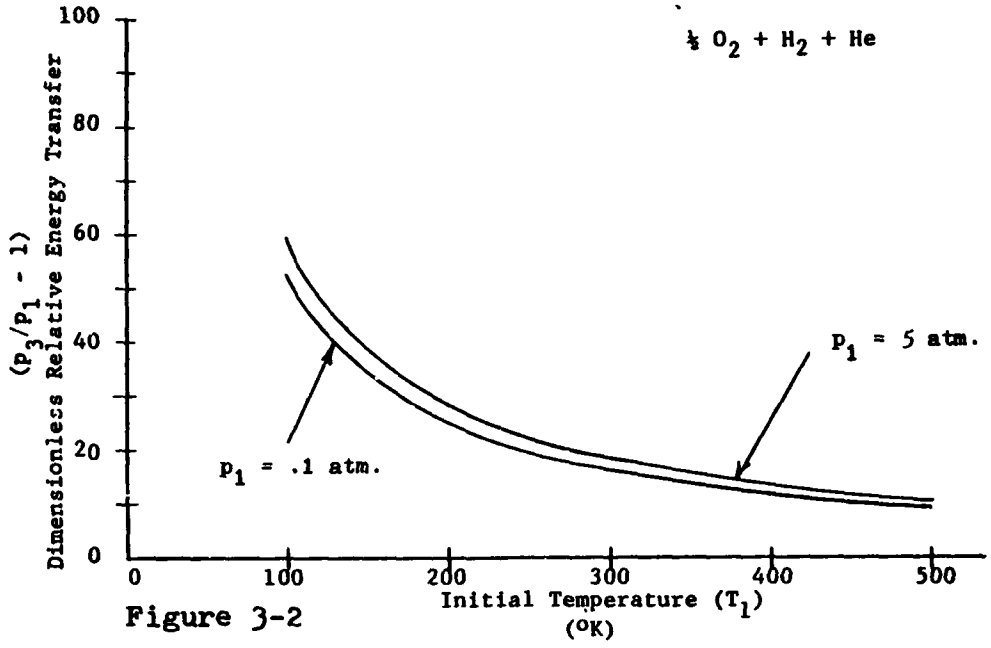

Figure 3-2

Dimensionless Relative Energy Transfer Vs. Initial Temperature

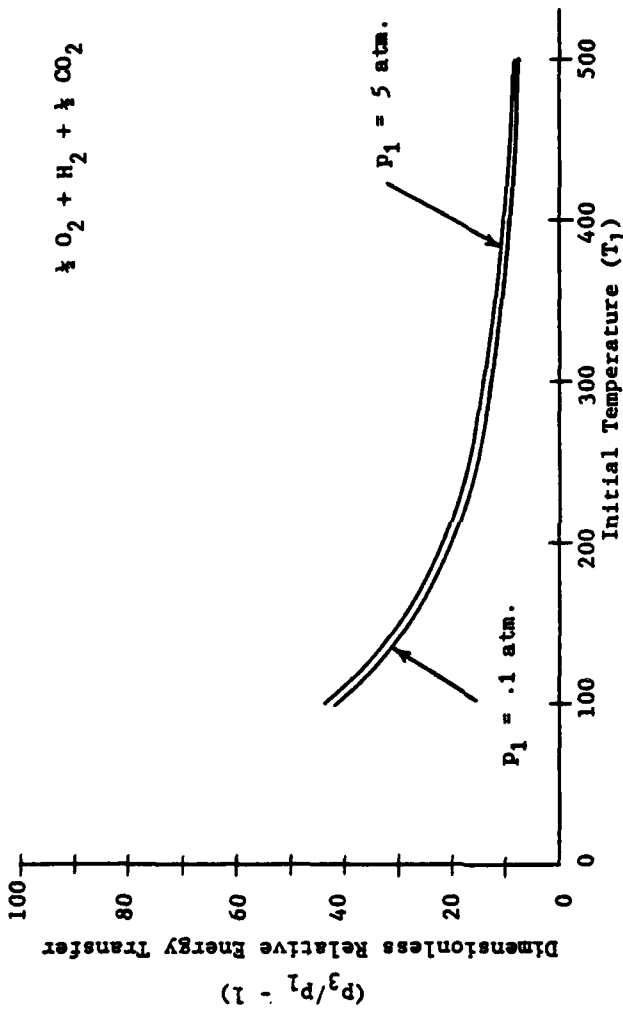

Figure 3-3

Dimensionless Relative Energy Transfer Vs. Initial Temperature

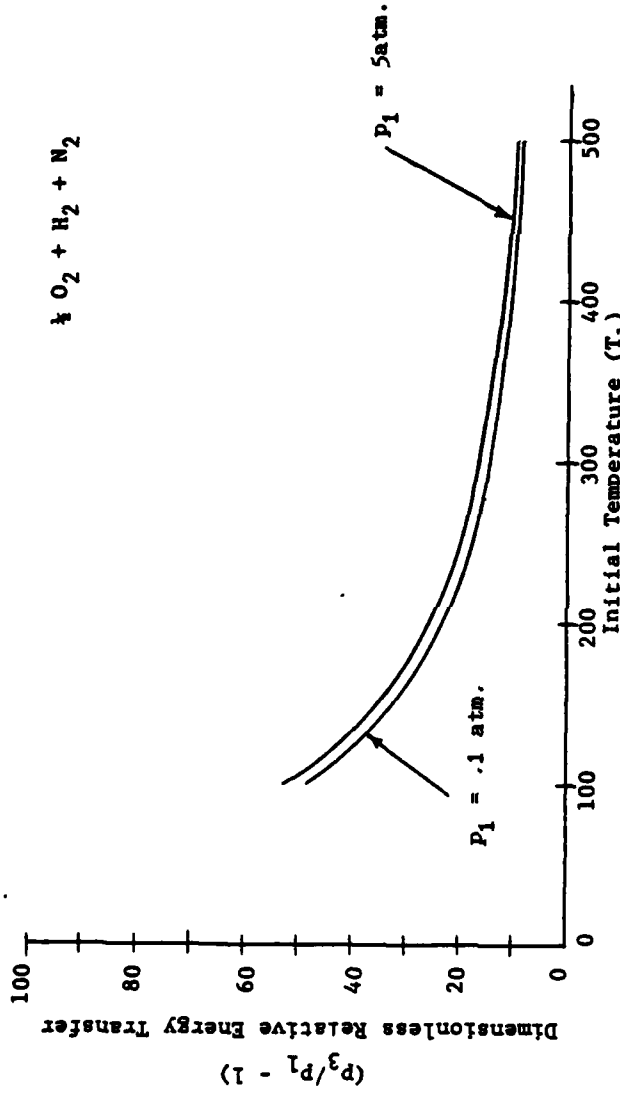

Figure 3-4

Dimensionless Relative Energy Transfer Vs. Initial Temperature

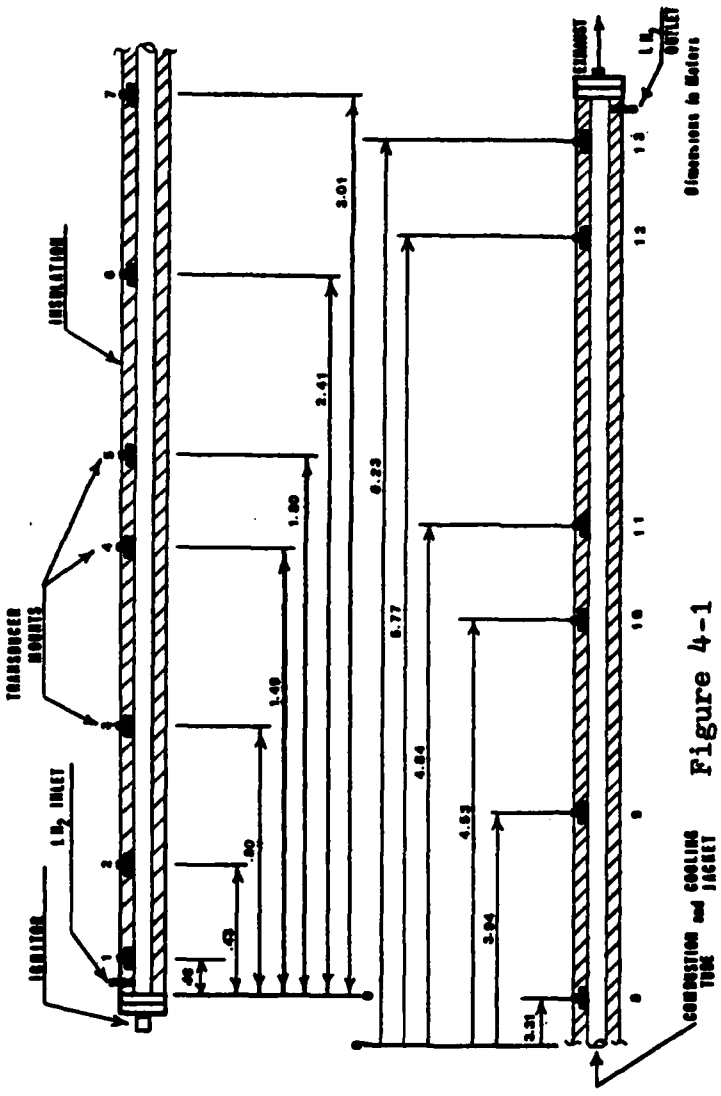

Figure 4-1
COMBUSTION TUBE

Figure 4-2

Ignitor and Inlet Assembly

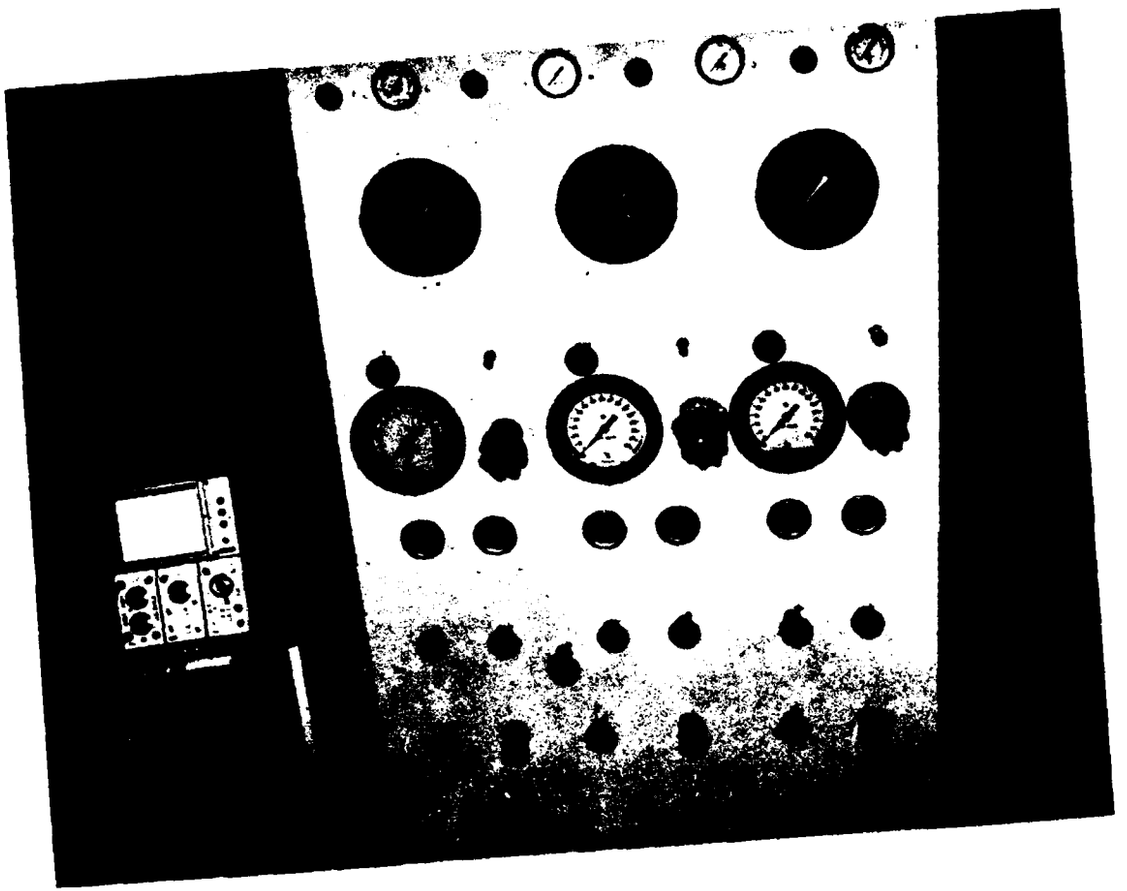

Figure 4-3

Gas Control Panel

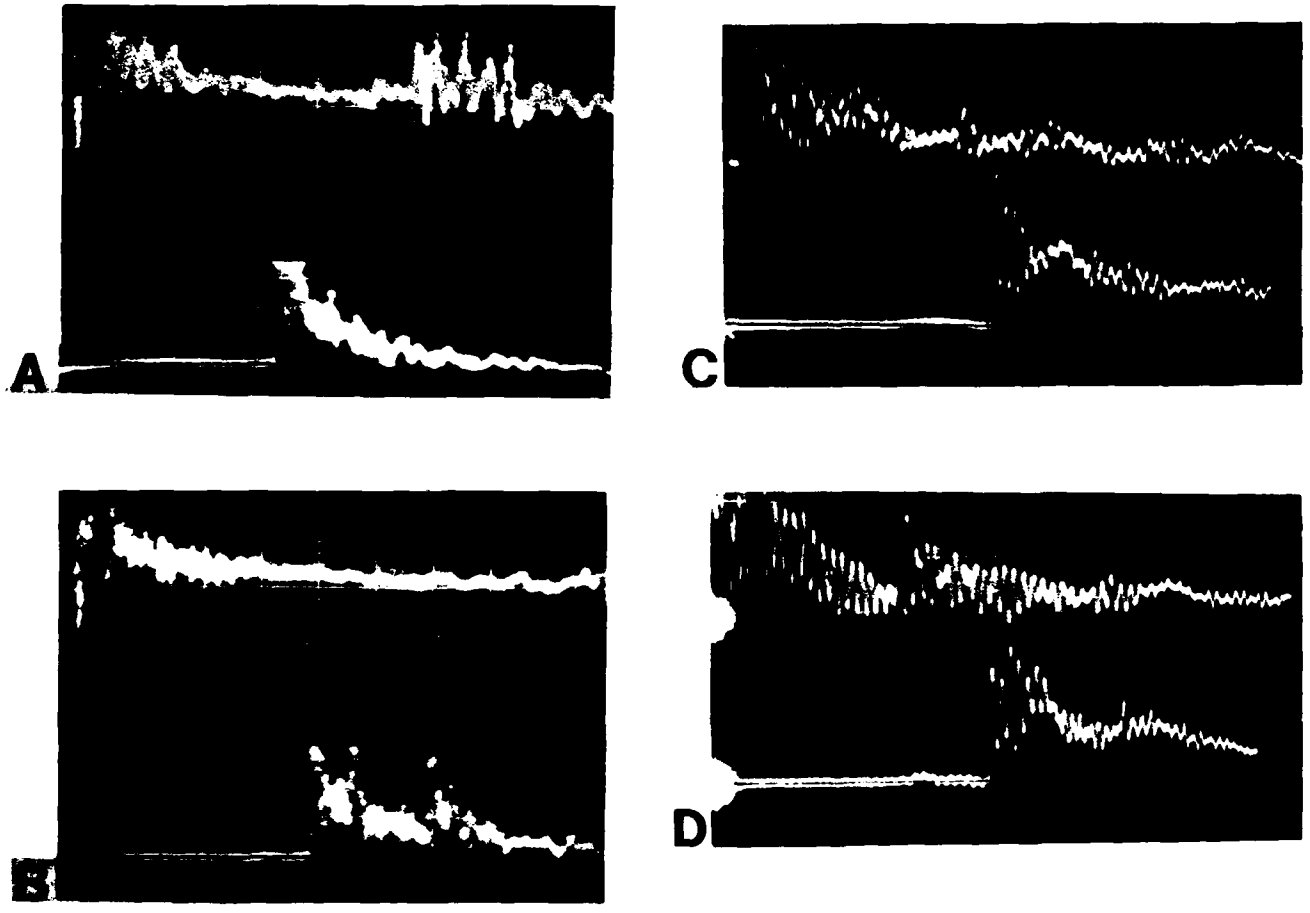

Figure 4-4

Typical Oscilloscope Photos

Figure 4-5

Experimental Setup

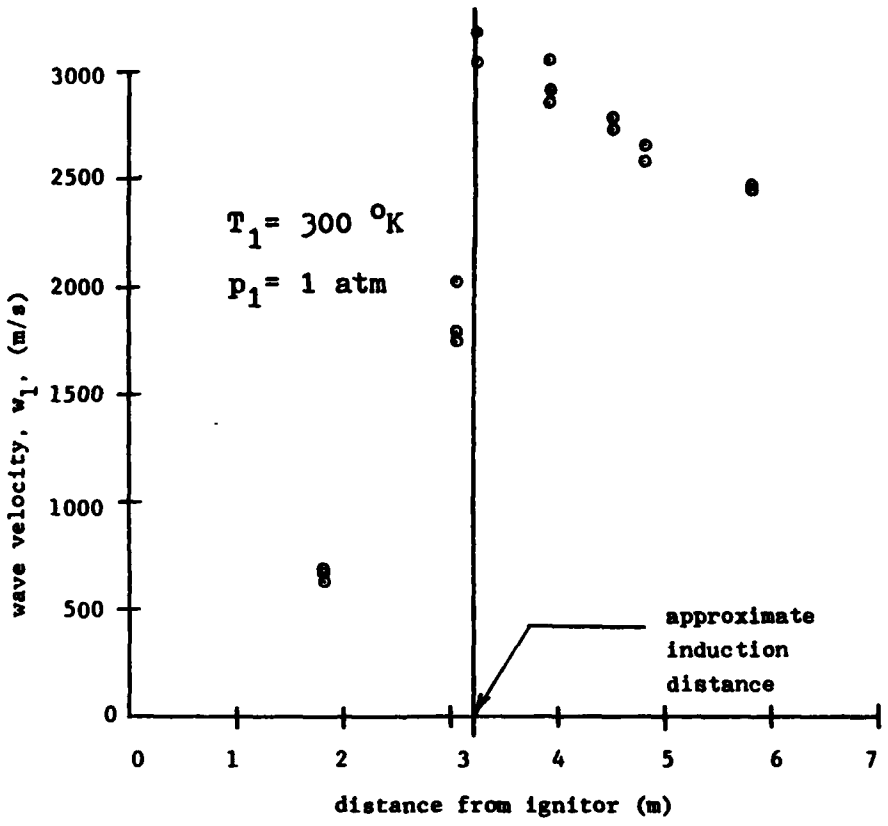

Figure 4-6
w_1 vs. distance from ignitor for $\frac{1}{2}O_2+H_2+N_2$

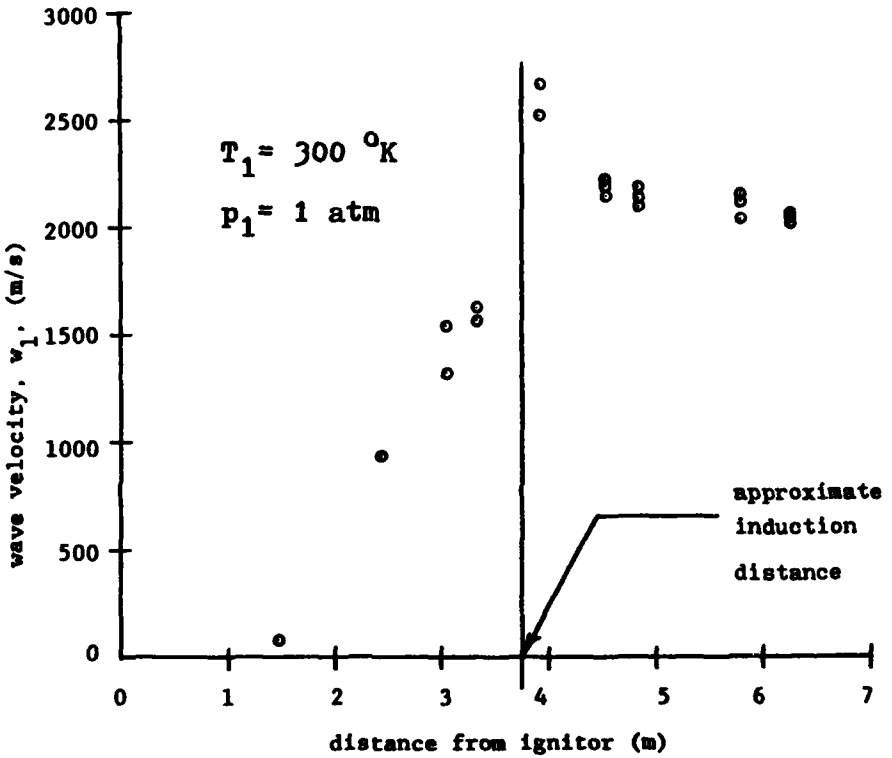

Figure 4-7
w_1 vs. distance from ignitor for $\frac{1}{2}O_2+H_2+\frac{1}{2}CO_2$

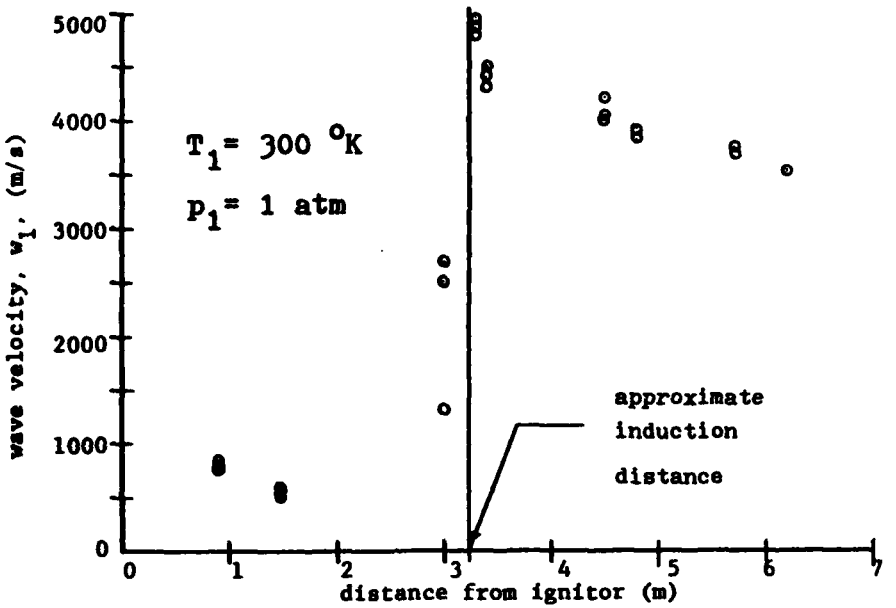

Figure 4-8

w_1 vs. distance from ignitor for $\frac{1}{2}O_2+H_2+He$

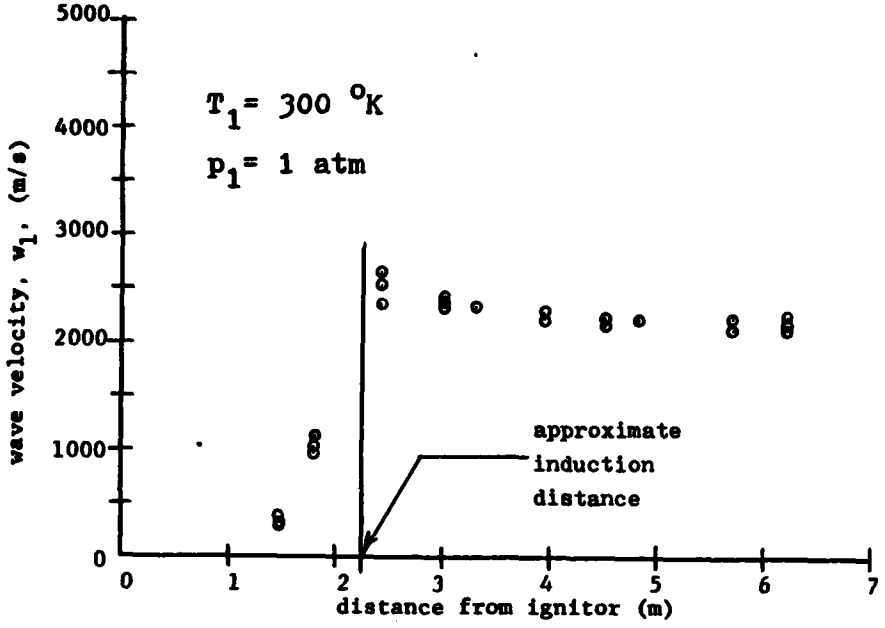

Figure 4-9
w_1 vs. distance from ignitor for $\frac{1}{2}O_2+H_2+$ Ar

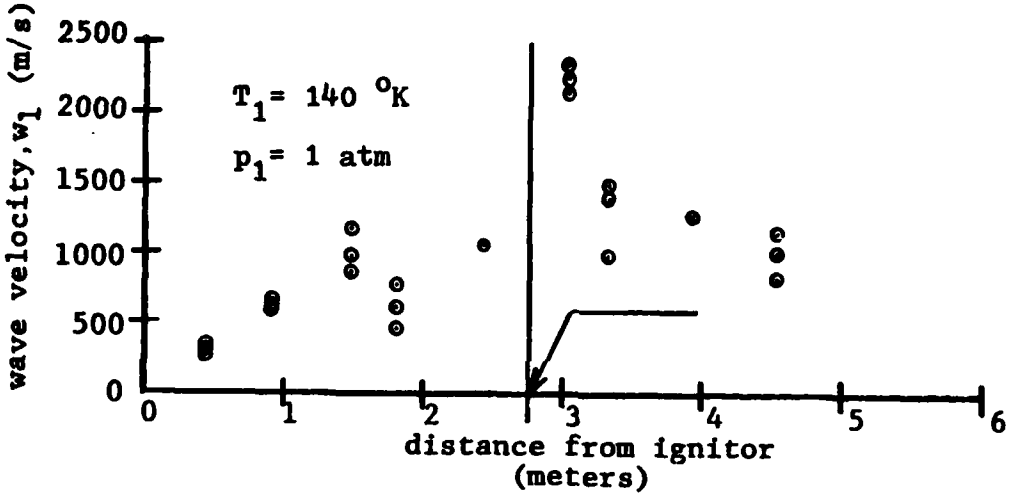

Figure 4-10

w_1 vs. distance from ignitor for $\frac{1}{2}O_2+H_2+He$

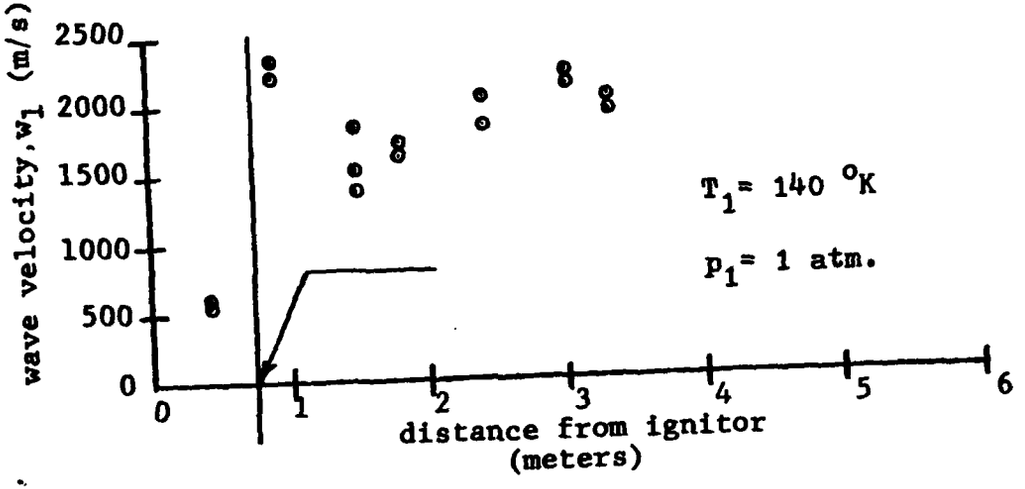

Figure 4-11

w_1 vs. distance from ignitor for $\frac{1}{2}O_2+H_2+Ar$

AD-A148 527 TRANSITION FROM DEFLAGRATION TO DETONATION AND EFFECT OF HEAT AND MASS AD..(U) OHIO STATE UNIV RESEARCH FOUNDATION COLUMBUS R EDSE ET AL. JUN 83 2/2

UNCLASSIFIED AFOSR-TR-84-1103 AFOSR-78-3604 F/G 21/2 NL

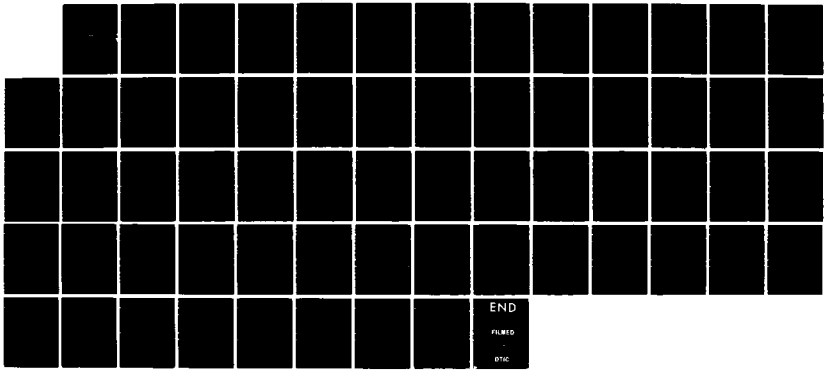

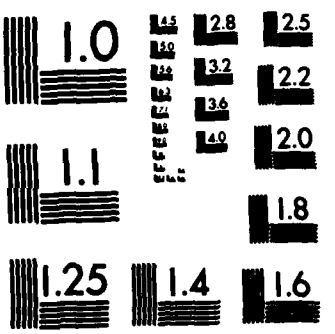

REFERENCES

1 Fourth (International) Symposium on Detonation, ACR-126, Office of Naval Research-Department of the Navy, Washington, D. C., October 1965.

2 Fifth (International) Symposium on Detonation, ACR-184, Office of Naval Research-Department of the Navy, Washington, D. C., August, 1970.

3 Sixth (International) Symposium on Detonation, ACR-221, Office of Naval Research-Department of the Navy, Washington, D. C., August 1976.

4 Sokolik, A. S., and Shchelkin, K. I., Detonation in Gaseous Mixtures. Variation of the Detonation Wave Velocity with Pressure, Journal of Physics and Chemistry, (USSR) Vol. 5, 1934, p. 1459.

5 Laffite, P., Compt. rend., Vol. 224, 1947, p. 1224.

6 Edse, R., and Lawrence, L. R., Jr., Detonation Induction Phenomena and Flame Propagation Rates in Low Temperature Hydrogen-Oxygen Mixtures, Combustion and Flame Journal, Vol. 13, No. 5, October 1969, pp 479 to 485.

7 Bollinger, Loren E., Fong, Michael C., Laughrey, James A., and Edse, Rudolph, Experimental and Theoretical Studies on the Formation of Detonation Waves in Variable Geometry Tubes, NASA Technical Note No. D-1983, June 1963.

8 Bollinger, Loren E., and Edse, Rudolph, Detonation Induction Distances in Combustible Gaseous Mixtures at Atmospheric and Elevated Initial Pressures: I Methane-Oxygen, II Carbon Monoxide-Oxygen, III Hydrogen-Oxygen., WADC Technical Report 58-591, March 1959.

9 Zeldovich, Ia. B., and Kompaneets, A. S., Theory of Detonation, Academic Press, New York, New York and London, 1960.

10 Rybanin, S. S., Theory of Detonation in Rough Tubes, Combustion, Explosion and Shock Waves, Vol. 5, No. 3, 1969, pp. 395-403.

11 Oppenheim, A. K., Stern, R. A., and Urtiew, P. A., On the Development of Detonation with Pre-Ignition, Combustion and Flame Journal, Vol. 4, No. 4, December 1960, pp. 335-341.

12 Schmidt, E., Steinicke, H., and Neubert, U., Flame and Schlieren Photographs of Combustion Waves in Tubes, Fourth Symposium (International) on Combustion, Williams and Wilkins, Baltimore, 1953, pp. 658-666.

13 Meyer, J. W., Urtiew, P. A., and Oppenheim, A. K., On the Inadequacy of Gasdynamic Processes for Triggering the Transition to Detonation, Combustion and Flame Journal, Vol. 14, February to June 1970, pp. 13-20.

14 Strehlow, R. A., Crooker, A. J., and Cusey, R. E., Detonation Initiation Behind an Accelerating Shock Wave, Combustion and Flame Journal, Vol. 11, No. 4, August 1967, pp. 339-351.

15 Atkinson, B., Bull, D. C., and Shuff, P. J., Initiation of Spherical Detonation in Hydrogen/Air, Combustion and Flame Journal, Vol. 39, No. 3, November 1980, pp. 287-300.

16 Urtiew, P. A., Laderman, A. J., and Oppenheim, A. K., Dynamics of the Generation of Pressure Waves by Accelerating Flames, Tenth Symposium (International) on Combustion, The Combustion Institute 1965, pp. 797-804.

17 Edse, Rudolph, and Strauss, William A., Stability and Burning Velocities of Laminar Carbon Monoxide-Air Flames at Pressures up to 93 Atmospheres, Journal of Chemical Physics, Vol. 25, No. 6, December 1956, pp. 1241-1245.

18 Edse, Rudolph, Studies on Bunsen Burner Flames at High Pressures with Hydrogen-Oxygen Mixtures, Proceedings of the Second Midwestern Conference on Fluid Mechanics, The Ohio State University, 1952, pp. 441-457.

19 Strauss, W. A., and Edse, R., Burning Velocity

Measurements by the Constant-Pressure Bomb Method, Seventh Symposium (International) on Combustion, At London and Oxford, August 28 to September 3, 1958, Butterworths Scientific Publications, London 1958, pp. 377-385.

20 Bollinger, Loren E., Strauss, William A., and Edse, Rudolph, Burning Velocities of Bunsen Burner Flames by the Flame Pressure Method, Industrial and Engineering Chemistry, Vol. 49, April 1957, pp. 768-773.

21 Lewis, Bernard, and von Elbe, Guenther, Combustion, Flames and Explosions of Gases, Second Edition, Academic Press, New York, New York and London, 1961.

22 Berets, D. J., Greene, E. F. and Kistiakowsky, G. B., Journal of the American Chemical Society, Vol. 72, 1950, p. 1080.

23 Dunn, R. and Wolfson, B. T., WADC Technical Note No. 54-13, 1956.

24 Eisen, C. L., Gross, R. A., and Rivlin, T. J., Theoretical Calculations in Gaseous Detonation, Combustion and Flame Journal, Vol. 4, No.2, June 1960, pp. 137-147.

25 Bollinger, Loren E., and Edse, Rudolph, Thermodynamic Calculations of Hydrogen-Oxygen Detonation Parameters for Various Initial Pressures, ARS Journal, February 1961, pp. 251-256.

26 Bollinger, Loren E., Laughrey, James A., and Edse, Rudolph, Experimental Detonation Velocities and Induction Distances in Hydrogen-Nitrous Oxide Mixtures, ARS Journal, January 1962, pp. 81-82.

27 Bollinger, Loren E., and Edse, Rudolph, Measurements of Detonation Induction Distances in Hydrogen-Oxygen and Acetylene-Oxygen-Nitrogen Mixtures at Normal and Elevated Initial Pressures and Temperatures, WADC Technical Report 57-414, June 1957.

28 Bollinger, Loren E., Fong, Michael C., and Edse, Rudolph, Experimental and Theoretical Analysis of Detonation Induction Distances, ARS Journal, May 1961.

29 Edse, R., and Costello, T.D., Ignition, Combustion, Detonation and Heat Addition to Established Flows, AFOSR Technical Report No. TR 81-0788, August 1981.

30 Edse, Rudolph, Ignition, Combustion, Detonation and Quenching of Reactive Mixtures, AFOSR Technical Report No. TR 80-0302, November 1979.

31 Jones, J. D., Flame speed measurements obtained during current experimentation in the Department of Aero/Astro Engineering, The Ohio State University, Columbus, Ohio 1982.

APPENDIX
Derivation Of Relative Energy Transfer

The relative energy transfer is equal to the difference between the stagnation enthalpy in the unburnt, unshocked gas mixture and the stagnation enthalpy of the gases at the tail of the stable detonation wave. This difference is expressed as,

$$\Delta h^{\circ} = h_f^{T_3} + u_3^2/2 - h_f^{T_1} \qquad \text{(A-1)}$$

The energy equation written relative to the wave speeds is,

$$h_f^{T_3} + w_3^2/2 = h_f^{T_1} + w_1^2/2 \qquad \text{(A-2)}$$

therefore,

$$h_f^{T_3} - h_f^{T_1} = (w_1^2 - w_3^2)/2 \qquad \text{(A-3)}$$

Substitution into equation (A-1) produces,

$$\Delta h^{\circ} = (w_1^2 - w_3^2)/2 + (w_1 - w_3)^2/2 \qquad \text{(A-4)}$$

and from the continuity equation,

$$w_3 = w_1 (v_3/v_1) \qquad \text{(A-5)}$$

so equation (A-4) becomes,

$$\Delta h^{\circ} = w_1^2 (1 - v_3/v_1) \qquad \text{(A-6)}$$

The Hugoniot equation is finally employed to express w_1 in terms of the pressure and specific volume ratio so that equation (A-6) becomes,

$$\Delta h^{\circ} = \left(R_1 T_1 (p_3/p_1 - 1)/(1 - v_3/v_1)\right) \cdot (1 - v_3/v_1) \qquad \text{(A-7)}$$

which reduces to,

$$\frac{\Delta h^{o}}{R_1 T_1} = \left(\frac{P_3}{P_1} - 1 \right) \qquad \text{(A-8)}$$

PART II

EFFECT OF HEAT AND MASS ADDITION ON THE PARAMETERS OF SUBSONIC DUCT FLOWS

TABLE OF CONTENTS

LIST OF TABLES

LIST OF FIGURES

Section

I. INTRODUCTION

II. THEORETICAL ANALYSIS

- A. General
- B. Compressor Maps
- C. Heat Addition Only
- D. Mass Addition
  - 1. General
  - 2. Solution of Problem
  - 3. Program Analysis
  - 4. Results

III. CONCLUSIONS AND RECOMMENDATIONS

LIST OF TABLES

Table		Page
1	Compressor Map Notation	3
2	Thermodynamic Values Of Air	52
3	Absolute Formation Enthalpies For Eleven Species At 0°K	53

LIST OF FIGURES

Figure		Page
1	Typical Compressor Map	5
2	Compressor Map Variation	6
3	Unheated Flow	8
4	Flow After Heat Addition	8
5	P_1 vs. Heat Addition	12
6	T_1 vs. Heat Addition	13
7	U_1 vs. Heat Addition	14
8	M_1 vs. Heat Addition	15
9	$\dot{m}_{air}$ vs. Heat Addition	16
10	P_2° vs. Heat Addition	17
11	U_2 vs. Heat Addition	18
12	T_2 vs. Heat Addition	19
13	M_2 vs. Heat Addition	20
14	Fuel Addition From Side	23
15	Tangential Fuel Addition	24
16	Temp. vs. Speed - Converging	26
17	Temp. vs. Speed - Diverging	27
18	$\dot{m}_{H_2}$ vs. $P_{H_2}^\circ$	38
19	$\dot{m}_{air}$ vs. $P_{H_2}^\circ$	39
20	$P_{c,1}$ vs. $P_{H_2}^\circ$	40
21	$T_{c,1}$ vs. $P_{H_2}^\circ$	41
22	$U_{c,1}$ vs. $P_{H_2}^\circ$	42

I. INTRODUCTION

This analysis investigated the effect of heat addition (due to fuel mass addition) on the thermodynamic and gas-dynamic properties of an established one-dimensional, chemically reacting, subsonic flow. In particular the effect of the fuel mass addition on the upstream conditions of the primary flow (air in this study) was examined.

It was assumed that the flow was adiabatic relative to the environment and friction was negligible between the flow and the walls of the duct. The length of the duct from the measuring point of the upstream primary flow conditions to the point where complete combustion has occured (chemical equilibrium prevails) is assumed to be long enough to allow for secondary flow injections (fuels), and complete homogenous mixing of all gases. Most importantly, it was assumed that at some point past the combustion zone, the flow becomes choked. This last assumption allows the problem to be solved and in practice is found in turbojet operations.

Only the theor tical analysis is included in this report. Gaseous hydrogen has been used as the fuel because of its high heat release and availability. Due to the complications involved in building an experimental device which closely approximates a basic gas generator, the experimental results have yet to be completed.

II. THEORETICAL ANALYSIS

A. General

The objective of this report was to theoretically simulate the effect of fuel flow changes on the temperature, pressure, and speed of the flow of a basic gas generator which is the heart of the turbojet, turbofan and turbo-prop engine. This problem has been approached in past literature under two areas, compressor-turbine matching and acceleration, deceleration problems of turbojets. The latter being more in tune to this report. However both areas have only been lightly discussed in compressor stall material, and quantitative information on them is scarce.

Industry has concentrated little effort towards studying acceleration, deceleration stalls from fuel flow changes for they feel that the acceleration and deceleration schedules built into the fuel controls of their production engines sufficiently handle the problem. However it is felt by these authors that pressure disturbances (from an increased fuel flow) are generated much faster than these schedules can react. Therefore engine failure results despite having been thought to be free of such a failure. As will be shown, this relatively simple assumption gives a feasable, realistic explanation to unexplained engine failures experienced by some of the high performance turbojets on fighter aircraft. The problem is more prevelent today since we require engines to operate near their peak performances.

B. Compressor Maps

Examining compressor maps of an engine, one can see how fuel flow controls or schedules do decrease the chance of stalls. Figure 1 shows a typical compressor map which lends to understanding the operating limits of compressors. The pressure rise through the compressor (P3/P2) is plotted against an altitude corrected air mass flow rate (m θ2/δ2). The notation for figures 1 and 2 is given below.

Table 1. Compressor map notation

δ - P/P_S	P - altitude pressure	P_S - standard press.
θ - T/T_S	T - altitude temp.	T_S - standard temp.
m - mass flow rate		
(2)- subscript for compressor inlet		
(3)- subscript for compressor exit		
(4)- subscript for turbine inlet		
N - compressor RPM's		

Under an ideal acceleration, an increase in fuel would increase the combustion temperature which in turn would increase the work done on the turbine, increasing the compressor RPM. The schedules now built into production engines maintain a path such as path Y. Along Y the temperature ratio does not increase so drastically that stall conditions are reached.

However this is not a complete picture of the gas generator. Nothing in the compressor maps accounts for the pressure waves being sent upstream to reduce the mass flow rate of air into the combustion chamber from the compressor. These pressure disturbances, as shown in this report, disrupt the flow from the compressor. This can lead to stall in the compressor.

Thus the entire compressor may be disturbed.

The arrow in figure 1 shows how the stall or surge line decreases as altitude is increased. Most likely the pressure disturbance from a fuel flow change also decreases the pressure ratio. Therefore if path Y is again followed, it is possible that it now passes through the stall zone.

As stated earlier it is believed by these authors that the actual path the engine takes is not like Y but more like path Z in figure 2. Here the temperature ratio increases much faster than the turbine and compressor speed. When the engine is operating at a higher CPR and higher RPM, as are todays engines for maximum performance, this increases the chances of such an occurance for one would be operating in the upper right hand vicinity of figures 1 and 2 where there is less room for deviation.

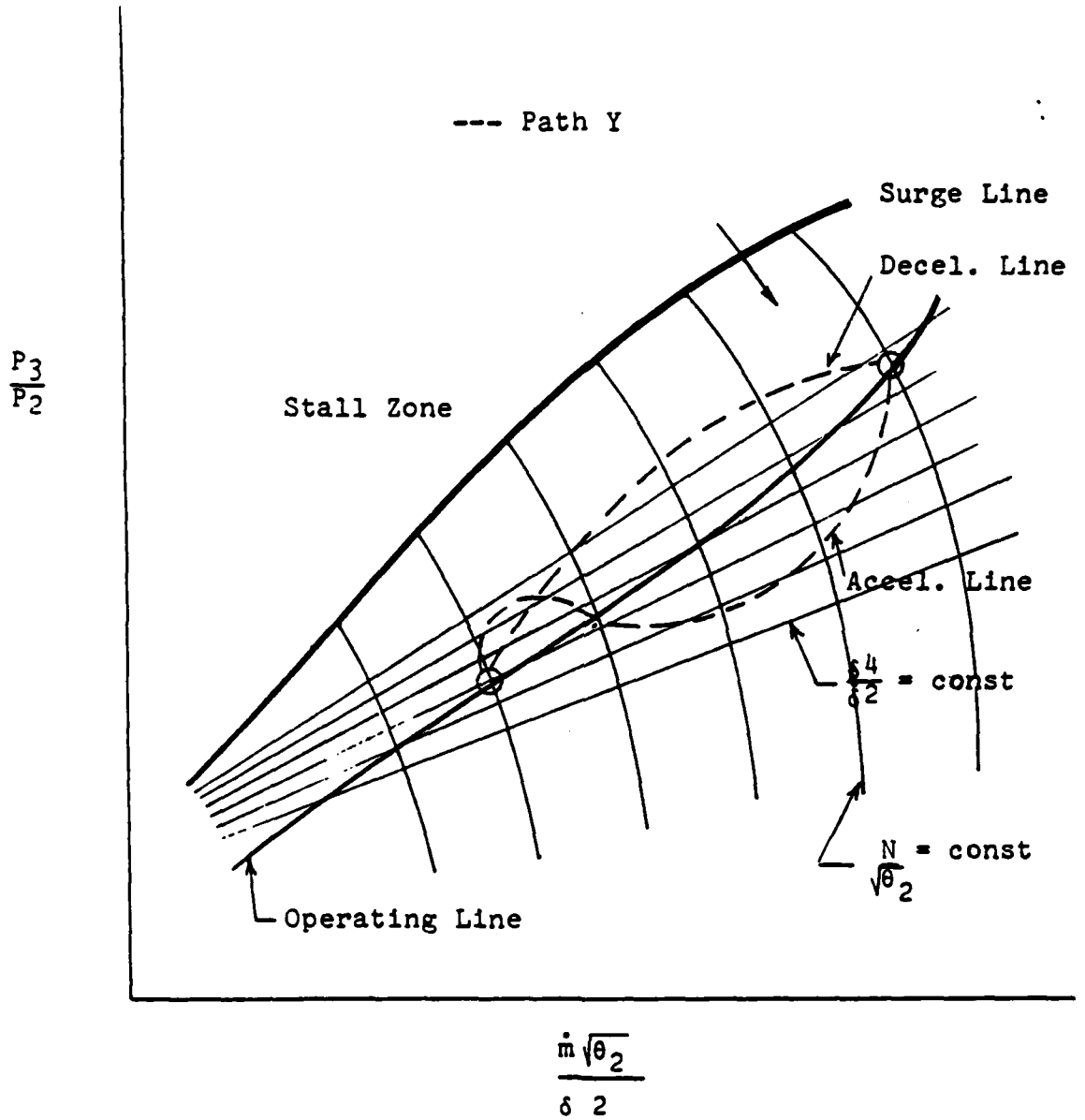

Fig. 1 - Typical compressor map

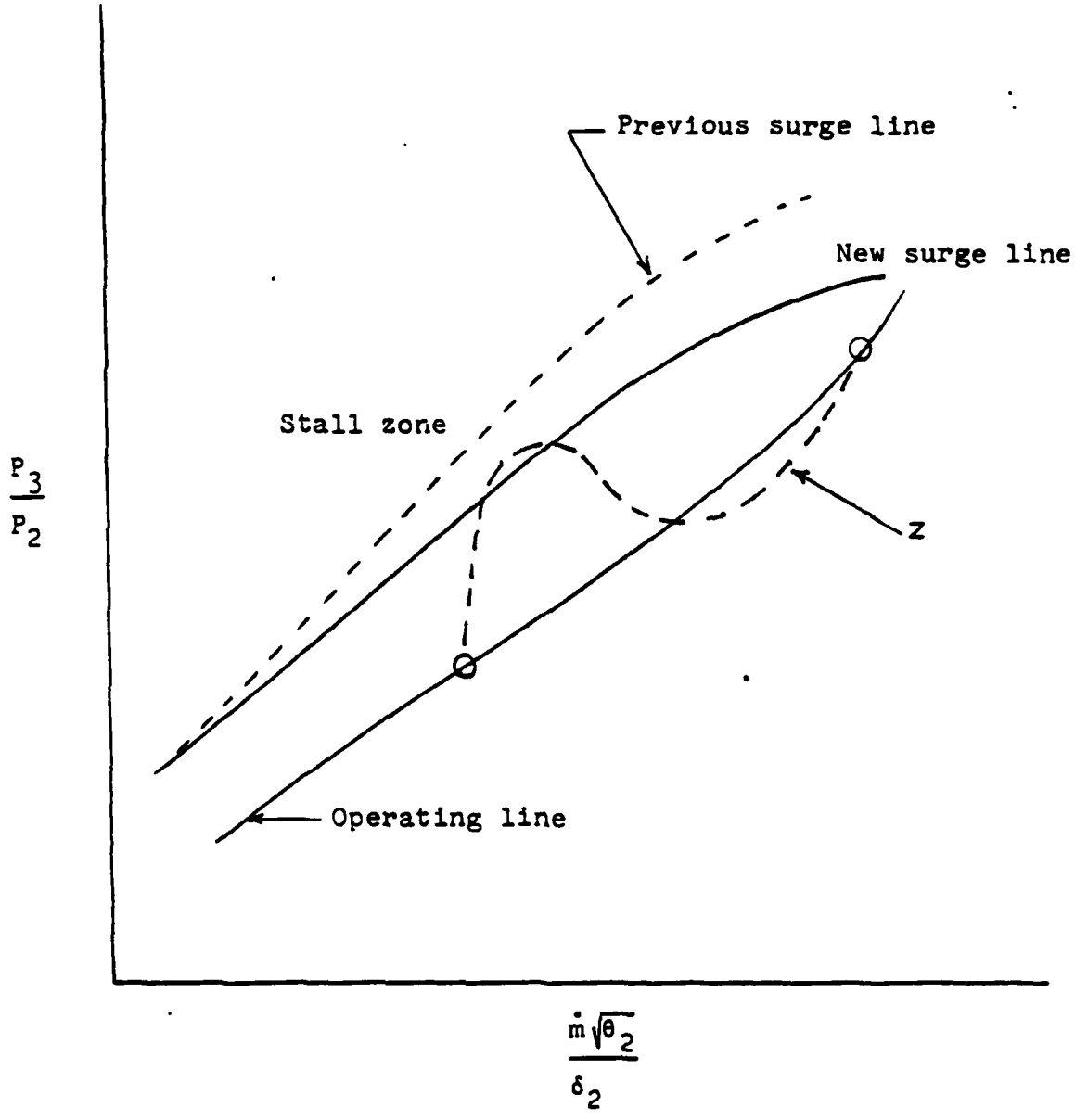

Fig. 2 - Compressor map variation

C. Heat Addition Only

Before studying flow changes due to fuel mass addition much insight into the problem is obtained by first looking at how heat addition alone causes changes to an unheated, subsonic, inviscid flow. A one-dimensional, constant area duct is used and the gas is assumed to be calorically perfect. Figures 3 and 4 illustrate the subscript notation used in this particular analysis.

At some point along the duct, heat is added to the flow producing a local change in pressure. Since the flow is subsonic, the pressure disturbance is transmitted both downstream and upstream through the duct, thus altering the initial conditions of the entire flow. In particular the pressure waves may cause the static pressure of the unheated gas to increase and bring about a reduction in the mass flow rate. This will now be shown to be true.

Two conditions are required. The first is that the static pressure downstream, that of the heated gas, remains constant, and, therefore, is that of the initial pressure ($P_2 = P_i$). The second condition is that the compression of the unheated gas as a result of heat addition, is isentropic and no energy is transferred to the initial gas because the rate of compression is moderate. This implies that $P_1^\circ = P_i^\circ$ and $T_1^\circ = T_i^\circ$. Thus the problem has only 3 unknowns, M_1, M_2, and T_2. None of the three can be solved for directly. One

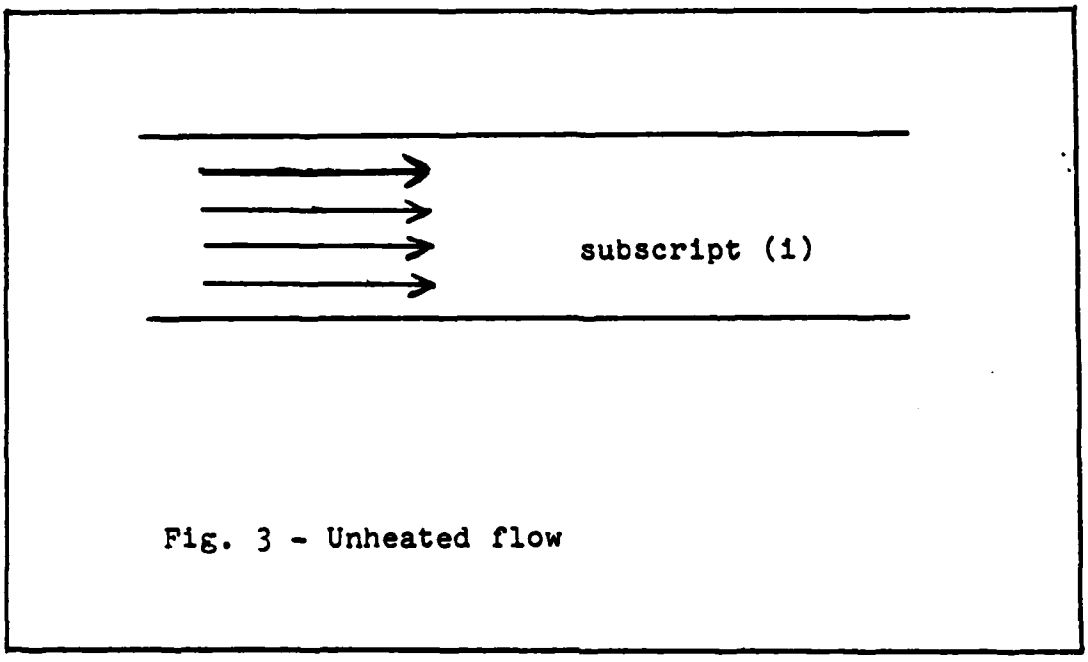

Fig. 3 - Unheated flow

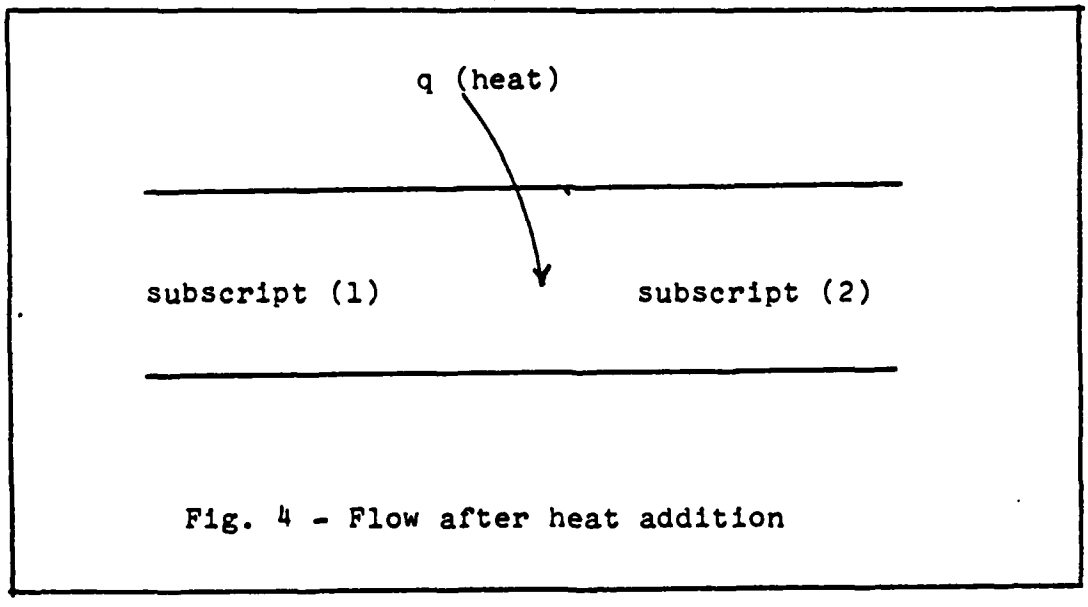

Fig. 4 - Flow after heat addition

solves the problem by applying the continuity, momentum, and energy equations.

The continuity equation written for figure 4 is

$$\rho_1 u_1 = \rho_2 u_2 \qquad \text{---(1)}$$

Letting $\rho u = \frac{pu}{RT} = \frac{\gamma pM}{\sqrt{\gamma RT}}$, and $P_2 = P_i$, equation (1) becomes

$$\frac{P_1 M_1}{\sqrt{T_1}} = \frac{P_i M_2}{\sqrt{T_2}}. \qquad \text{---(2)}$$

With no work being performed on the gas, the momentum equation can be written

$$P_1(1+\gamma M_1^2) = P_1(1+\gamma M_2^2). \qquad \text{---(3)}$$

The energy equation for this flow is

$$T_2^\circ = T_1^\circ + \frac{q}{Cp}$$

or

$$T_2^\circ = T_1\left(1+\frac{\gamma-1}{2} M_1^2 + \frac{q}{C_p T_1}\right) \qquad \text{---(4)}$$

where $T_i^\circ = T_1^\circ$ and q = Joules per Kg of air, Cp = J/Kg.K. So q/C_pT_i is a dimensionless heat release factor. The isentropic relationships give

$$P_1 = P_i\left(\frac{1+\frac{\gamma-1}{2} M_1^2}{1+\frac{\gamma-1}{2} M_1^2}\right)^{\frac{\gamma}{\gamma-1}} \qquad \text{---(5)}$$

and

$$T_1 = T_1^\circ/(1+\tfrac{\gamma-1}{2} M_1^2), \quad T_2 = T_2^\circ/(1+\tfrac{\gamma-1}{2} M_2^2) \qquad \text{-(6)}$$

Substition of equations (4),(5), and (6) into (2) gives a relationship between two unknowns M_1, M_2, and three knowns, M_i, T_1, and q. It is listed below.

$$M_1\sqrt{1+\frac{\gamma-1}{2}M_1^2}\left(\frac{1+\frac{\gamma-1}{2}M_1^2}{1+\frac{\gamma-1}{2}M_1^2}\right)^{\frac{\gamma}{\gamma-1}} = \frac{M_2\sqrt{1+\frac{\gamma-1}{2}M_2^2}}{\sqrt{1+\frac{q}{C_pT_1^\circ}}} \quad ---(7)$$

A second relationship between M_1 and M_2 is obtained by substition of equation (5) into the momentum expression, equation (3). This gives for M_2

$$M_2 = \sqrt{\frac{1}{\gamma}\left\{(1+M_1^2)\left(\frac{1+\frac{\gamma-1}{2}M_1^2}{1+\frac{\gamma-1}{2}M_1^2}\right)^{\frac{\gamma}{\gamma-1}} - 1\right\}} \quad ---(8)$$

Equations (7) and (8) now contain only two unknowns M_1 and M_2. Neither can be solved for explicity so some type of trial and error iteration must be used. Once M_1 and M_2 are found for a given heat input ($q/C_pT_i^\circ$), the static temperature of the heated gas can be found from equations (4) and (6) which can be written as

$$T_2 = T_1\left(\frac{M_2}{M_1}\right)^2\left(\frac{1+\frac{\gamma-1}{2}M_1^2}{1+\frac{\gamma-1}{2}M_1^2}\right)^{\frac{\gamma+1}{\gamma-1}}$$

Also $$P_2^\circ = P_1\left(1+\frac{\gamma-1}{2}M_2^2\right)^{\frac{\gamma}{\gamma-1}}$$

Completing the analysis, the final mass flow rate is found from the mass flow rate general expression.

$$\frac{\dot{m}}{A} = \rho u = \frac{\gamma PM}{\sqrt{\gamma RT}} = \frac{\gamma P^\circ M}{\left(1+\frac{\gamma-1}{2}M^2\right)^{\frac{\gamma+1}{2(\gamma-1)}}\sqrt{\gamma RT^\circ}}$$

With $T_1^\circ = T_i^\circ$ and $P_1^\circ = P_i^\circ$ this gives

$$\frac{\dot{m}_{final}}{\dot{m}_i} = \frac{M_1}{M_i}\left(\frac{1+\frac{\gamma-1}{2}M_i^2}{1+\frac{\gamma-1}{2}M_1^2}\right)^{\frac{\gamma+1}{2(\gamma-1)}} \qquad ---(9)$$

These expressions show that heat addition to a flow as described earlier, increases the upstream static pressure, slows down the flow, and decreases the mass flow rate. It is easy to see that if some high precision device such as a compressor were located upstream of the flow, it would react to the heat addition downstream. Figures 5-13 show the effects of heat addition ($q/C_pT_i^\circ$) to an inviscid subsonic flow passing through a constant area duct. Equations (1) - (9) were used to obtain these figures with $P_2 = P_i$ = 1 atm, $P_1^\circ = P_i^\circ$, $T_1^\circ = T_i^\circ$, and $T_i = 288^\circ K$.

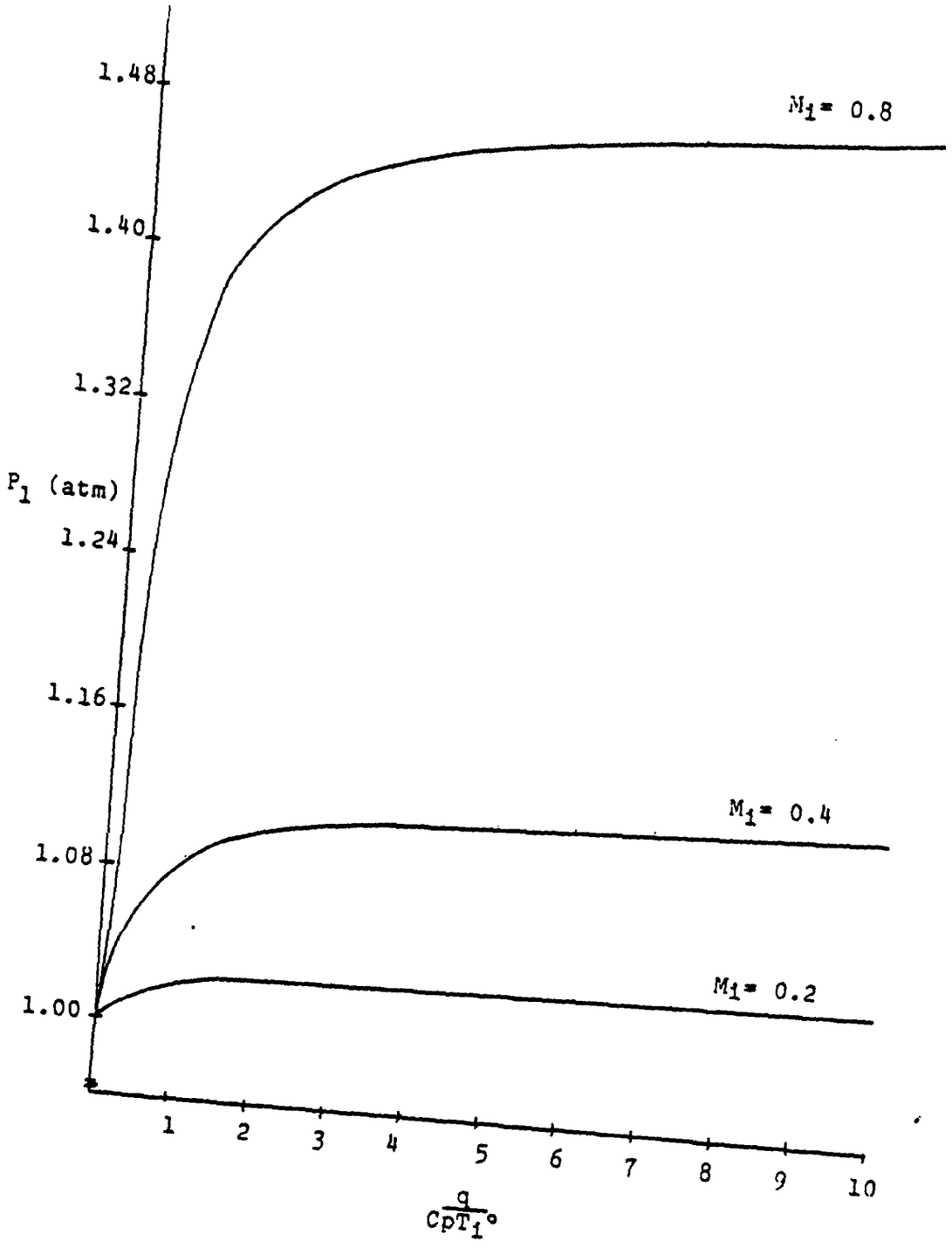

Fig. 5 - Upstream static pressure vs. heat addition

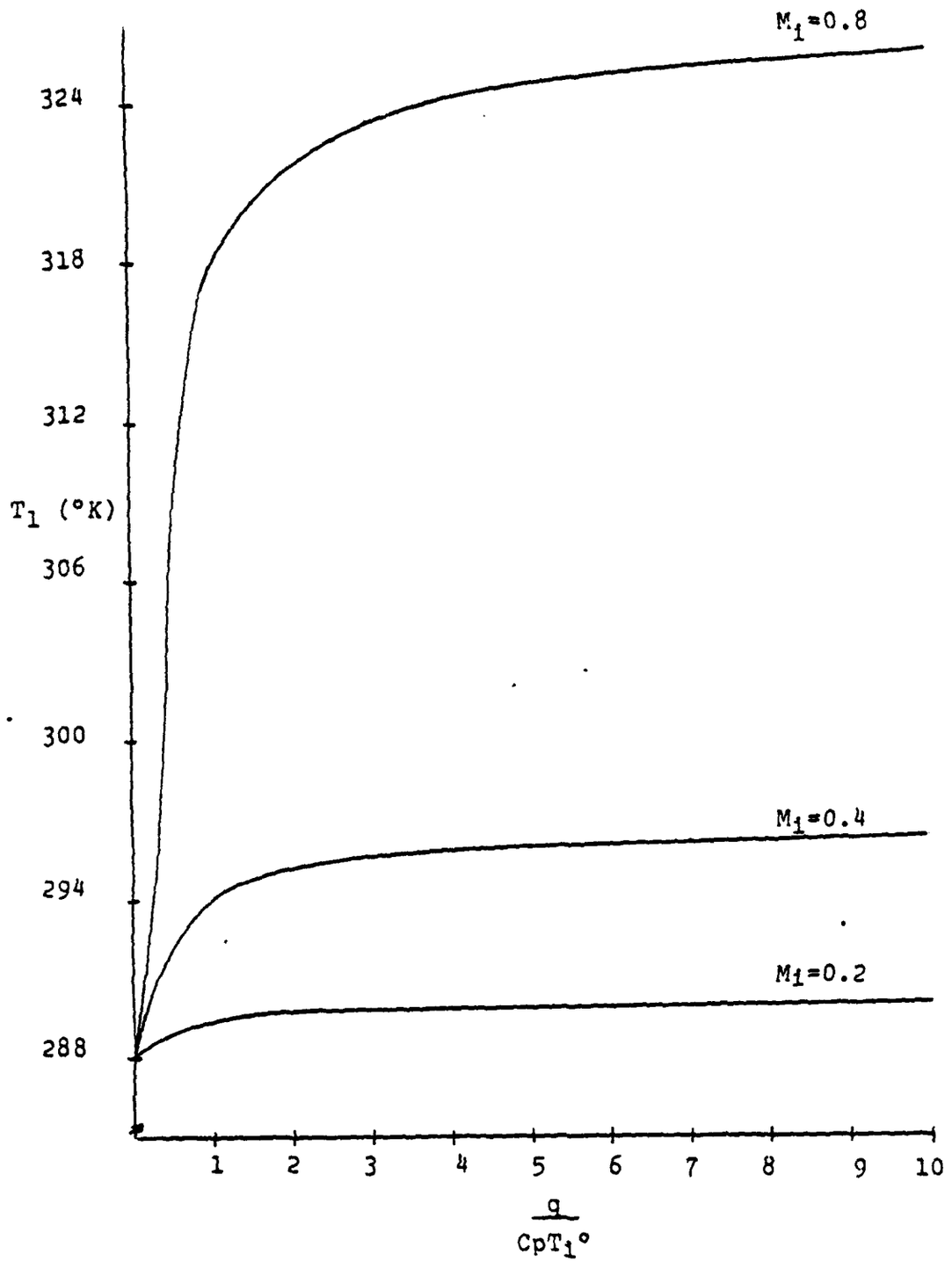

Fig. 6 - Upstream temperature vs. heat addition

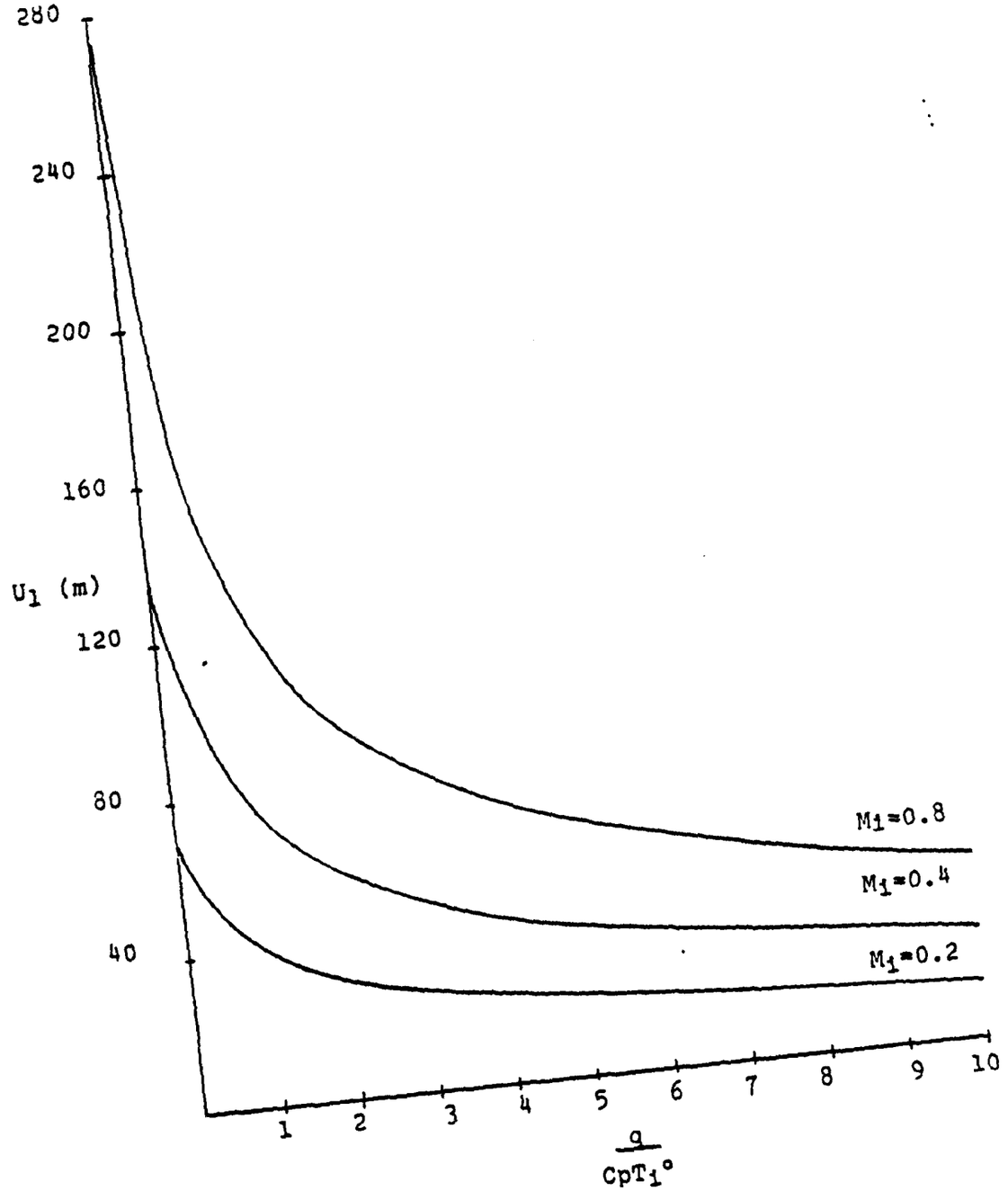

Fig. 7 - Upstream flow speed vs. heat addition

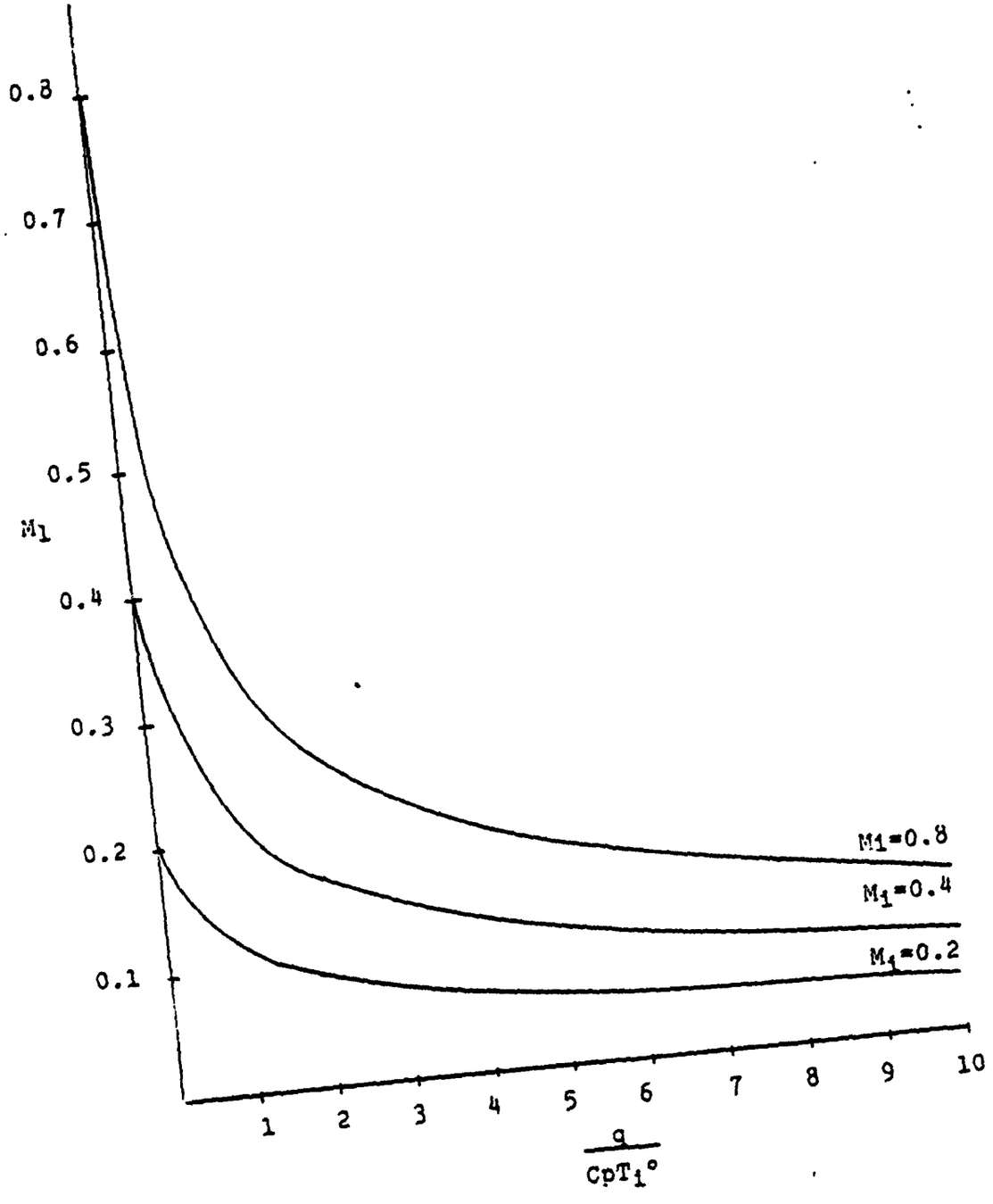

Fig. 8 - Upstream mach # vs. heat addition

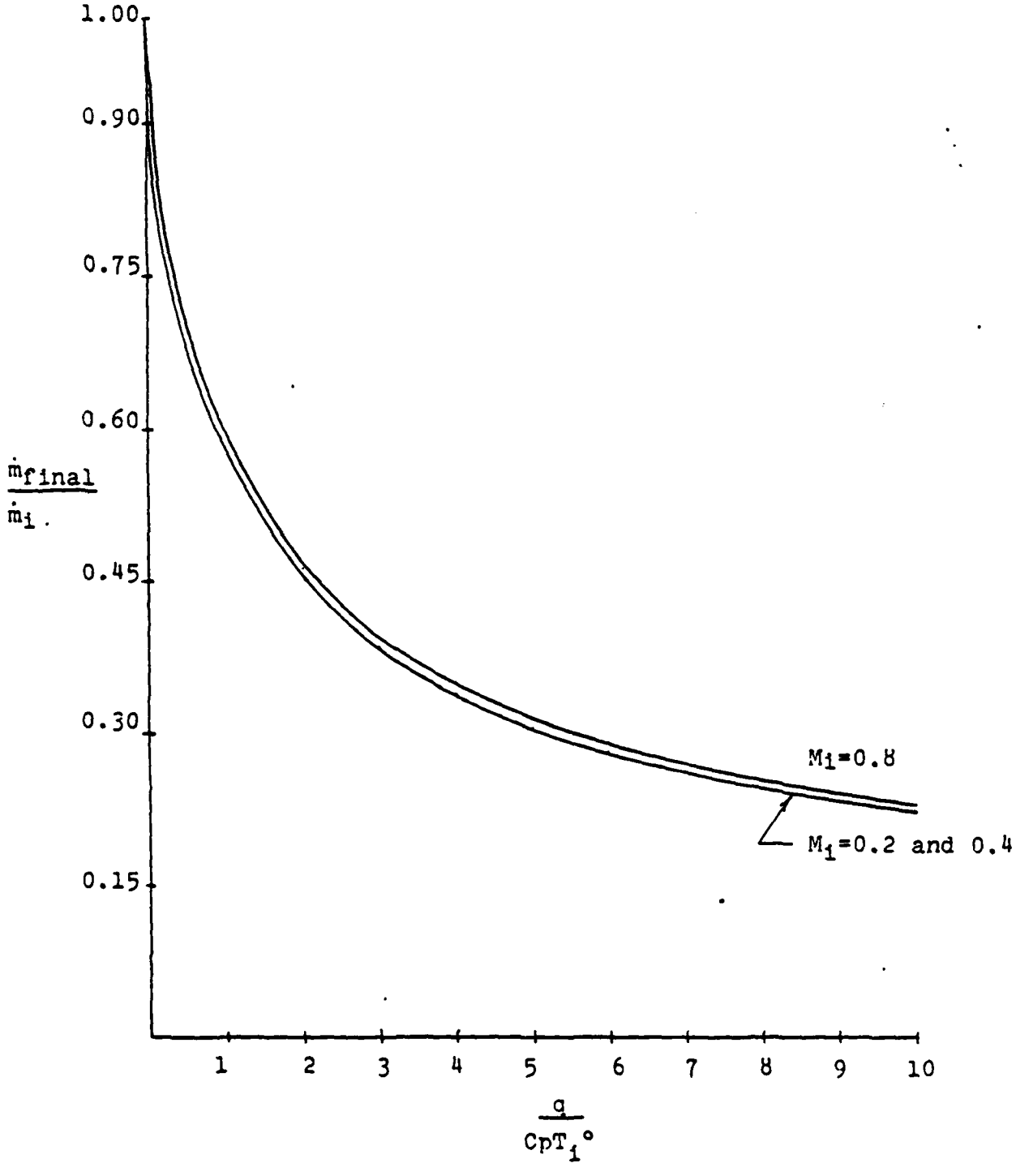

Fig. 9 - Mass flow rate vs. heat addition

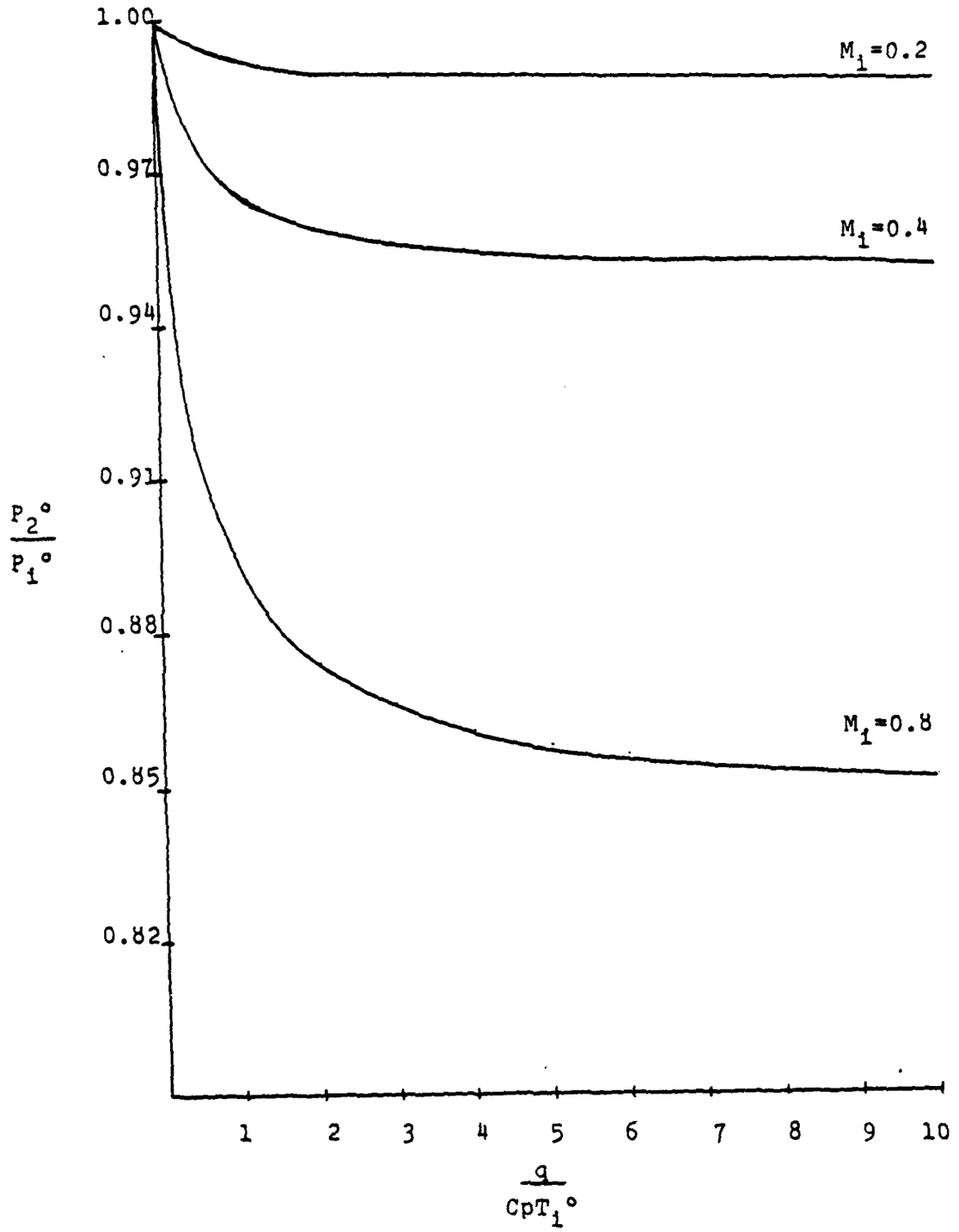

Fig. 10 - Stagnation pressure of heated gas vs. heat addition

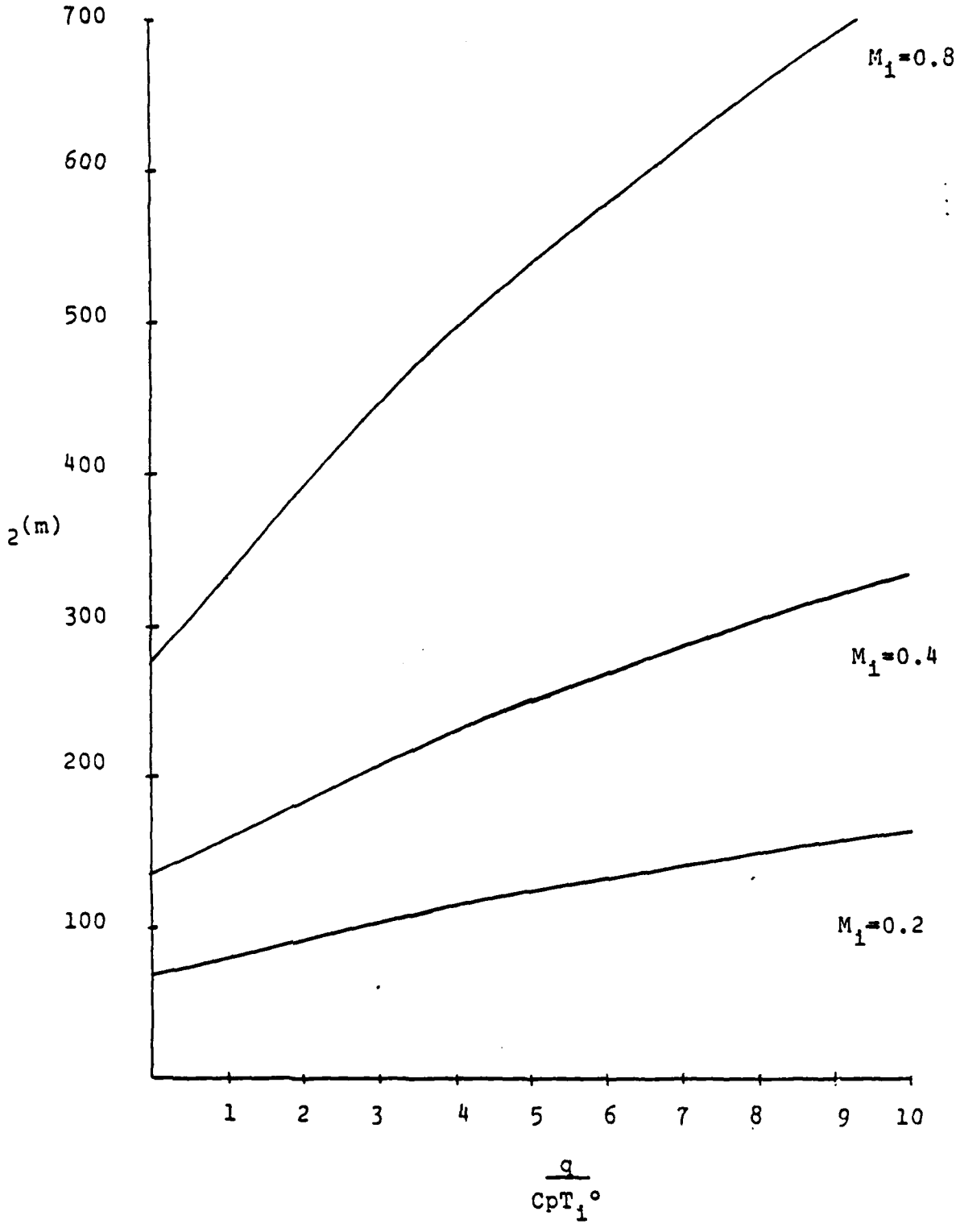

Fig. 11 - Speed of heated gas vs. heat addition

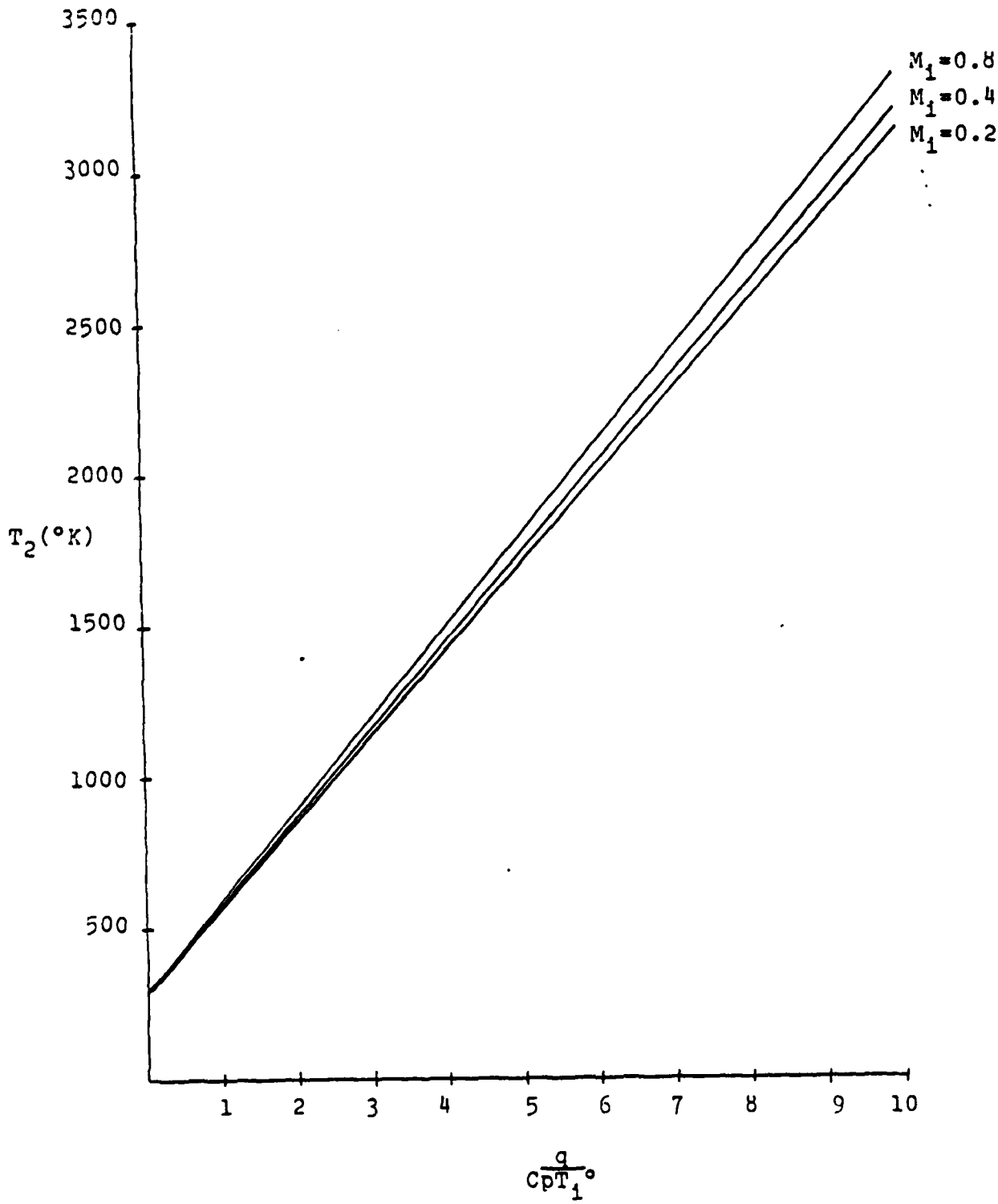

Fig. 12 - Temperature of heated gas vs. heat addition

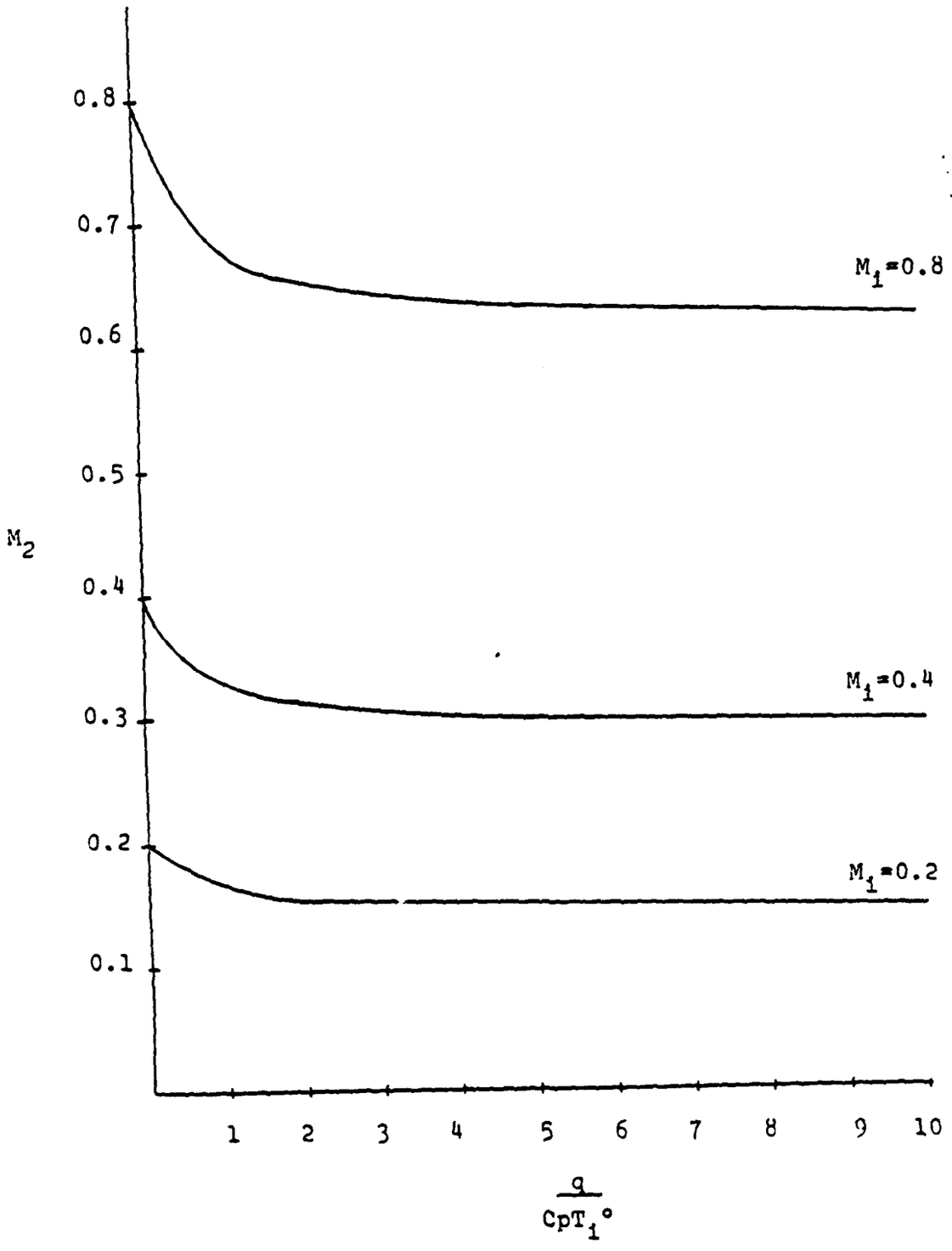

Fig. 13 - Mach # of heated gas vs. heat addition

D. Mass Addition

1. General

The effects of mass addition due to a fuel flow change will now be discussed in this section. The additional mass in the flow releases heat upon combustion. Both the increased heat and the presence of the additional mass alter the flow conditions upstream and downstream. The flow is considered to be steady, one-dimensional, inviscid, adiabatic with the environment, and it is assumed that complete homogeneous mixing has occured before combustion.

The following analyis is based on the special condition that at some point past the combustion zone the flow is choked. This is a realistic assumption for turbine nozzles are often choked over a good part of their operating range. Extending this analysis one can see that with a choked afterburner, the turbine-afterburner operation of the turbojet may be disrupted by way of fuel changes to the afterburner. Therefore had choked flow not been assumed, the problem would have to be solved with incorrect assumptions placed on the combustion gas. (This was tried and produced inaccurate results)

Many attempts were made to formulate solutions which accurately simulated fuel flow changes and their effect on the flow. Primarily, modifications to the previously completed heat addition of section C were attempted. But these

attempts either required non-realistic assumptions as mentioned before, or produced equations with too many unknowns. Always the equations of motion had to be satisfied. The difficulty of the entire problem arises because the upstream conditions change. One can not simply set up the equations of motion by adding the primary and secondary flows then solving for the combustion flow. Because the primary flow changes, an iteration process must be used. This technique is outlined in the next subsection.

2. Solution of Problem

The addition of gases to a primary flow through a duct may be accomplished in either of the three ways shown in figures 14 - 15. The secondary flows can be added from the side and may or may not increase the duct area (fig. 14) or the fuel can be added tangentially (fig. 15). the setup in fig. 15 was used for it simplified the momentum equation and in the future would make the physical apparatus easier to construct. It is realized that in combustion chambers the mixing of the fuel and combustion occurs almost simultaneously, but in this analysis the process is separated for simplicity.

Two ways can be used to get the values of the combustion chamber variables. The most rigorous one involves using equilibrium constants to calculate the mole fractions of each species in the combustion gas. However since the temperature in turbojet combustion chambers is always lower than

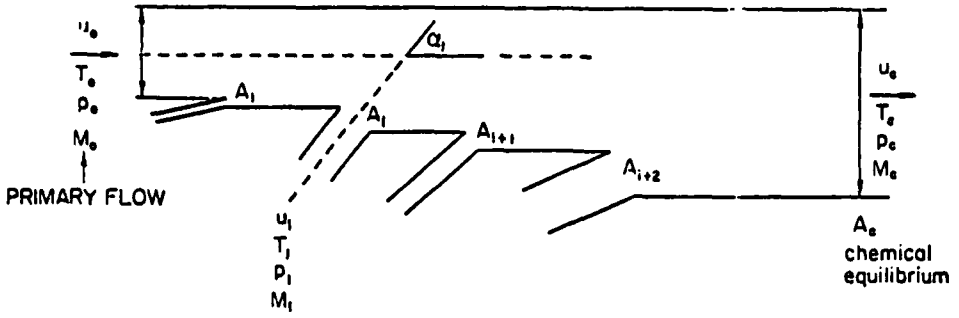

$$A_e = A_e + \sum_{i=1}^{n} A_i \cdot \cos \alpha_i$$

FOR TANGENTIAL INJECTION ALL $\alpha_i = 0$

FOR NORMAL INJECTION ALL $\alpha_i = \pi/2$

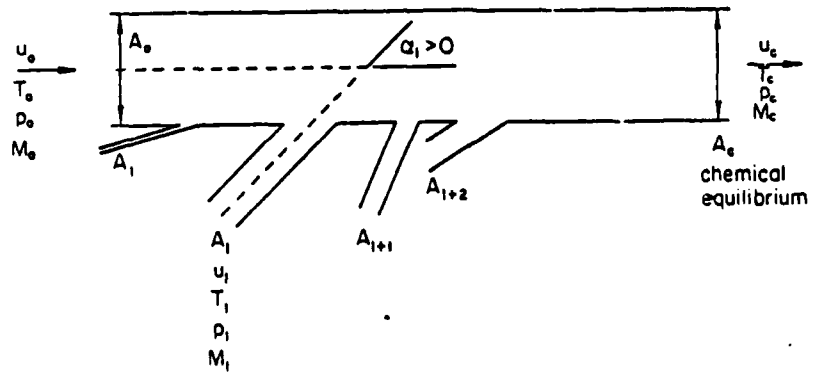

FOR NORMAL INJECTION ALL $\alpha_i = \pi/2$

Fig. 14 - Fuel addition from side

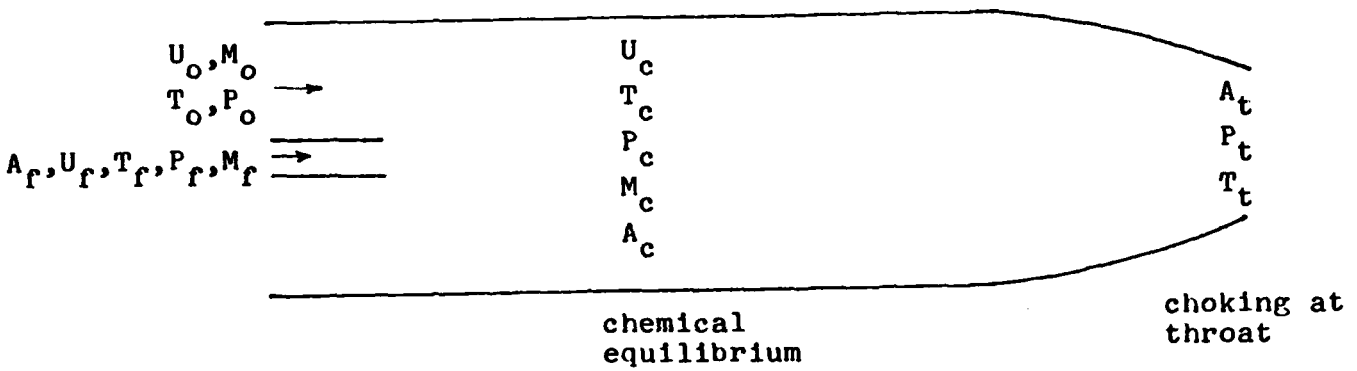

$$A_o + A_f = A_c$$

Fig. 15 - Tangential fuel addition

2000°K, dissociation is minimal and the method is tedious. (For a complete description of this method see reference 3). Instead, dissociation is disregarded and the combustion gas is assumed to consist of nitrogen, oxygen, water vapor, and carbon dioxide only.

Both methods do use the same general approach in calculating the speed and temperature of the combustion gas. This involves calculating the speed from two different equations. One is derived from the momentum and continuity equations and the other derived from the energy equation. Both require an estimated combustion temperature. The two speeds are compared for a certain temperature and a new estimate of the temperature is made based on their differences. This iteration is continued until the value of the speeds from each equation are practically the same. This also gives the correct temperature. Once the speed and temperature are known the pressure is found from the continuity equation.

It should be noted at this point that problems encountered most often when programming this problem, involved the calculation of the two speeds mentioned above. Figures 16 and 17 give qualitative pictures of how the speeds change with temperature. Referring to fig. 16, for an initial temperature estimate points A are found from each equation and plotted. A new temperature estimate will give points B. It is easy to see how they will converge to a solution. The intersection of the lines on the negative slope of the

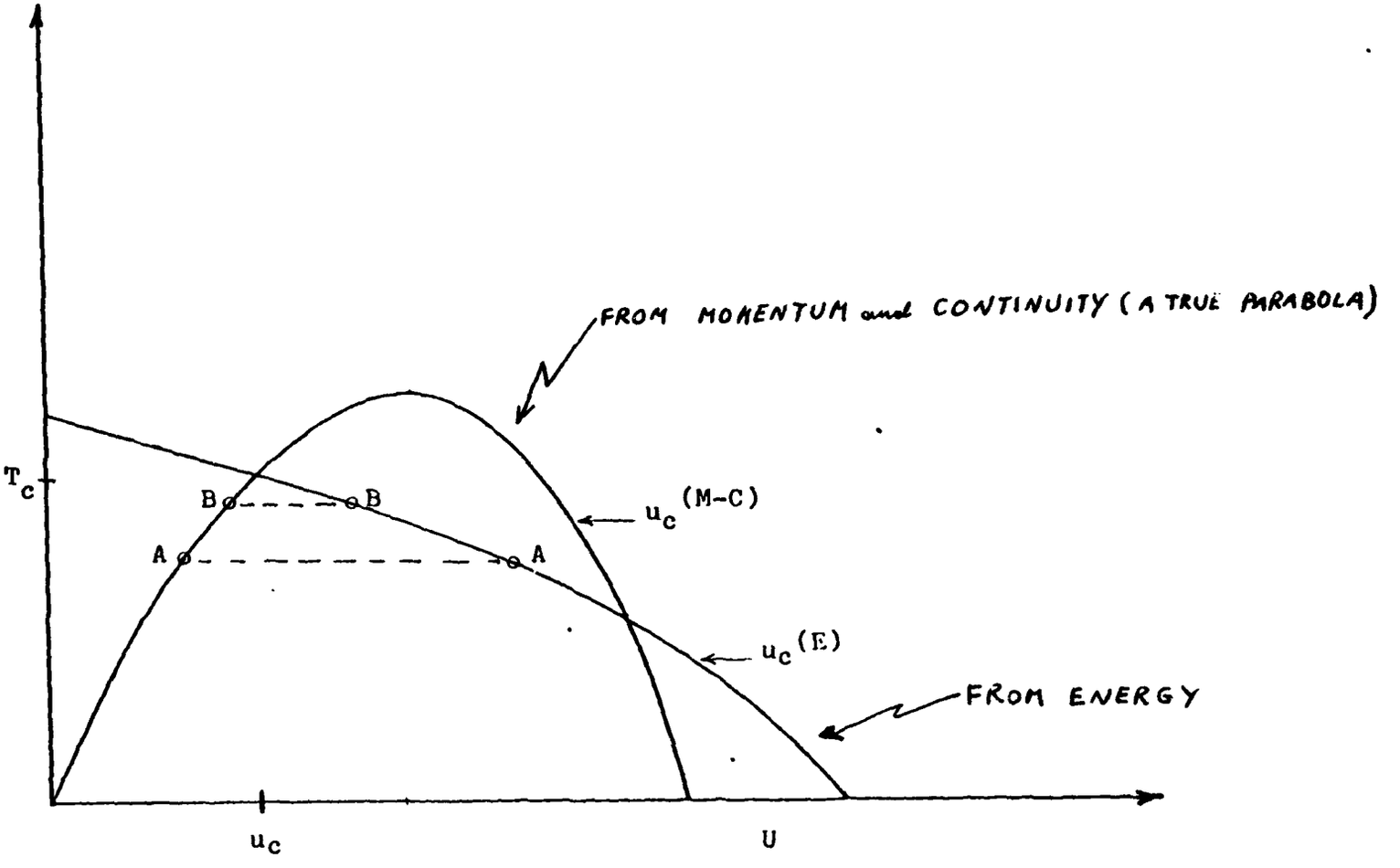

Fig. 16 - Speed vs. temperature - converging

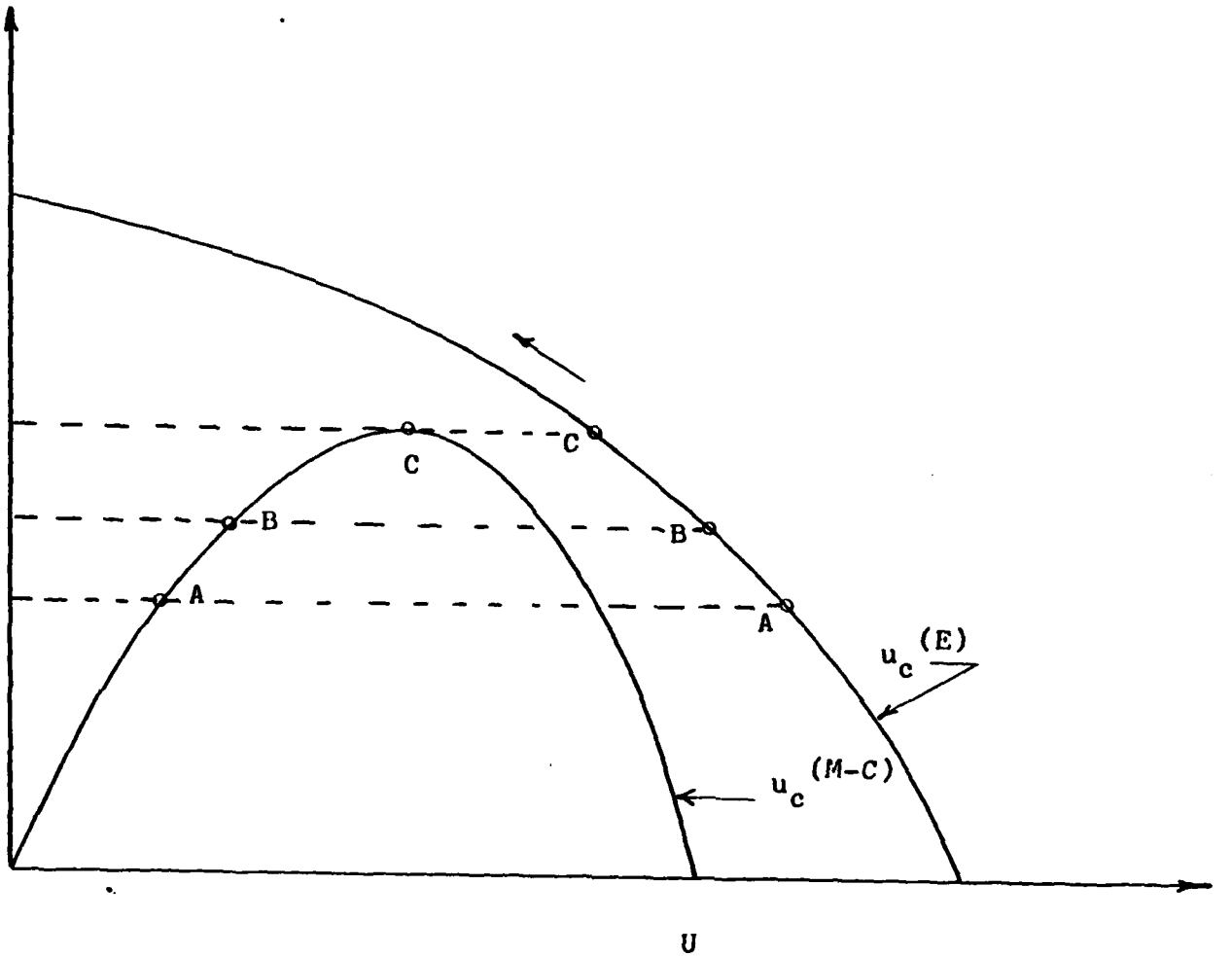

Fig. 17 - Speed vs. temperature - diverging

momentum-continuity line is a physically impossible solution (flow goes from sub to supersonic) and is not looked into in this report.

when heat addition leads to choked flow (initial gas speed is too high), there is no solution as shown in Fig.17. In this case for the lower temperature estimates the speeds are obtainable but never converge. For higher temperature estimates negative square roots are obtained when running the program. Points A,B, and C in fig. 17 show the first three temperature estimates. After a new estimate from points C, the equation for the speed derived from energy soon produces this negative root due to the temperature increasing while the maximum value allowable from energy has already been reached. A glance at the energy equation in the next subsection will illustrate this further. If this occurs then the speed of the air and/or fuel flow must be decreased to obtain a solution.

3. Program Analysis

The following detailed discussion of the program will enable the reader to fully comprehend the technique used in solving this problem. Each step will be numbered for reference. The reduced sensible enthalpies, $\left(\frac{H-E_o}{\mathcal{R}T}\right)_i^T$, formation enthalpies, $\left(\frac{h_f}{\mathcal{R}}\right)_i^T$, dimensionless specific heats, $\left(\frac{C_p}{\mathcal{R}}\right)_i^T$, and entropy coefficients, $\left(C_s\right)_i^T$ which are needed can be found in thermodynamic tables (JANNAF, AFCSR TR 3641)

for temperatures ranging from 100 to 6000 K. A linear interpolation method is used to calculate values for temperatures between those in the tables. In general the program leads to a calculated throat area. This area is compared to a specified area and the upstream Mach # is modified until the calculated area is equal to the specified area.

The program begins by establishing a steady combustion for a fixed fuel flow. The areas of the primary flow and fuel line are known. The mass flow of the air, as well as as the stagnation temperature and pressure of both the fuel and the air before they are mixed are specified. Since the injection speed of the gaseous fuel is sonic, fuel flow changes occur from changes in the fuels' stagnation pressure. Gaseous hydrogen has been chosen as the fuel.

$M_{c,1}$ is calculated before the fuel is added.

1: $M_{c,1} = \dot{m}_{air} \sqrt{\gamma R_{air} T_{c,1}}/(P_{c,1} A_{c,1} \gamma)$

The mass flow of the fuel is found.

2: $\dot{m}_f = A_f P_f^\circ / \sqrt{\frac{R_f T_f}{\gamma_f} \left(\frac{\gamma+1}{2}\right)^{\frac{\gamma+1}{\gamma-1}}}$

The next step is skipped the first run through.

3: $\dot{m}_{air} = A_{c,1} P_{c,1}^\circ \sqrt{\gamma}\, M_{c,1} / \left(\sqrt{R_{air} T_{c,1}^\circ} (1+\frac{\gamma-1}{2} M_{c,1}^2)^{\frac{\gamma+1}{2(\gamma-1)}} \right)$

The fuel-air flow mixture ratio is then

4: $f = \dot{m}_f / \dot{m}_{air}$

Next the static pressure of the fuel as well as the static temperature and pressure, and the speed of the upstream primary flow (air) are calculated.

5: $P_f = P_f^\circ \; / \; (1+\frac{\gamma-1}{2} M_f^2)^{\gamma_f/\gamma_f-1}$

6: $T_{c,1} = T_{c,1}^\circ \; / \; (1+\frac{\gamma-1}{2} M_{c,1}^2)$

7: $P_{c,1} = P_{c,1}^\circ \; (T_{c,1}/T_{c,1}^\circ)^{\gamma/\gamma-1}$

8: $U_{c,1} = M_{c,1} \sqrt{\gamma R_{air} T_{c,1}}$

The maximum speeds possible for the combustion gas are calculated. They are based on momentum-continuity and on energy and lead to the two speeds discussed earlier in subsection C.

9: $U_{c,2\ max}^{(M-C)} = (f(U_f + \frac{R_f T_f}{U_f}) + (U_{c,1} + \frac{R_{air} T_{c,1}}{U_{c,1}})) \; / \; (1+f)$

10: $U_{c,2\ max}^{(E)} = \sqrt{(2((R_f T_f (\frac{H-E_o}{\mathcal{R}T})_{fuel}^{T_f} + U_f^2)f) + A) / \; (1+f)}$

where $A = R_{air} T_{c,1} (\frac{H-E_o}{\mathcal{R}T})_{air}^{T_{c,1}} + \frac{U_{c,1}^2}{2}$

Now the moles of O_2, air and the moles of the combustion gas are found. These will lead to the value of the

formation enthalpy of the combustion gas.

11: $\nu_{O_2} = \mathfrak{M}_f / (4.76\, f \mathfrak{M}_{air})$

12: $\nu_{air} = \mathfrak{M}_f / (f \mathfrak{M}_{air})$

13: $\nu_{cg} = \nu_{air} + 1/2$

The gas constant of the combustion gas is then

14: $R_{cg} = R_{air}(1+(f\mathfrak{M}_{air}/2\mathfrak{M}_f))/(1+f)$

The formation enthalpy per unit mass of the combustion gas is given in terms of the absolute formation enthalpies per kmole. These absolute formation enthalpies for different species are listed in table 2.

15: $$\left(\frac{h_f}{RT}\right)_{cg}^{T_{c,2}} = \left(\left(\frac{H_f}{\mathcal{R}T}\right)_{H_2O}^{T_{c,2}} + \nu_{air}\left(\frac{H_f}{\mathcal{R}T}\right)_{air}^{T_{c,2}} - \frac{1}{2}\left(\frac{H_f}{\mathcal{R}T}\right)_{O_2}^{T_{c,2}}\right)/\nu_{cg}$$

Calculation of the two speeds based on the equations of motion is now possible. The temperature is iterated on until the values of the two speeds agree to a desired accuracy. A new estimate of the combustion gas temperature is obtained by using a multiplying factor times the difference in the two speeds. This factor depends on the rates at which the speeds change. For this step

a value of X = 0.03 was used.

$$16: \quad U_{c,2}^{(M-C)} = \frac{1}{2} U_{c,2\ max}^{(M-C)} - \sqrt{\left(\frac{U_{c,2\ max}^{(M-C)}}{2}\right)^2 - R_{cg}T_{c,2}}$$

$$17: \quad U_{c,2}^{(E)} = \sqrt{U_{c,2\ max}^{(E)\ 2} - 2R_{cg}T_{c,2}\left(\frac{h_f}{RT}\right)_{cg}^{T_{c,2}}}$$

$$18: \quad \text{IF ABS } (U_{c,2}^{(E)} - U_{c,2}^{(M-C)}) < 10^{-7} \quad \text{GO TO \#20}$$

$$19: \quad T_{c,2}^{est(n+1)} = T_{c,2}^{est(n)} + X(U_{c,2}^{(E)} - U_{c,2}^{(M-C)}) \quad \text{GO TO \#15}$$

The pressure of the combustion gas is then found from the continuity equation.

$$20: \quad P_{c,2} = (1+f)R_{cg}T_{c,2} \Big/ \left(U_{c,2}\left(\frac{R_{air}T_{c,1}}{P_{c,1}U_{c,1}} + f\,\frac{R_f T_f}{P_f U_f}\right)\right)$$

The conditions at the point of choking, the throat, are now found. An estimated temperature for the throat is needed to get the formation enthalpy per kmole of the gas there. Since the speed is sonic the temperature will be lower than that of the combustion zone. Therefore

$$21: \quad \left(\frac{h_f}{RT}\right)_{cg}^{T_t} = \left(\left(\frac{H_f}{RT}\right)_{H_2O}^{T_t} + \nu_{air}\left(\frac{H_f}{RT}\right)_{air}^{T_t} - \frac{1}{2}\left(\frac{H_f}{RT}\right)_{O_2}^{T_t}\right)/\nu_{cg}$$

and the specific heat is

22: $$\left(\frac{C_p}{R}\right)_{cg}^{T_t} = \left(\left(\frac{C_p}{R}\right)_{H_2O}^{T_t} + \nu_{air}\left(\frac{C_p}{R}\right)_{air}^{T_t} - \frac{1}{2}\left(\frac{C_p}{R}\right)_{O_2}^{T_t}\right)/\nu_{cg}$$

so

23: $$\gamma_{cg}^{T_t} = \left(\frac{C_p}{R}\right)_{cg}^{T_t} / \left(\left(\frac{C_p}{R}\right)_{cg}^{T_t} - 1\right)$$

24: $$\mathfrak{M}_{cg} = \mathfrak{M}_f(1+f) \,/\, \left(\frac{\mathfrak{M}_f}{\mathfrak{M}_{air}} + \frac{1}{2} f\right)$$

Since the stagnation enthalpy of the flow does not change, this value is calculated at the throat and is compared to the value from the combustion zone. A new throat temperature is estimated based on the old value and the difference in the stagnation enthalpiy values. The temperature is iterated on until the two enthalpy values are approximately the same. A multiplying factor X=0.3 was used for this iteration.

25: $$\left(\frac{h_f}{R}\right)_{cg}^{T^\circ_{c,2}\ \text{calc}} = \left(T_t\left(\frac{h_f}{RT}\right)_{cg}^{T_t} \mathfrak{M}_{cg}\right) + \frac{T_t \gamma_{cg}^{T_t}}{2\mathfrak{M}_{cg}}$$

26: $$\Delta\left(\frac{h_f}{R}\right)_{cg}^{T^\circ_{c,2}} = T_{c,2}\left(\frac{h_f}{RT}\right)_{cg}^{T_{c,2}} \mathfrak{M}_{cg} + \frac{U^4_{c,2}}{2} - \left(\frac{h_f}{R}\right)_{cg}^{T^\circ_{c,2}\ \text{calc}}$$

27: IF ABS $\left(\Delta\left(\frac{h_f}{R}\right)_{cg}^{T^\circ_{c,2}}\right) < 10^{-4}$ GO TO #29

28: $$T_t^{est(n+1)} = T_t^{est(n)} + X\left(\Delta\left(\frac{h_f}{R}\right)_{cg}^{T^\circ_{c,2}}\right)$$ GO TO #21

The entropy coefficients of the gas at the combustion zone and at the throat are then found and are used to determine the static pressure of the gas at the throat.

$$29: \quad \left(c_s\right)_{cg}^{T_{c,2}} = \left(\left(c_s\right)_{H_2O}^{T_{c,2}} + \nu_{air}\left(c_s\right)_{air}^{T_{c,2}} - \tfrac{1}{2}\left(c_s\right)_{O_2}^{T_{c,2}}\right)/\nu_{cg}$$

$$30: \quad \left(c_s\right)_{cg}^{T_t} = \left(\left(c_s\right)_{H_2O}^{T_t} + \nu_{air}\left(c_s\right)_{air}^{T_t} - \tfrac{1}{2}\left(c_s\right)_{O_2}^{T_t}\right)/\nu_{cg}$$

$$31: \quad P_t = P_{c,2} T_t \left(c_s\right)_{cg}^{T_t} \Big/ T_{c,2}\left(c_s\right)_{cg}^{T_{c,2}}$$

Now a calculated throat area is found. This is then compared to the specified area. If the two are different a new value for the Mach # of the upstream primary flow ($M_{c,1}$) is calculated and the entire program is run again iterating on $M_{c,1}$ until the two areas are the same. The multiplying factor here is X=500.

$$32: \quad A_t^{calc} = \frac{(\dot{m}_f + \dot{m}_{air})\sqrt{(R_{cg} T_t / \gamma_{cg})}}{P_t}$$

$$33: \text{ IF ABS } (A_t^{spec} - A_t^{calc}) < 10^{-10} \qquad \text{GO TO \#35}$$

$$34: \quad M_{c,1} = M_{c,1} + X(A_t^{spec} - A_t^{calc}) \qquad \text{GO TO \#3}$$

The last calculations give the stagnation pressure and temperature of the combustion gas. An estimate for the stagnation temperature is obtained assuming a perfect gas. The temperature is iterated on until the stagnation enthalpy is correct.

35: $$T^{\circ,est}_{c,2} = T_{c,2} + \frac{U^2_{c,2}}{2}\frac{\gamma-1}{\gamma R_{cg}}$$

36: $$\left(\frac{h_f}{RT}\right)^{T^\circ_{c,2}\ calc}_{cg} = \left(\left(\frac{H_f}{RT}\right)^{T^\circ_{c,2}}_{H_2O} + \nu_{air}\left(\frac{H_f}{RT}\right)^{T^\circ_{c,2}}_{air} - \frac{1}{2}\left(\frac{H_f}{RT}\right)^{T^\circ_{c,2}}_{O_2}\right)/\nu_{cg}$$

37: $$\left(\frac{h_f}{R}\right)^{T^\circ_{c,2}\ calc}_{cg} = T_{c,2}\left(\frac{h_f}{RT}\right)^{T^\circ_{c,2}\ calc}_{cg} /\mathfrak{M}_{cg}$$

38: $$\Delta\left(\frac{h_f}{R}\right)^{T^\circ_{c,2}}_{cg} = \left(\frac{h_f}{R}\right)^{T^\circ_{c,2}}_{cg} - \left(\frac{h_f}{R}\right)^{T^\circ_{c,2}\ calc}_{cg}$$

The first value on the right side of eq. 38 is obtained from line 25.

39: IF ABS $\left(\Delta\left(\frac{h_f}{R}\right)^{T^\circ_{c,2}}_{cg}\right) < 10^{-7}$ GO TO #41

40: $T^\circ_{c,2} = T^\circ_{c,2} + X\left(\Delta\left(\frac{h_f}{R}\right)^{T_{c,2}}_{cg}\right)$ GO TO #36

Finally

41: $$\left(C_s\right)_{cg}^{T_{c,2}^{\circ}} = \left(\left(C_s\right)_{H_2O}^{T_{c,2}^{\circ}} + \nu_{air}\left(C_s\right)_{air}^{T_{c,2}^{\circ}} - \frac{1}{2}\left(C_s\right)_{O_2}^{T_{c,2}^{\circ}}\right)/\nu_{cg}$$

42: $$P_{c,2}^{\circ} = P_{c,2}(T_{c,2}^{\circ})\left(C_s\right)_{cg}^{T_{c,2}^{\circ}} / (T_{c,2}^{\circ})\left(C_s\right)_{cg}^{T_{c,2}^{\circ}}$$

43: PRINT VALUES

44: STOP

Figures 18-31 show the results of a program run using the equations listed on the previous pages. The fuel used was gaseous hydrogen.

4. Results

Figures 18-31 illustrate the effect of a fuel flow change on the upstream properties of a subsonic flow. It is evident that the upstream conditions change due to the downstream addition of heat and mass. Even though the upstream pressure rise was small, the speed decreased by 20% and the mass flow by 20%.

Presently an experimental device is being constructed to test these results.

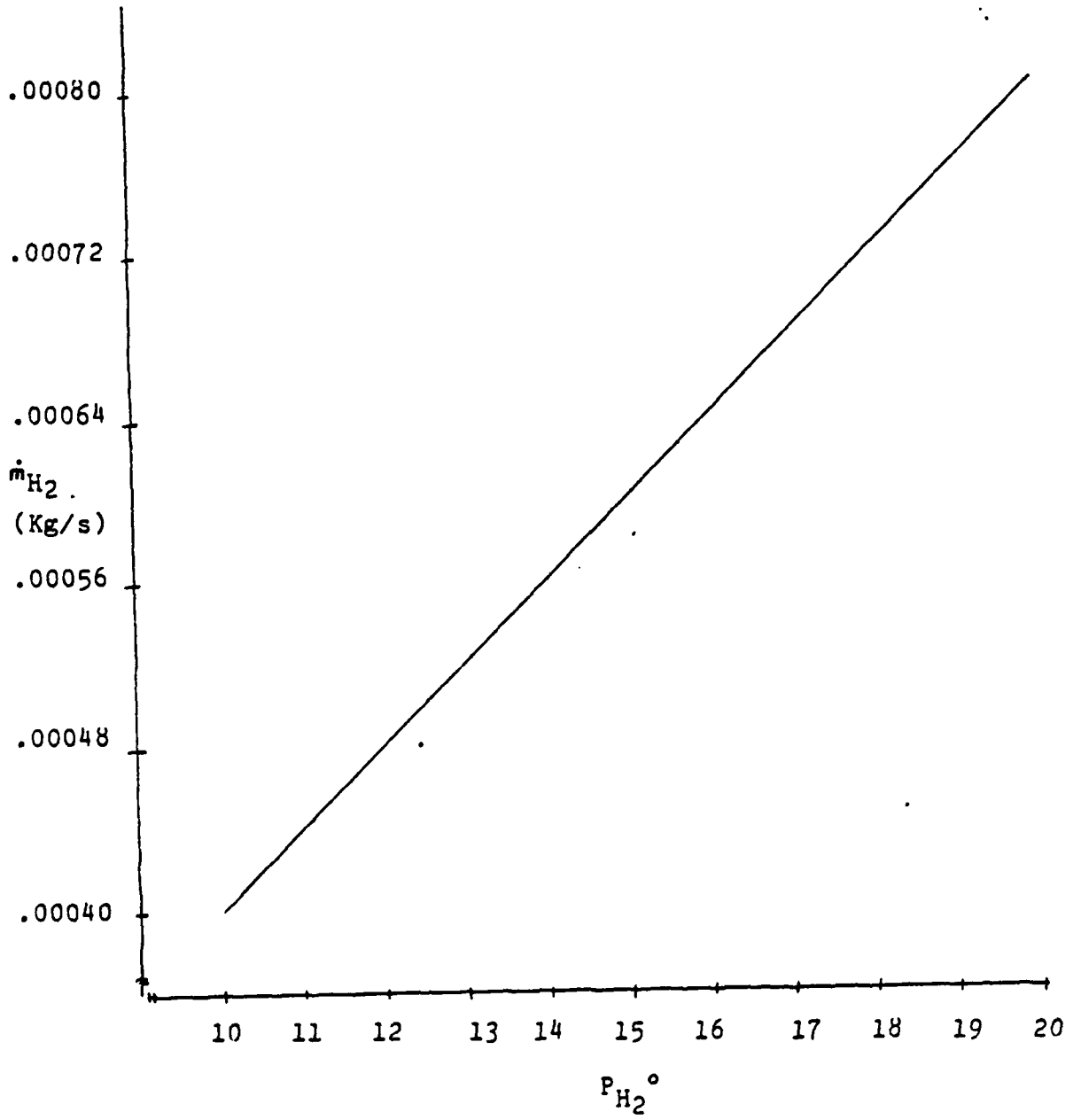

Fig. 18 - Fuel mass flow ($\dot{m}_{H_2}$) vs. $P_{H_2}°$

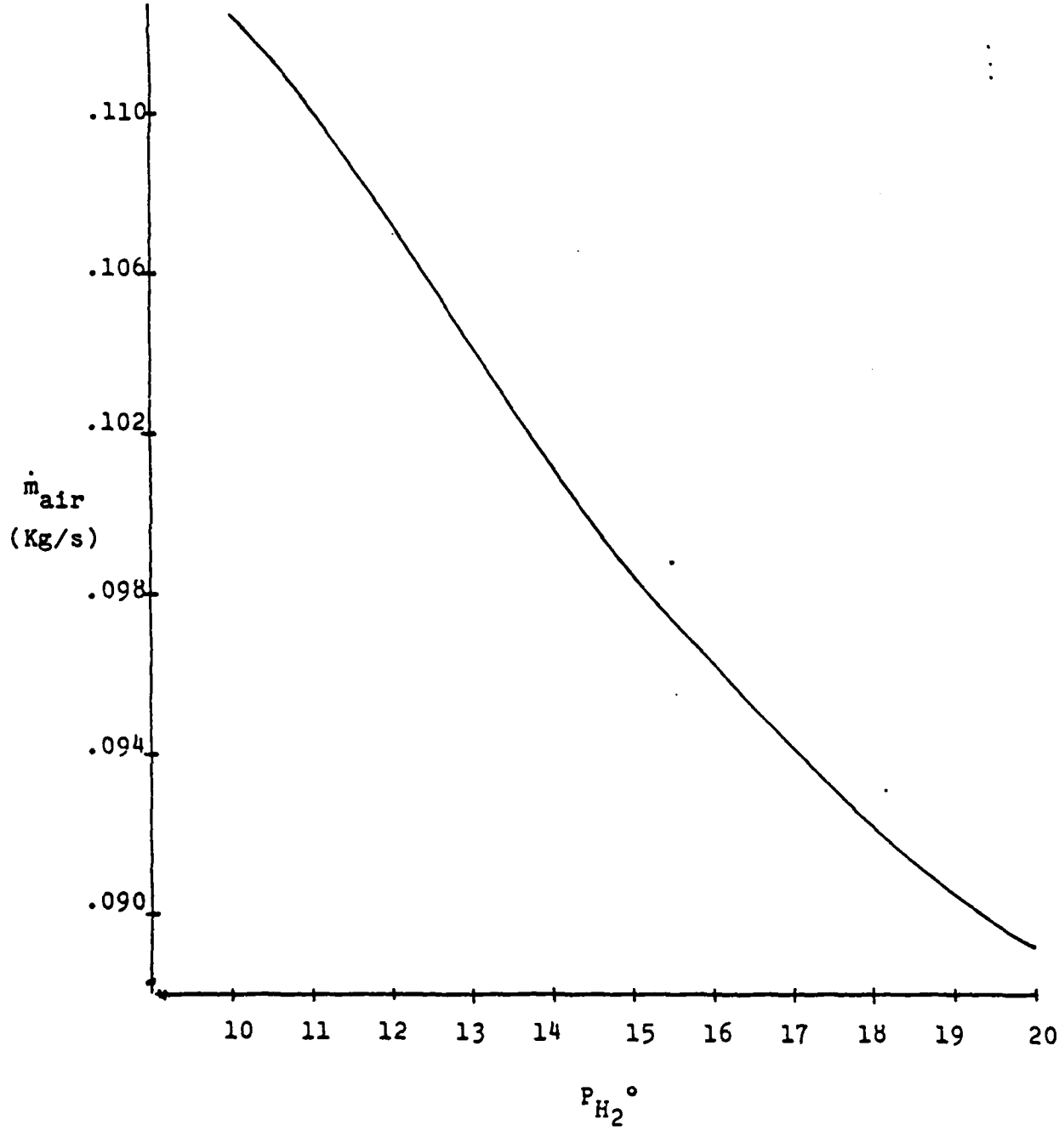

Fig. 19 - Primary mass flow ($\dot{m}_{air}$) vs. $P_{H_2}°$

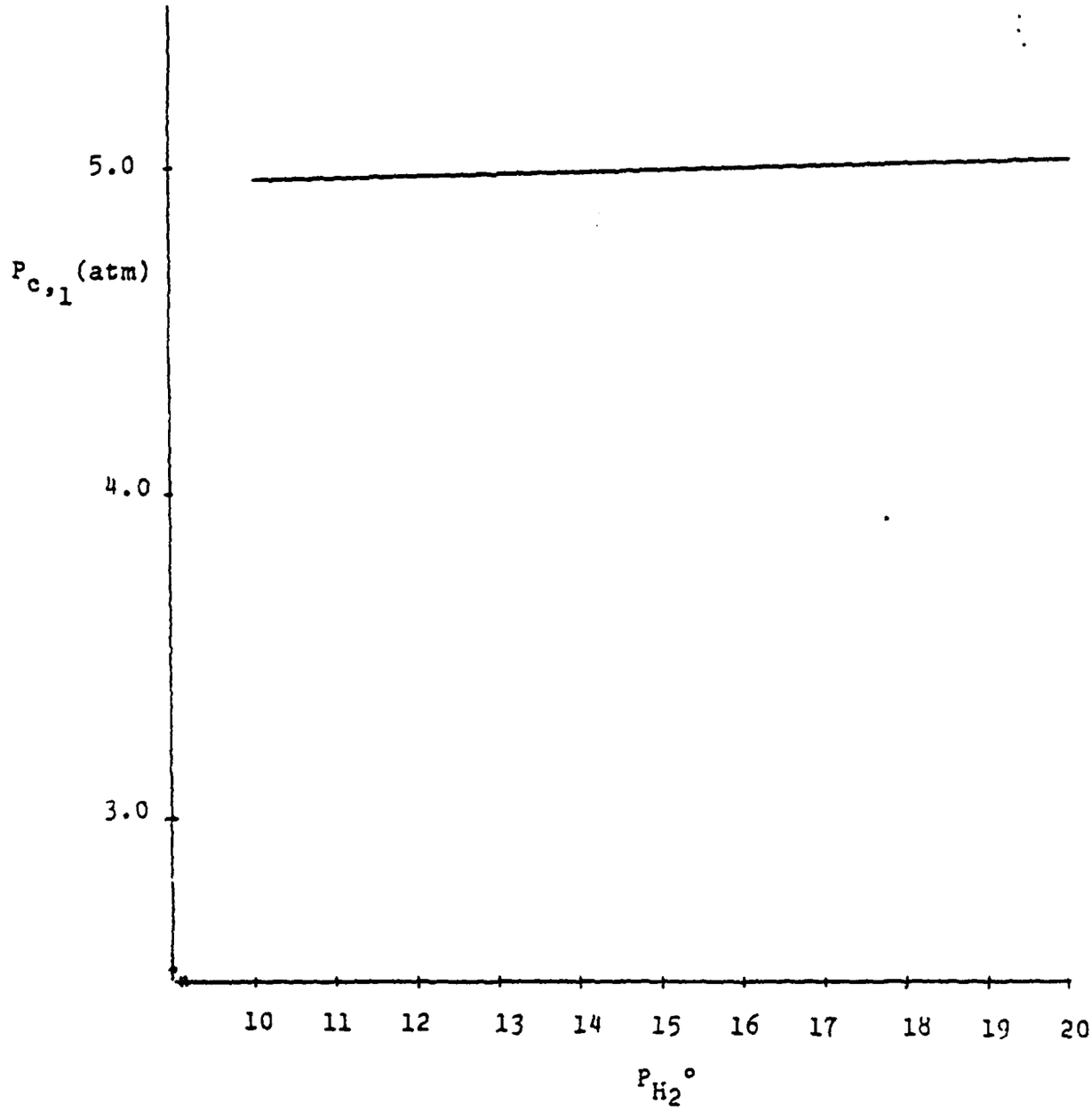

Fig. 20 - Upstream static pressure($P_{c,1}$) vs. $P_{H_2}°$

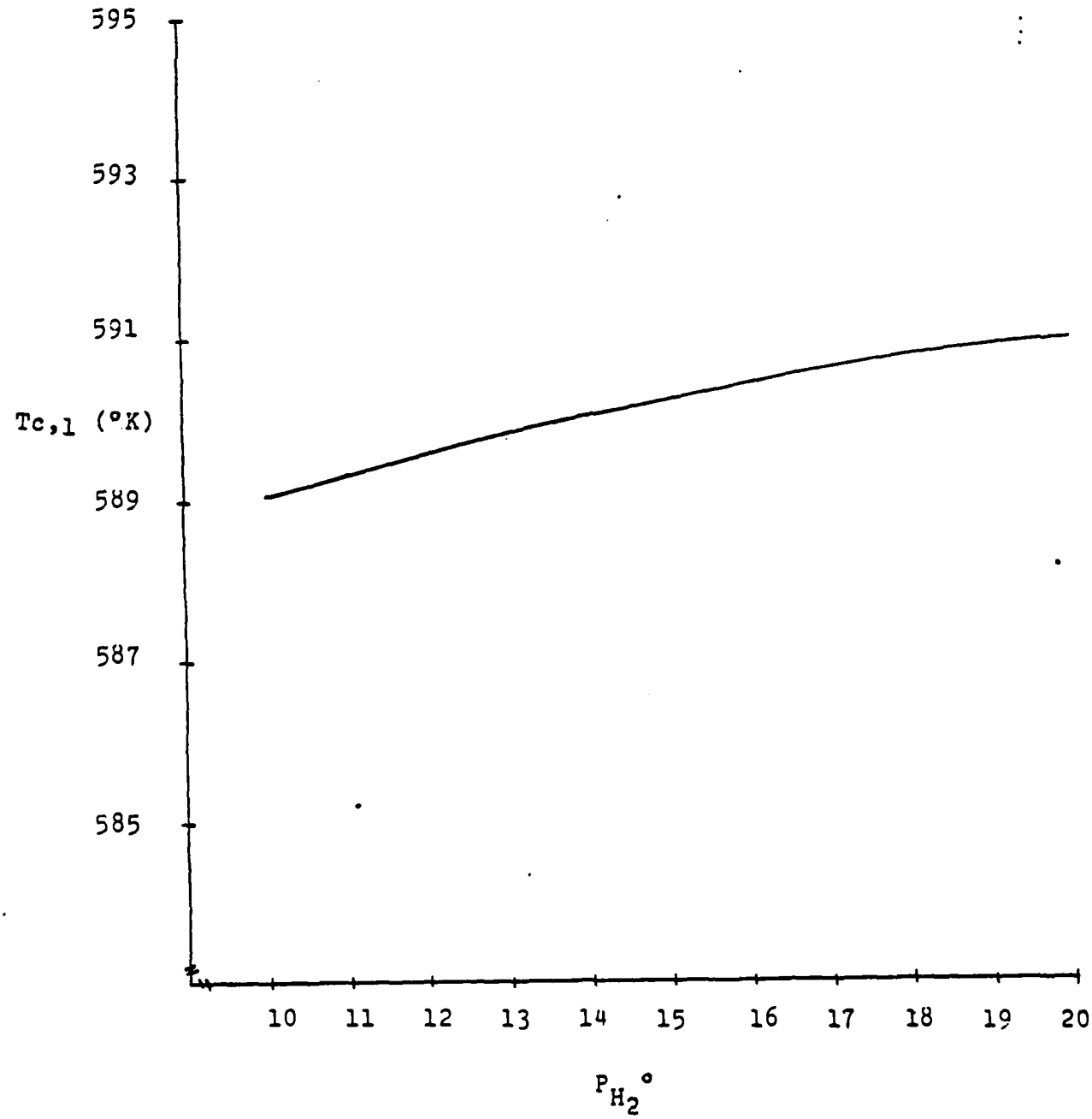

Fig. 21 - Upstream static temperature $T_{c,1}$ vs. $P_{H_2}°$

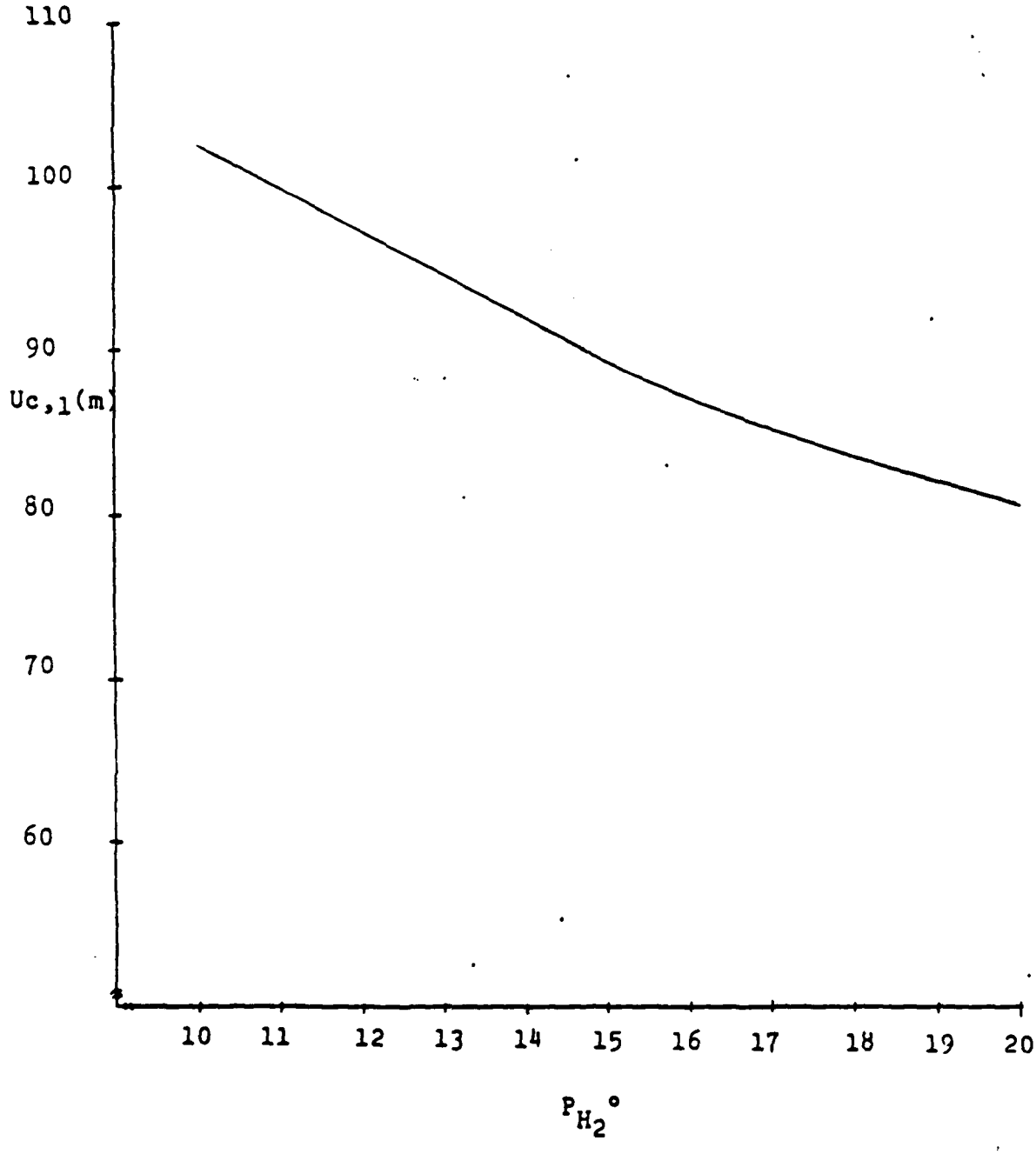

Fig. 22 - Upstream flow speed $Uc,_1$ vs. $P_{H_2}°$

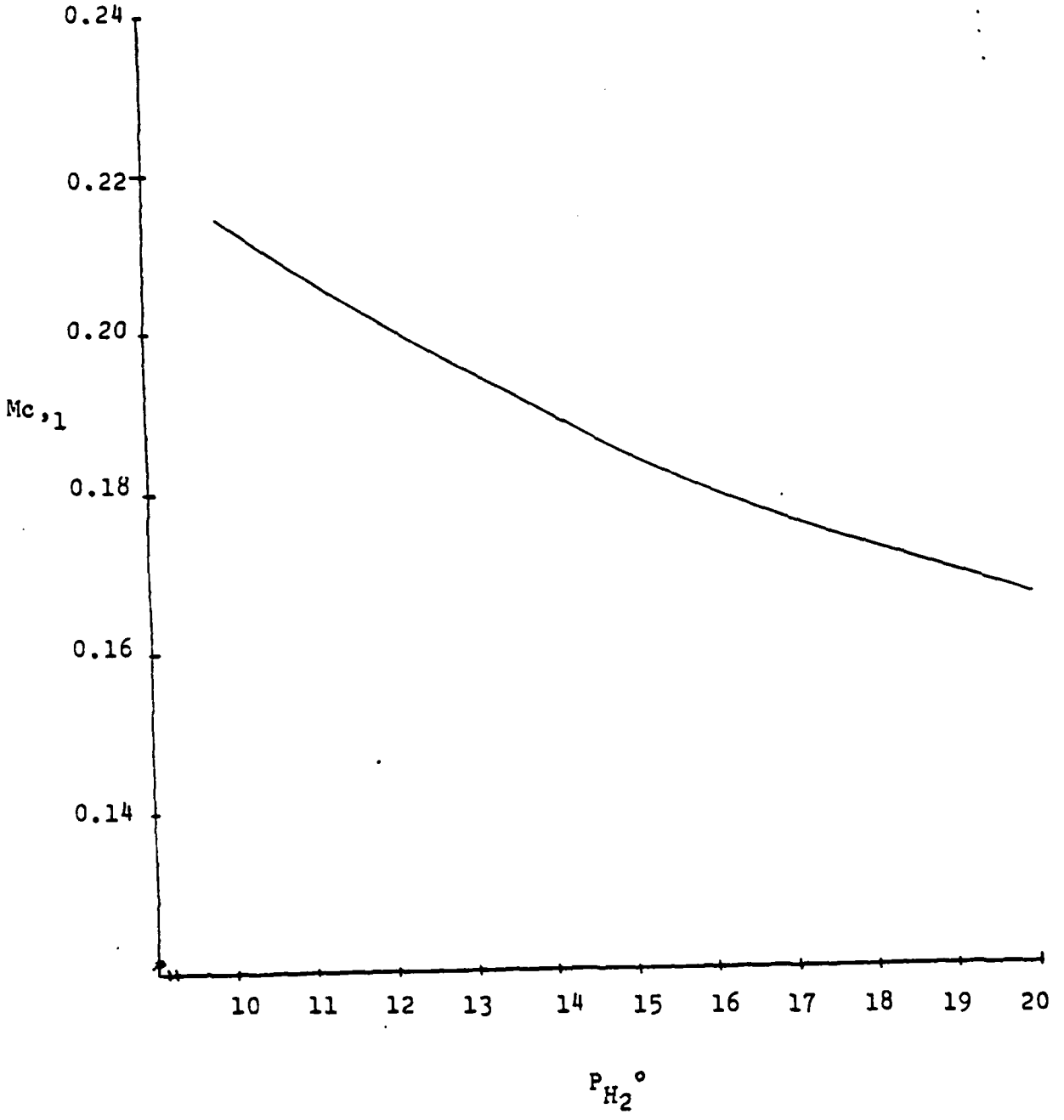

Fig. 23 - Upstream mach # $Mc_{,1}$ vs. $P_{H_2}{}^{\circ}$

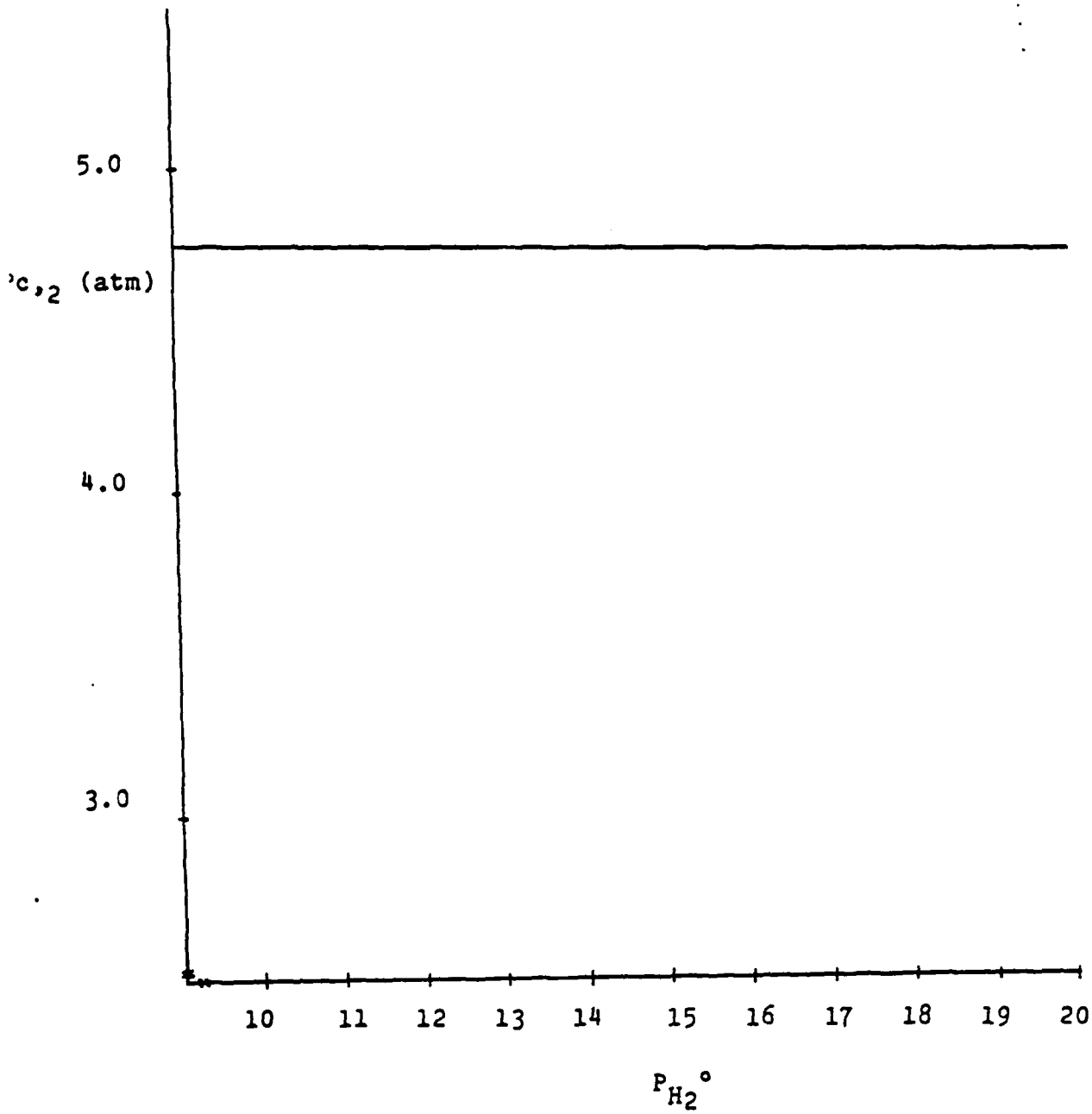

Fig. 24 - Combustion gas static pressure ($Pc,_2$) vs. $P_{H_2}°$

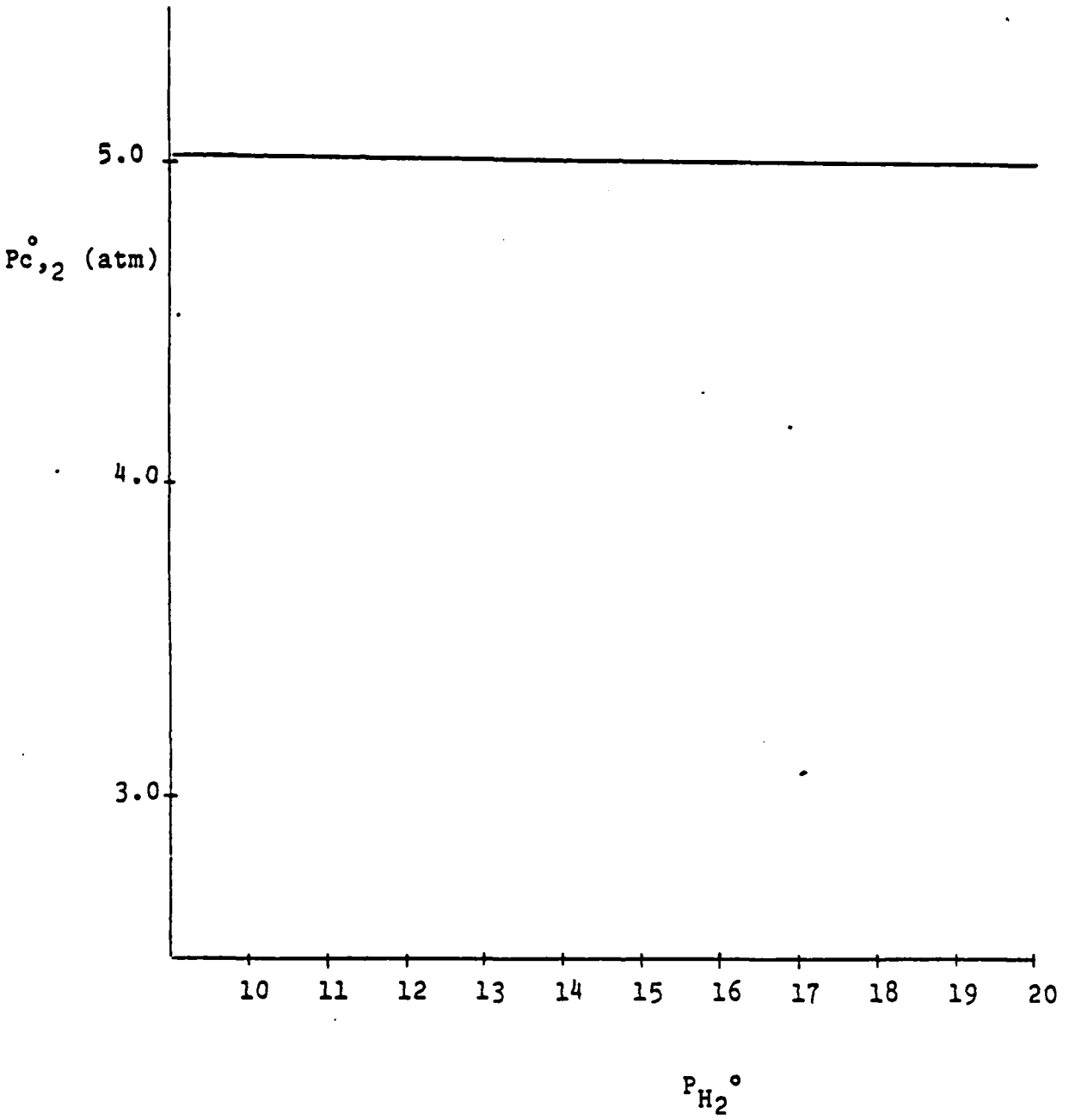

Fig. 25 - Combustion gas stagnation pressure ($P_{c,2}^{\circ}$) vs. $P_{H_2}^{\circ}$

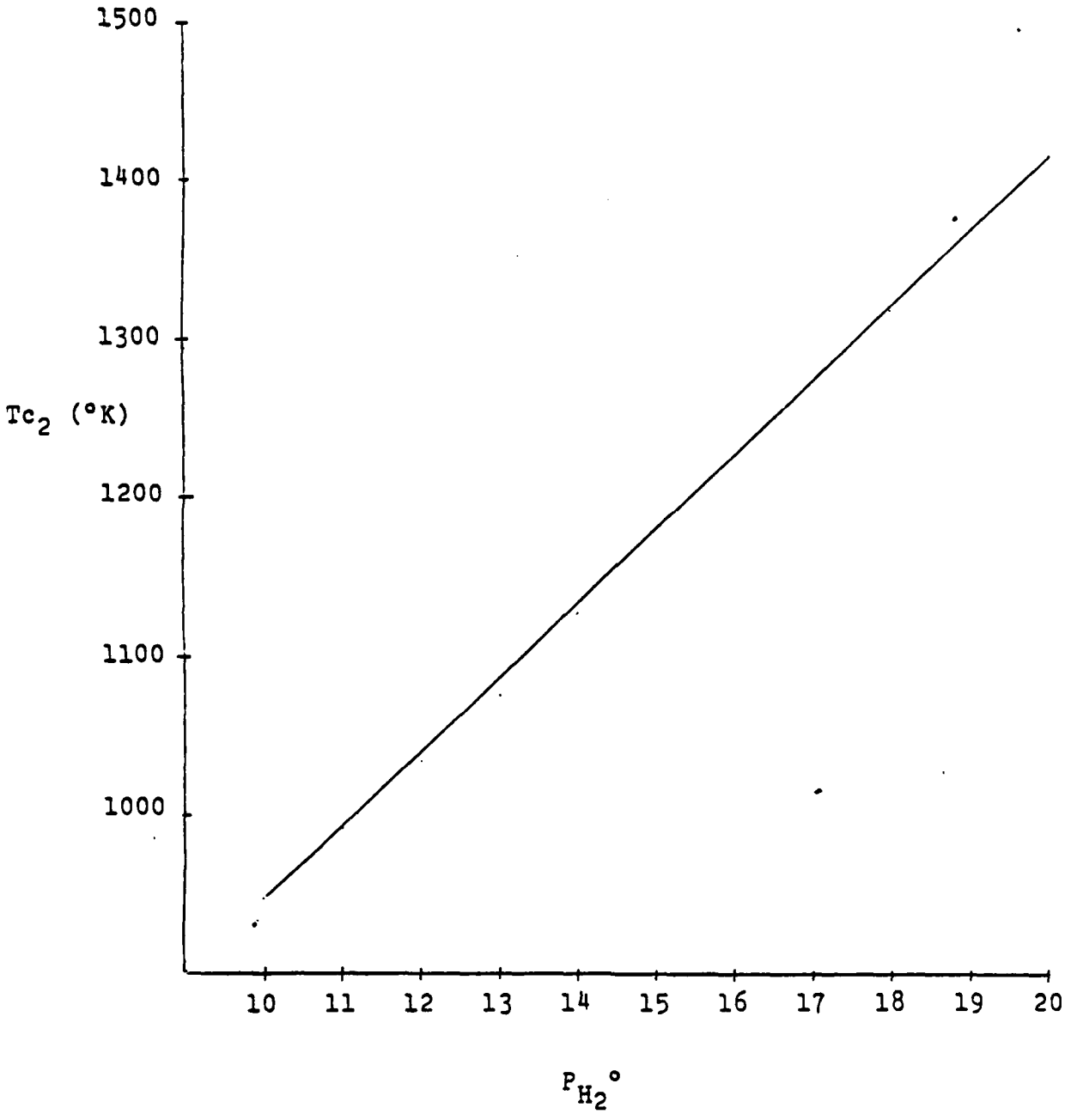

Fig. 26 - Combustion gas static temp. ($Tc_{,2}$) vs. $P_{H_2}°$

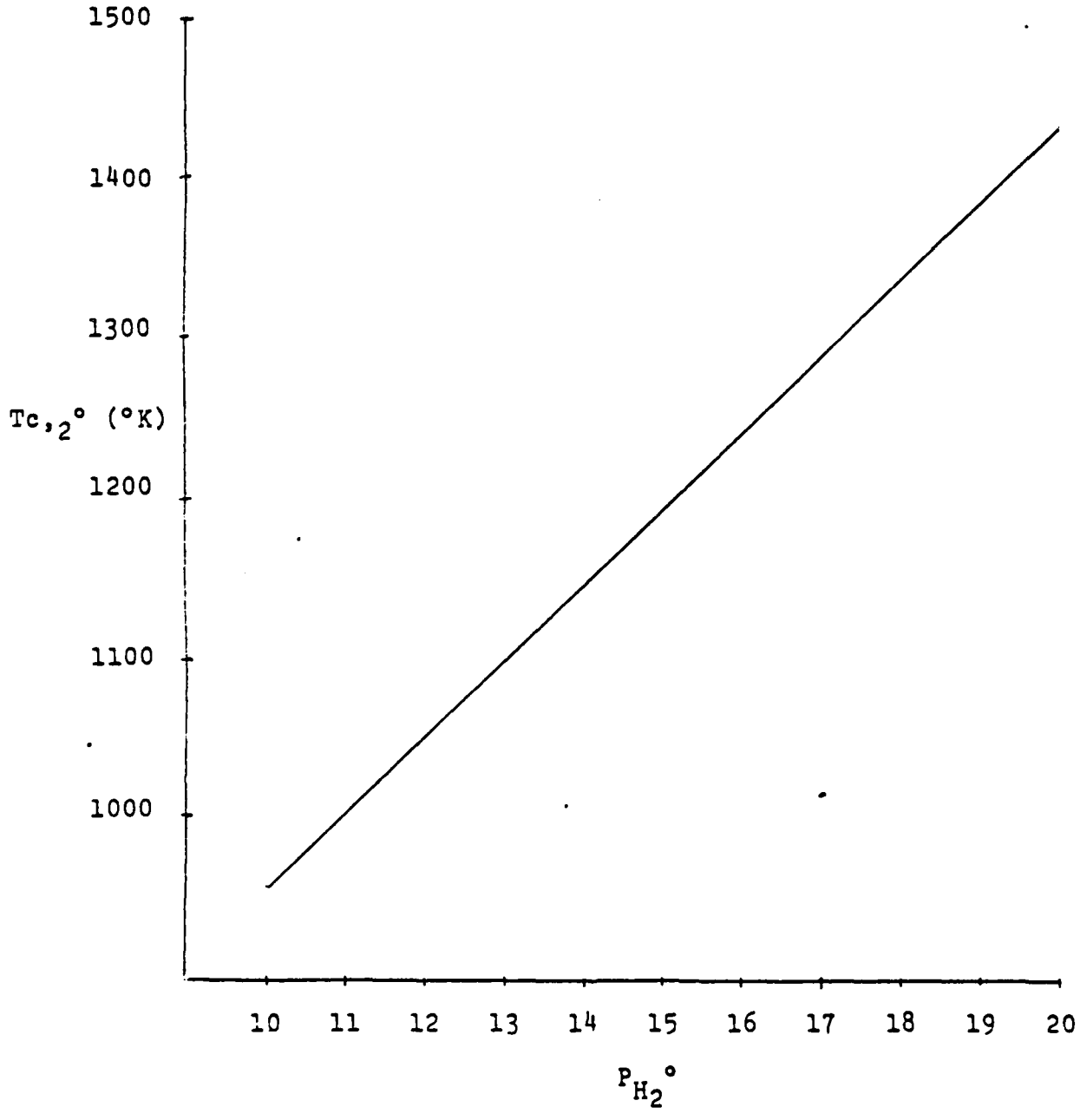

Fig. 27 - Combustion gas stag. temp. ($Tc,_1°$) vs. $P_{H_2}°$

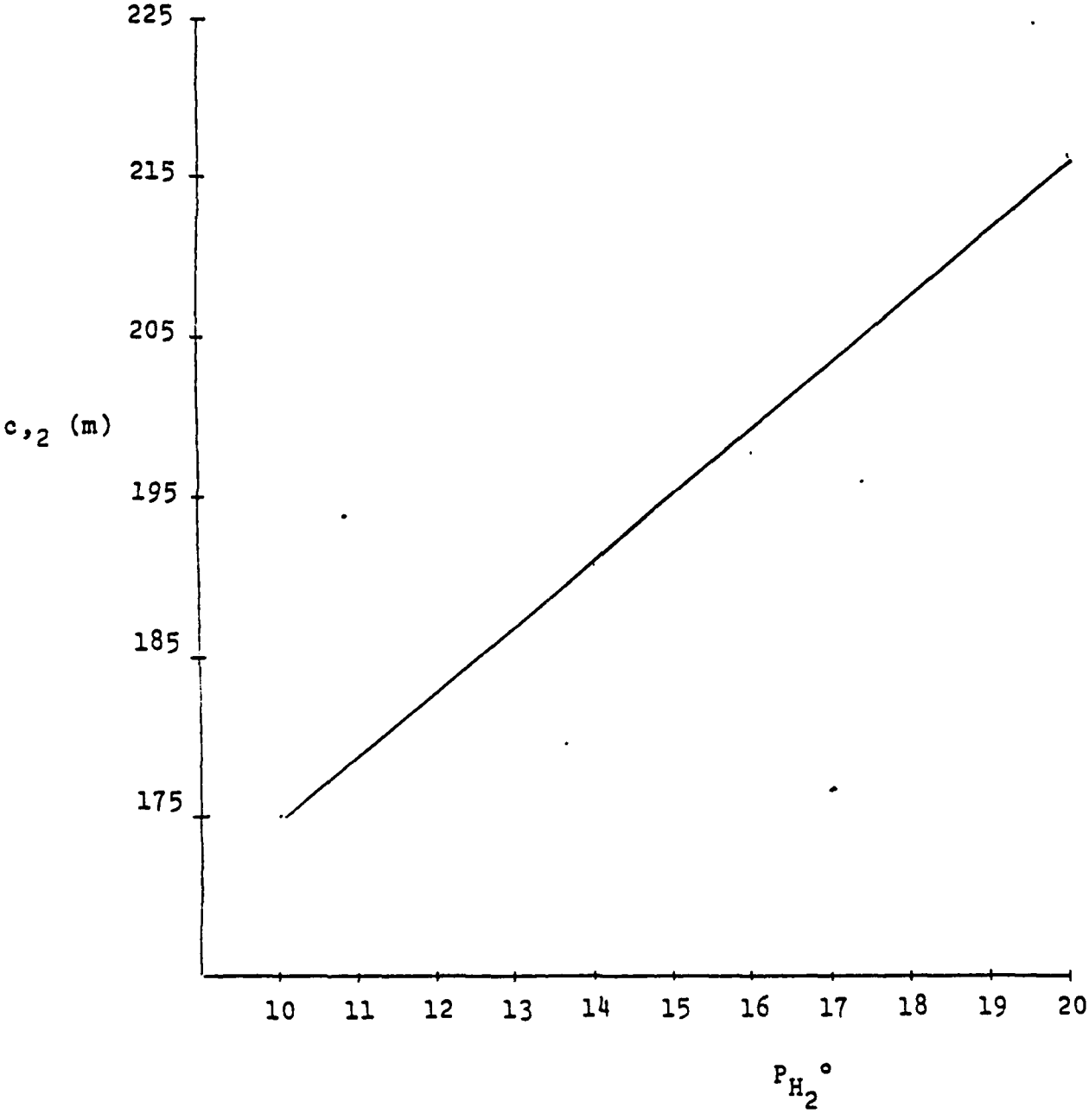

Fig. 28 - Combustion gas speed ($Uc_{,2}$) vs. $P_{H_2}^{\circ}$

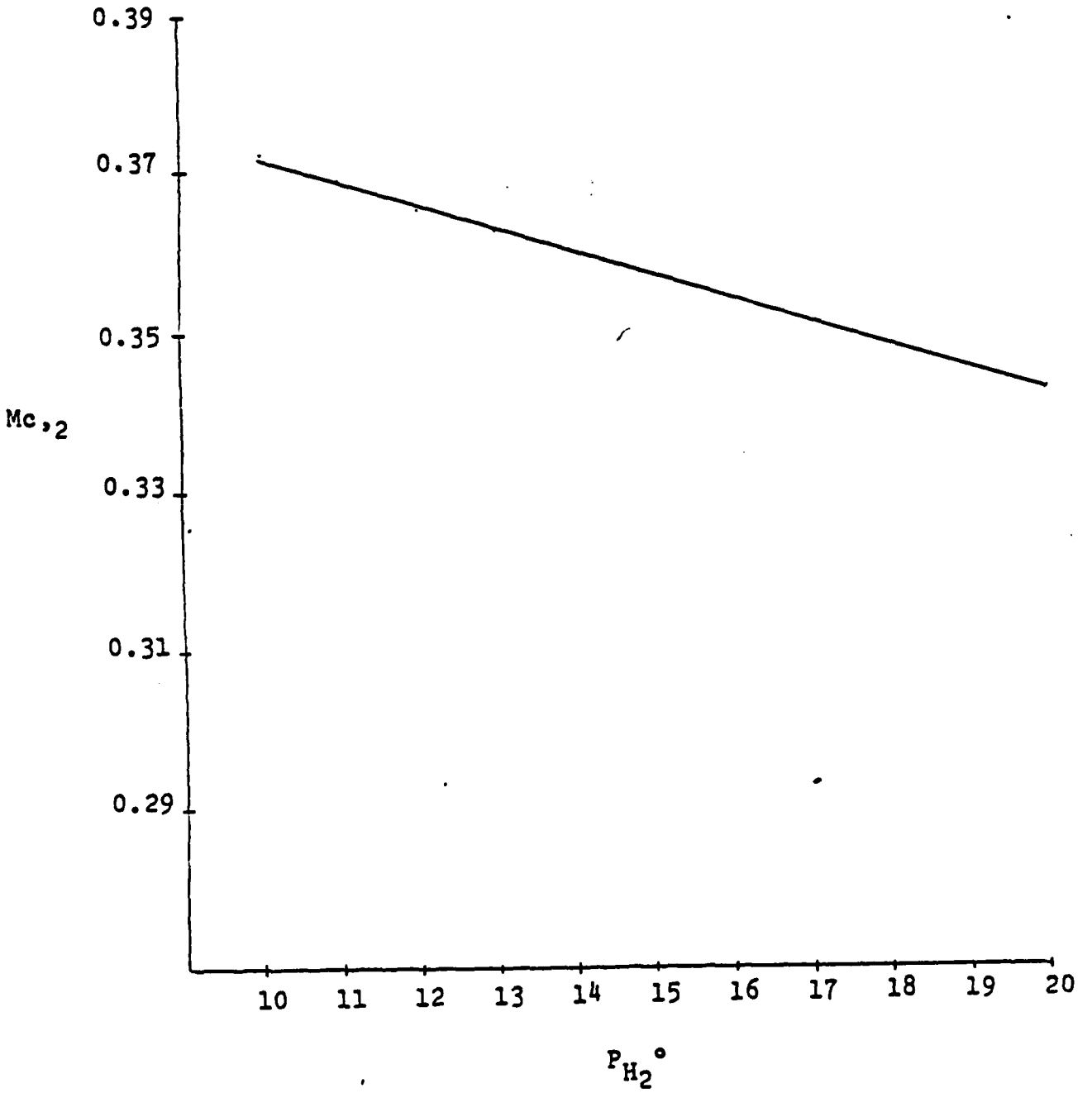

Fig. 29 - Combustion gas mach # ($Mc_{,2}$) vs. P_{H_2}

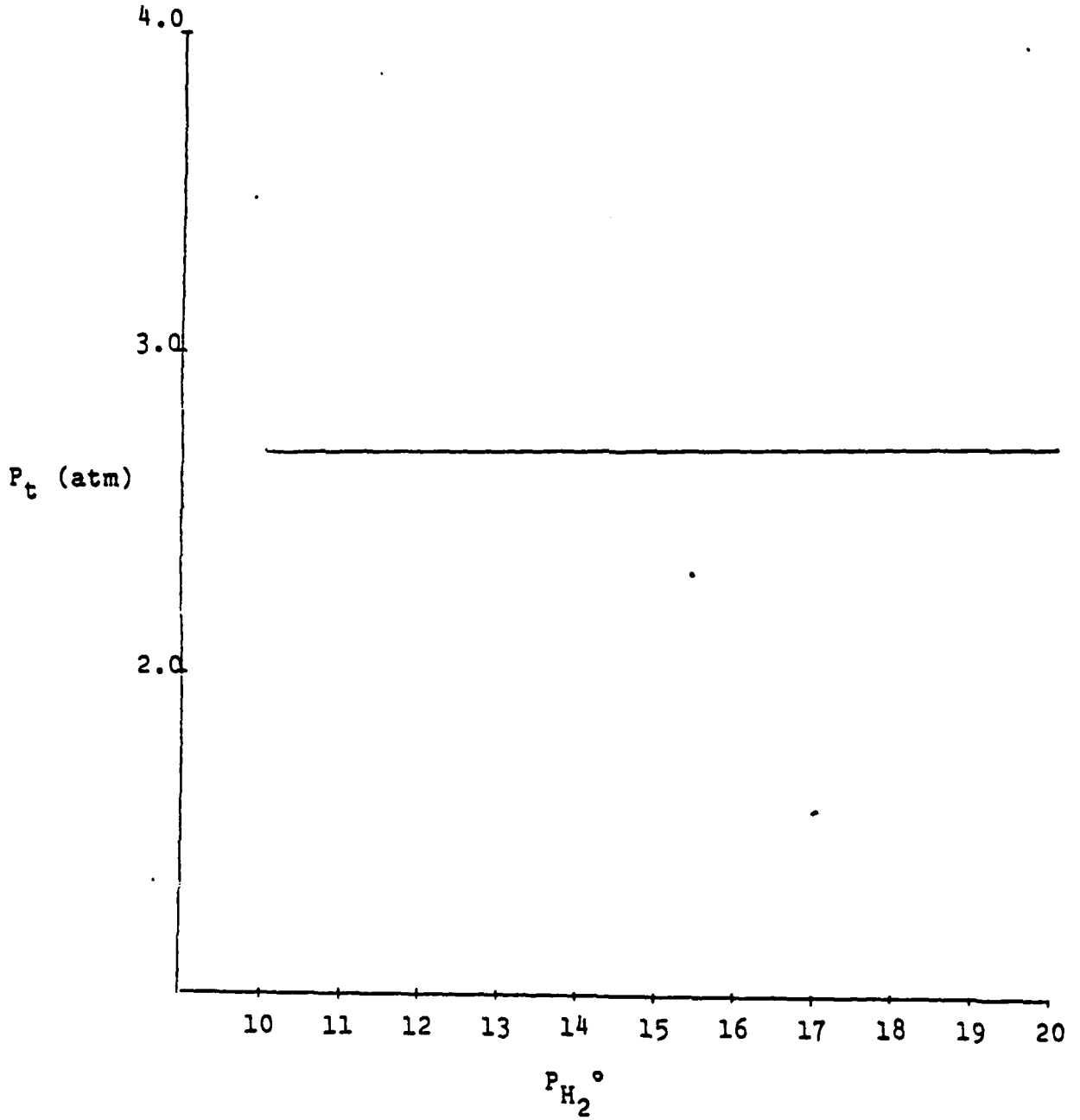

Fig. 30 - Static pressure at throat (P_t) vs. $P_{H_2}°$

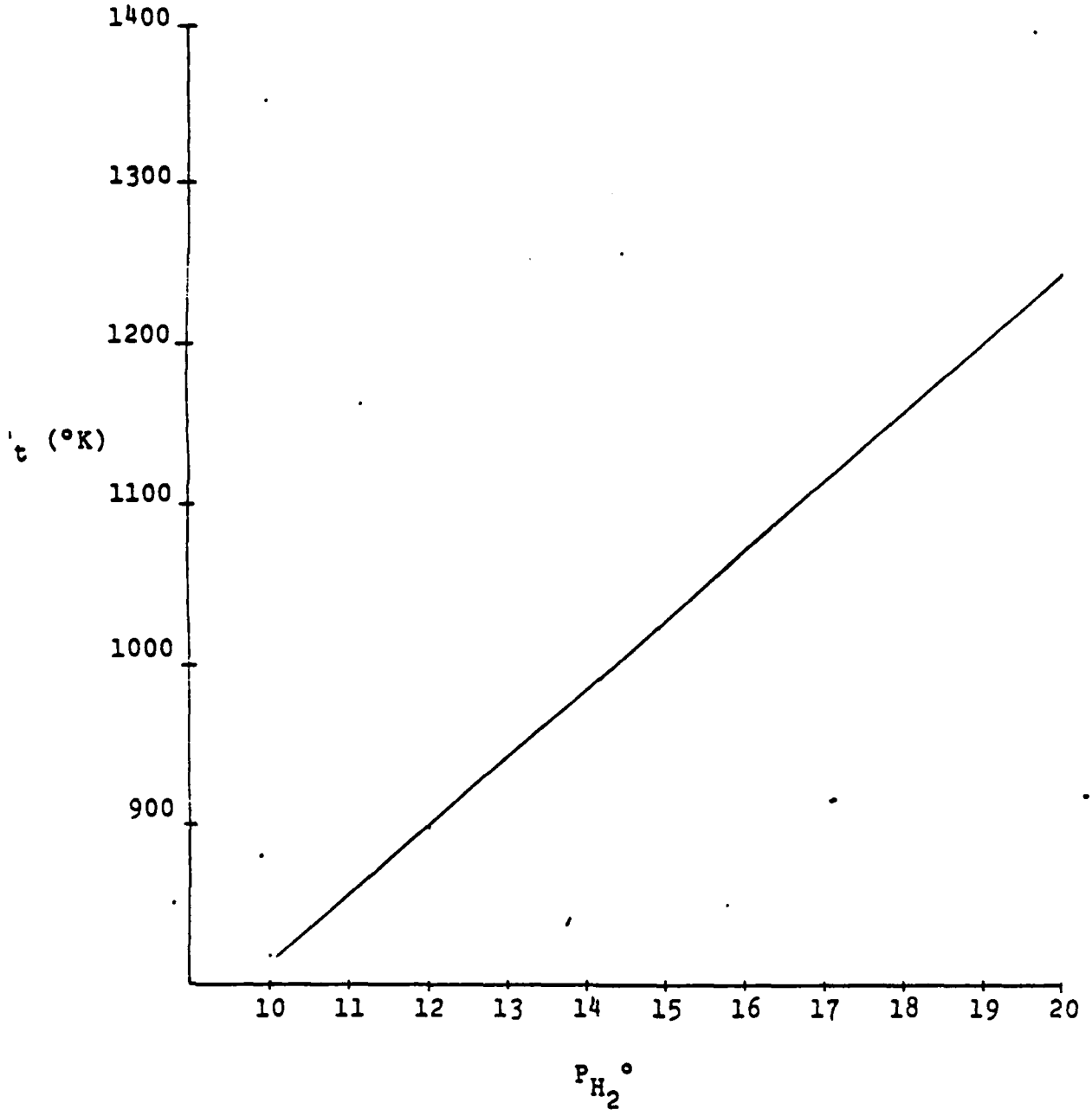

Fig. 31 - Static temperature at throat (T_t) vs. $P_{H_2}°$

Table 2 - Thermodynamic Values of Air

Temp. °K	$\left(C_s\right)^T_{air}$	$\left(\frac{h_f}{RT}\right)^T_{air}$	$\left(\frac{C_p}{R}\right)^T_{air}$
100	4.24293	3.48805	3.50021
200	4.14739	3.49302	3.50142
300	4.10166	3.49805	3.50951
400	4.07375	3.50441	3.53964
500	4.05556	3.51745	3.59503
600	4.04349	3.53555	3.67121
700	4.03564	3.56180	3.75530
800	4.03084	3.59063	3.83840
900	4.02821	3.62299	3.91735
1000	4.02701	3.65572	3.98804
1100	4.02689	3.68882	4.05031
1200	4.02758	3.72108	4.10616
1300	4.02870	3.75313	4.15385
1400	4.03017	3.78297	4.19756
1500	4.03199	3.81218	4.23507
1600	4.03384	3.83960	4.26844
1700	4.03593	3.86581	4.29844
1800	4.03801	3.89023	4.32586
1900	4.04025	3.91302	4.35070
2000	4.04236	3.93666	4.37358

Table 3
Absolute Formation Enthalpies

For Eleven Species

At 0 Degrees Kelvin

Species	$\left(\frac{E_f^o}{\mathcal{R}}\right)_i$ (K)
CO	-13688
CO_2	-47286
H	25982
H_2	0
H_2O	-28736
N	56613
N_2	0
NO	10799
O	29685
O_2	0
OH	4675

REFERENCES

1. Edse, R., Dhiman, O., Marasco, E., Ignition, Combustion, Detonation, and Quenching of Reactive Mixtures, AFOSR-TR-77-0059, September 1976.

2. Edse, R., Unpublished Notes.

END

FILMED

2-85

DTIC